VERTICAL FORESTS

The Impact of Green Balconies on the Microclimate by Solar Shading, Evapotranspiration and Wind Flow Change

Caithlin Ann Marugg

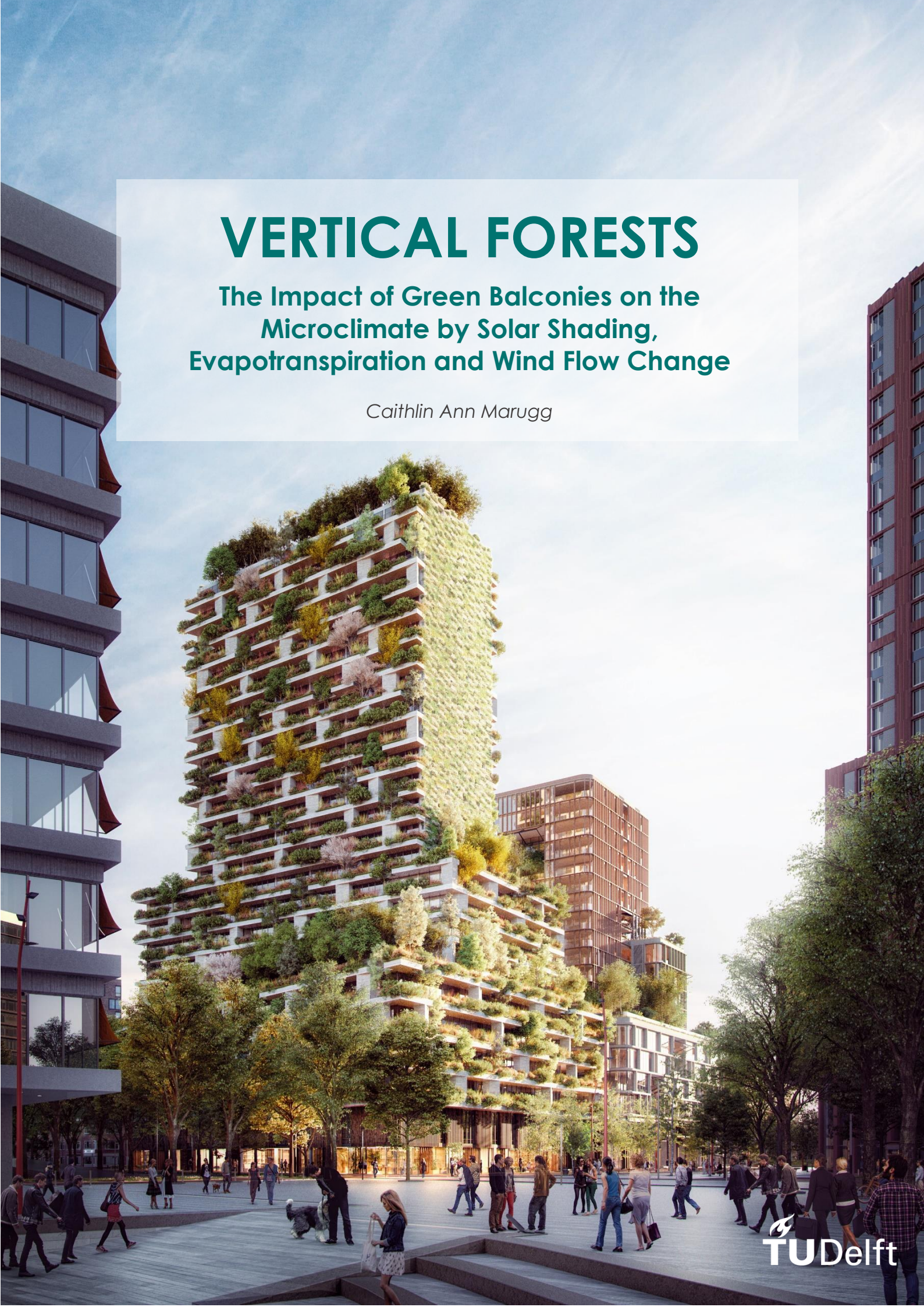

TUDelft

Vertical Forests

The Impact of Green Balconies by Solar Shading, Evapotranspiration and Wind Flow Change

by

Caithlin Ann Marugg

4127978

In partial fulfillment of the requirements for the degree of
Master of Science
in Building engineering
at Delft University of Technology

Thesis committee

Prof. dr. ir. A.A.J.F. van den Dobbelsteen | TU Delft
Dr. ir. M.J. Tenpierik | TU Delft
Dr. ir. H.R. Schipper | TU Delft
Ir. L. Cartigny | Arcadis

An electronic version of this thesis is available at http://repository.tudelft.nl

Cover image: Wonderwoods, Stefano Boeri Architett

TU Delft

Table of Contents

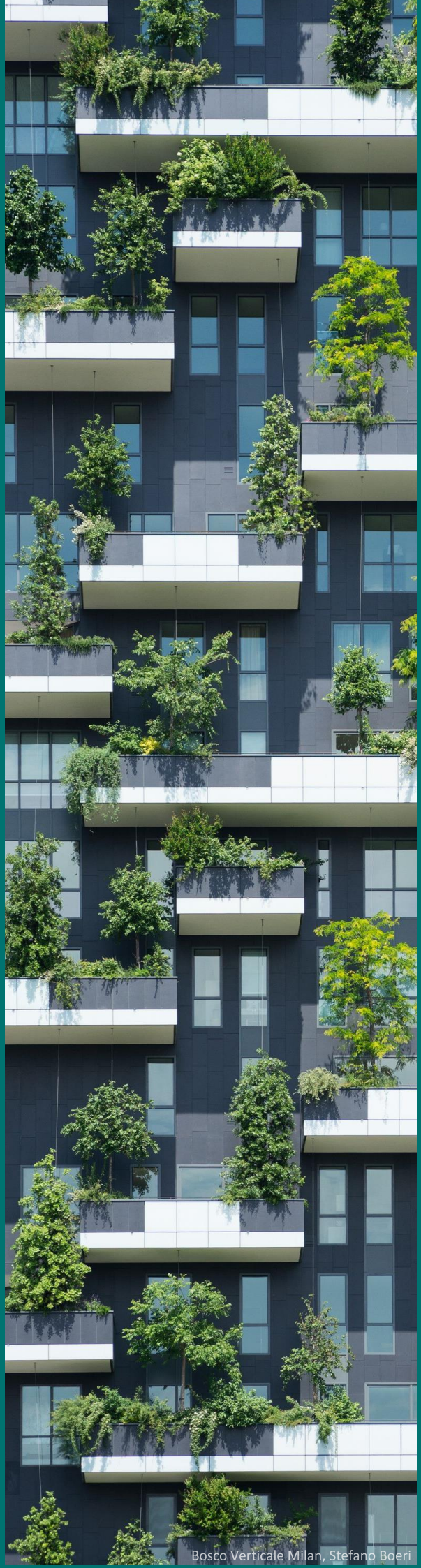

Bosco Verticale Milan, Stefano Boeri

Part I

Research Definition

1 Introduction

In the future most of us will be living in cities. The attraction that large cities have on people is undeniable and the migration of people from rural areas to an urban one is an increasing trend that seems unstoppable. And while only two percent of the earth's area is urbanized, that two percent consumes eighty percent of our energy (Hall, 2016).

Urbanization poses new challenges to us as a society. The built environment is becoming more densely populated and the limited availability of space requires us to utilize it in a smart way. But we still desire the city to provide a livable environment. Currently our buildings mainly consist of cold harsh materials such as steel, concrete and glass. These materials have made it possible for us to build megacities at an incredibly fast pace. But as we see the cities evolving around us we start to realize that a city built up of mineral materials alone is not a very livable city. Access to nature has an important role in making our cities more livable. We all know about the calming and healing effects that nature can have on our well-being. Vegetation can reduce stress, promote socialization, increase productivity and stimulate creativity (Mangone, 2015). And it is possible for us to enjoy both the benefits of the city and nature if we find smart ways to incorporate greenery into the high-density high-rise cities of the future.

In new construction projects the integration of greenery has an increasingly prominent role in the architectural design. This might have to do with the green building trend, which some architects have translated literally into the building appearance. There are several ways of integrating greenery into a building. Recently, the application of green roofs and green facades have become common practice. This had led to a considerable amount of research into the effects of these systems on the urban microclimate and building energy performance.

In 2014 the completion of Bosco Verticale (Vertical Forest) in Milan took building-integrated greenery to a whole new level. The two residential towers designed by Stefano Boeri Architetti were innovative because of the extensive application of green balconies (Figure 1). The goal of the project was to accommodate a vertical densification of nature and to increase the biodiversity in the urban environment. The name

Figure 1: Bosco Verticale (Vertical Forest) project in Milan (Stefano Boeri Architetti, 2018)

of the project is a reference to the vegetation that is featured on the building, it is similar to what can be found in one hectare of forest. Over 700 trees and 13.000 plants were distributed across balconies close to the building façade. The project attracted a lot of attention worldwide and won the 2015 CTBUH Best Tall Building Award. Since the extensive application of green balconies has been proven to be feasible, there have been more commissions to build similar Vertical Forest projects across the globe.

In the meantime, sustainability is an ongoing topic of conversation. There is an increased awareness of the anthropogenic contribution to global warming and the subsequent effects of climate change are already being experienced. Especially in large cities climate effects are amplified due to the high population density, high amount of impervious surfaces and low tree coverage. Therefore urban environments typically have to deal with issues such as air pollution and heat stress (Kats & Glassbrook, 2018).

The demand for sustainability is also reflected in current building design practice. Clients request buildings that are environmentally responsible and resource-efficient. Also the building codes are putting strict limitations on the conductivity of the thermal shell and require buildings to be more energy efficient. To reach sustainability goals a better understanding of the interaction between the building and its direct environment is of great importance.

Even though green balconies are seen more frequently in new construction projects, not a lot of research has yet been done on their impact. The trees on the green balconies are not only aesthetically pleasing, but will also have an effect on the local microclimate. Trees are known to have a cooling effect, increase relative humidity, reduce wind speeds, block daylight and improve air quality. Some research has been done on the effects of trees near a building façade, but there is very limited research on the specific application of trees on balconies (Raji, et al., 2015).

Research on this topic poses some difficulties. Modeling of trees is complex because of the irregular shape and significant differences in characteristics for every single tree. Direct measurements could be useful to deal with this complexity. But because of sheer size an experimental setup of a green balcony within a controlled laboratory setting is hard to realize. Empirical research on the other hand brings other complications. Firstly, access to measuring locations is limited since the application of green balconies is relatively new. And secondly, research performed in an outdoor setting will strongly be influenced by local climate variations.

Despite research limitations, there is still a need to get a better understanding of the impact that green balconies have on the urban environment and the building itself. With more we can make a better consideration in which context green balconies should be applied and which design strategies can optimize the benefits of vegetation. In the context of urbanization and sustainability, green balconies could potentially make our cities more comfortable and healthy environments.

2 Problem Context

This chapter defines the problem context of this research project. It focuses on issues in the built environment that are typical of this time and are related to building-integrated greenery. The main problems that will be treated are urbanization, sustainable building design and health and comfort in buildings.

2.1 Urbanization

Already more than half of the world population is living in cities and predictions show that by 2030 this will be up to 60 percent. By then, one in four will live in a city that has at least one million inhabitants (United Nations, 2015).

The world's cities are growing both in size and in number. In 2016, there were 512 cities with at least one million inhabitants and in 2030 this number is projected to 662 cities. Some cities can be defined as megacities because they provide a home to more than ten million inhabitants. In 2016 there were 31 of these megacities, by 2030 this is expected to grow to 41 (United Nations, 2016). Currently a minority of the people live in megacities, but they will become home to 8,7 percent of the world population in the nearby future (Figure 2). The population in all city types is expected to increase, whereas the proportion of the population living in rural areas is expected to decrease slightly.

Most megacities are located in less developed regions on the southern hemisphere. India and China have five and six megacities respectively. The newest megacities are also projected to be located in developing countries. But the share of the population that lives in cities is projected to increase in all regions of the world. However, most of the world's fastest growing cities are located in Asia and Africa. 47 cities grew twice as fast as the average annual rate between 2000 and 2016. Of these rapidly growing cities, 6 are located in Africa and 40 in Asia, with 20 in China alone. In China this leads to urbanization challenges such as segregation of migrants, over-pricing of housing and urban sprawl that overtakes cultivated land rapidly (Cao & Cao, 2013).

It will be a challenge to accommodate the rapid growth of cities while still realizing sustainable urban development. The expanded automobile ownership that is associated with urbanization leads to many negative effects on cities, including traffic congestion and air pollution (Wang & He, 2015). But not only the increased traffic leads to an increase in carbon emissions, also buildings are an important contributor, both directly and indirectly. In 2010 buildings accounted for approximately one third of global black carbon emissions and also accounted for 32% of global final energy use (IPCC, 2014).

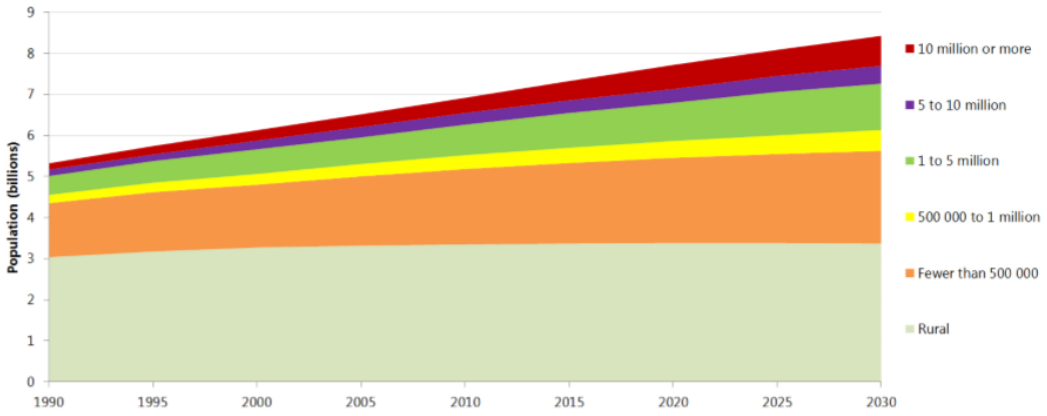

Figure 2: World population by size class of settlement 1990-2030 (United Nations, 2016)

The rapid process of urban renewal has led to demolition of large areas of old buildings that are replaced with uniform looking tall concrete and glass structures. This led to the realization of "a thousand cities, the same face" (Wu, 2012). There are many large cities that lack character and visual variety as a result of large construction projects constructing similar buildings with little attention to architectural variety.

As rural areas are converted to urban areas, fundamental changes are made to the natural ecosystems. Landscapes created entirely by humans lead to homogenization in resource spatial variability (Yan, et al., 2018). Aronson, et al. (2014) studied the impact of urbanization on biodiversity on a global scale and found that the species density in cities decline by 92% for native birds and 75% for native plants in comparison to non-urban areas. In recent decades, urban biodiversity has been increasingly recognized by the scientific community and policy makers as an important driver for global preservation efforts (Alvey, 2006).

Urbanization also has a negative effect on the storm water systems in the city. This is largely due to the highly impervious areas in urban conglomerations that result in increased surface run-off (Lee & Heaney, 2003). Another well-known effect of the urban area is the increased air temperature in cities, also described as the urban heat island effect.

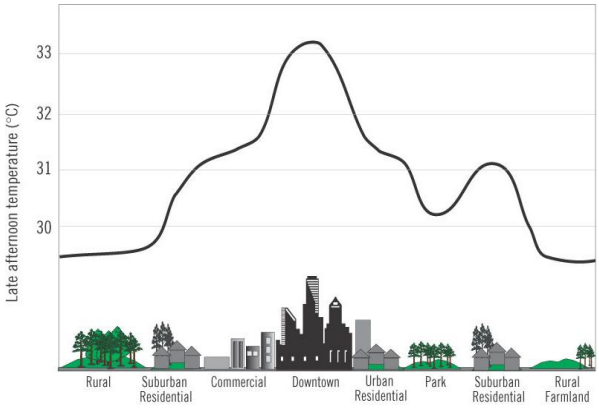

Figure 3: Late afternoon temperatures in different type of areas (UWO, 2018)

2.1.1 Urban heat island effect

Urbanization has a negative impact on the environment by an increased production of pollution, changes in the physical and chemical properties of the atmosphere and covering up the earth's surface. The cumulative heating effect that results from all these factors is called the urban heat island (UHI) effect. UHI is the temperature increase in any man-made area which results in a distinct "warm island" that is located in a "cool sea" when compared to the surrounding natural rural area (Arrau & Peña, 2016). As a result of the UHI effect the air temperature in large cities can be up to 7°C warmer than its surroundings (Wilby, 2003)(Figure 3).

Surprisingly, anthropogenic heat output originating from heating, air conditioning and transport is only a small component of the urban heat balance with around 50 W/m^2. As a reference, incoming solar radiation in the UK peaks around 800 W/m^2 (Ennos, 2015). What happens to this incoming solar radiation plays an important role in the temperature difference between urban and rural areas. In rural areas 20-25% of short-wave radiation is reflected back into the sky by grass and 15% by trees. Of the energy that is absorbed, over half is used by plants to evaporate water, which results in a local cooling effect. In cities this energy balance is dramatically different. The often darker man-made materials have a lower albedo so only 15% of the sun's radiation is reflected or even less in urban canyons. Of the absorbed radiation almost all

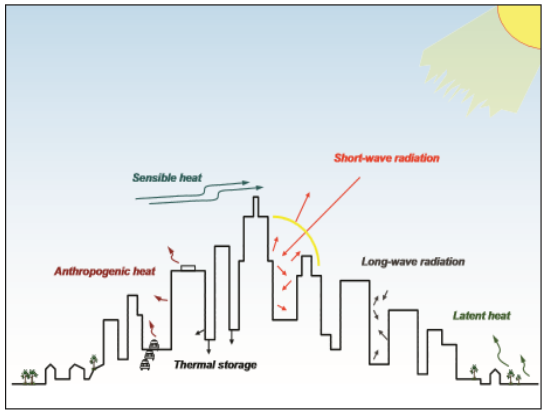

Figure 4: Types of urban surface energy transfer (EPA, 2008)

energy is used to heat up pavements and roofs which also heats the air directly above. At night cities cool down slowly because heat is stored in stony materials, pollution traps long-wave radiation and less sky is visible from urban canyons.

There are two main types of UHIs. A distinction is made between surface and atmospheric urban heat islands (EPA, 2008). The surface UHI has the most significant effect, because exposed urban surfaces can get hotter than air. Surface temperatures are typically measured indirectly by remote sensing. When at the end of the day the heat trapped by urban surfaces is slowly released, the atmospheric UHI effect occurs. The polluted air and tree canopies keep the hot air close to the city surface and result in locally warmer ambient temperatures. The air temperatures are typically measured directly with fixed weather stations.
There are many factors that influence the UHI effect (Voogt, 2004), these include:

- Weather and geographic location
- Urban geometry
- Urban material properties
- Vegetation
- Anthropogenic heat

Urban geometry refers to the dimensioning and spread of buildings in the city. In high-density cities, the view factor to the cooler sky is limited. Building surfaces are often obstructed by surrounding buildings which means heat is radiated to other buildings rather than escaping into the atmosphere (Figure 4). Urban material properties influence how sunlight is reflected, emitted and stored. Solar reflectance is the most important determinant of surface temperature, but thermal emissivity and heat capacity of urban materials also influence the UHI. Most urban materials have a higher heat capacity than rural materials and therefore store a lot of heat internally.

Trees and vegetation provide shade which lowers surface temperature, also they reduce air temperatures through evapotranspiration. Additionally, pollutants are deposited on vegetation and volatile organic compounds and smog are lessened.

Anthropogenic heat can come from a variety of sources such as HVAC systems in buildings and emissions and heat from urban transportation (Piselli, et al., 2018).

Some impacts of UHIs are positive, such as longer plant-growing seasons, but the negative effects are more prevalent. In summer there will be an increased cooling demand which leads to higher energy consumption. But even more concerning is the impact that the UHI has on human health, which will be discussed in Paragraph 2.3.1.

2.1.2 Urban air pollution

Urban air pollution is a topic that is closely linked to the urban heat island effect, because both mechanisms interact and amplify one another. The consequences of urban air pollution were clearly visible in European cities after the Industrial Revolution. The infamous London fog in 1952 caused many fatalities and hospital admissions. Subsequently legislation for air quality was drafted in many regions, but this did not solve all issues. The rapidly growing megacities in mainly Asia, Africa and Latin America still have high levels of ambient air pollution that form an immediate health hazard (Figure 6) (Gurjar, et al., 2008).

Rapid urbanization has resulted in more air pollution emissions due to transportation, energy production and industrial activity all being concentrated in a densely populated area. The transmission of the pollution is strongly influenced by wind and ambient air properties. Different pollutants also have a different effect on human health. Stieb considered CO, NO_2, O_3, SO_2 and $PM_{2.5+10}$ levels as critical to evaluate the air quality in cities (Stieb, et al., 2005).

Air pollution from combustion relates to a wide variety of acute and chronic health effects. The most serious effects such as lung cancer are caused by particulate matter, which are particles small enough to enter deep into the lung and blood stream. Analyses show that particulate

Figure 6: Urban air pollution in Beijing (Shan, 2011)

matter is associated with 5% of lung-related cancer, 2% of cardiorespiratory mortality and 1% of respiratory infections mortality worldwide (WHO, 2002). According to the Global Health Obvervatory, 90% of the population in cities in 2014 was exposed to particulate matter concentrations that exceeded the WHO air quality guidelines. Worldwide, ambient air pollution contributes to 5,4% of all deaths (WHO, 2018).

2.1.3 Urban noise

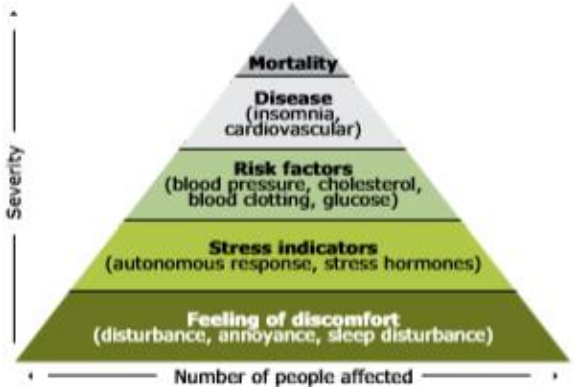

Figure 5: Pyramid of noise effects and severity (EEA, 2014)

Persistent or high-level noise leads to a number of direct and indirect health impacts. Figure 5 shows how exposure to noise can affect health and well-being. For most people noise disturbance leads to regular disturbance, annoyance and sleep disturbance. Severe annoyance and sleep deprivation over a long period of time can cause physiological and psychological stress, which could possibly lead to risk factors such as high blood pressure and high cholesterol levels. Then there is a small chance that these risk factors could lead to disease and finally, mortality. There is an increased cardiovascular risk if daytime noise exceeds the sound pressure level of 65 dB. Actually, chronic exposure to 75 dB is considered dangerous since the noise might cause hearing loss (EEA, 2014).

In urban areas people are living and working in greater proximity to noise pollution and this can seriously affect the quality of life. The most common sources of noise pollution are traffic, aircrafts and railways, industry as well as construction sites. Traffic noise is the most important source of environmental annoyance (Ising & Kruppa, 2004). According to the European Environment Agency, in large cities the percentage of people exposed to unacceptable levels is two to three times higher than the national average. Levels higher than the acceptable level of 65 dB occur in most cities (Santamouris, 2001).

2.1.4 Urban winds

Cities are the roughest type of surfaces there are, so they have a significant influence on wind distribution. Wind governs the dispersion of heat and pollutants from trees, squares and buildings (Hooff & Blocken, 2010). Urban wind distribution is a complicated field of research. A small difference in topography can cause a large irregularity in the air flow making it difficult to predict. Wind distribution is influenced by topography, building geometry, and many more local factors such as trees.

Grimmond & Oke (1998) characterized wind variation with height over cities by making a distinction between two specific sublayers: the free surface layer or urban boundary layer which exists above the rooftops and the obstructed sublayer or urban canopy layer which extends to the height of buildings (Figure 7). It can be said that in general the wind speed in the canopy layer is significantly lower than undisturbed wind. The urban canopy layer also has a distinct flow field that is determined by the local urban properties (Grimmond & Oke, 1998).

Especially the wind flow at night is interesting, because the urban heat island effect causes air flow to converge in the urban area (Oke, 1981). Because of temperature differences the wind flow pattern is very irregular and this results in short bursts of wind from the countryside.

In urban canyons large differences in wind speed between the canopy layer and street level can be found. An urban canyon is defined as a street with tall continuous buildings on both sides of the (narrow) road. Urban canyons have a low sky view factor and therefore do not radiate a lot of heat to the cool sky. But canyons also have a significant effect on both the speed and direction of winds. If the wind is parallel to the canyon, the wind is accelerated. A non-uniform width will add to this acceleration by the Venturi effect. When wind is perpendicular to the canyon, the turbulence of wind is greatest near the downwind side of the building due to stronger wind shears. The width of the urban canyon influences the type of flow (Figure 8).

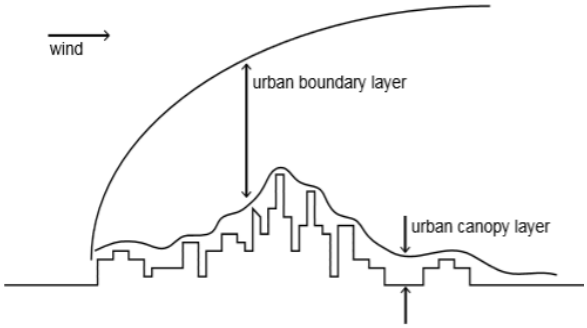

Figure 7: Urban boundary and canopy layer (Oke, 1981)

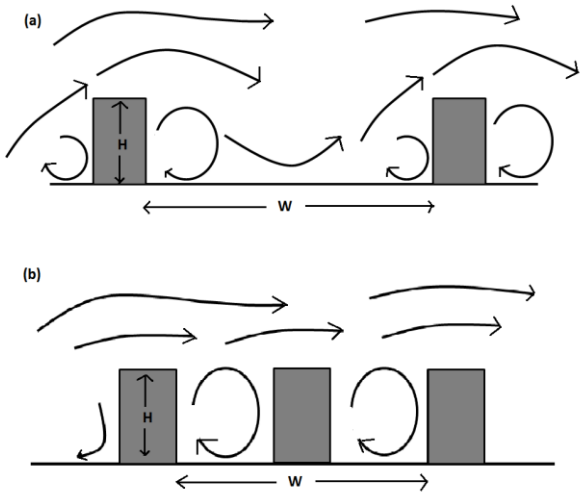

Figure 8: Effect of urban canyon width on wind flow patterns (Nunez & Oke, 1977)

To conclude there are two cases when urban winds are stronger than rural winds. Firstly, when the high-speed air layers are deflected downwards by tall buildings or channeled as jets along canyons in the same direction as the air flow. Secondly, when the air flow from the countryside is strong enough to overcome the frictional drag from the urban area (Santamouris, 2001).

2.2 Building energy use

Buildings use up a lot of energy due to material processing, construction and also in the operations phase. Globally, energy use of buildings accounts for 30-40% of all primary energy used (Kelso, 2010). Energy is a very important element for technological and economic development of a country. With increasing oil prices and a growing awareness of

the exhaustibility of fossil fuels, there is a need to diminish energy consumption. Since the first oil crisis in 1975 many different countries have been trying to increase energy efficiency with energy policies. However, not all policies were effective and many countries still see their energy usage rise yearly. In the European Union buildings consume approximately 40% of the total energy and produce 36% of the carbon dioxide emissions (Pikas, et al., 2014).

2.2.1 Near-zero energy buildings

The 2015 Paris agreement has set specific goals to mitigate climate change effects globally. Lowering the environmental impact of buildings and improving their energy efficiency are important elements to achieve these goals. A growing awareness about the use of natural resources and responsibility to the environment puts building energy performance even higher on the agenda. A well-known approach to sustainable building design is the three step strategy Trias Energetica (Duijvestein, 1989).

1. Energy demand reduction
2. Renewable energy employment
3. Clean and efficient use of fossil fuels

Nearly zero-energy buildings (nZEB) are buildings with a very high energy performance. The low amount of energy that these buildings do require comes mostly from renewable resources. To minimize environmental impact from buildings the EU directive on the Energy Performance of Buildings has expressed that by the end of 2020 all new buildings will need to be near-zero energy buildings. All new public buildings must be nearly zero-energy by 2018 (European Parliament and Council, 2010). This poses a significant adjustment to current building practices. And while this policy is focused on energy savings, these buildings should still have good quality from the end-user perspective. Thermal comfort is one of the key drivers to household energy use, so it is important to examine the level of thermal comfort while considering the energy performance (Berry, et al., 2014).

2.2.2 Bioclimatic design

Buildings have always been designed to protect mankind from the exterior environment. Bioclimatic design aims at constructing buildings that are in harmony with the natural surroundings and local climate while ensuring conditions of thermal comfort. This is reached by energetical interaction with the environment. A constant balance needs to be found between the building envelope and construction, the climate and location and the needs of the user (Manzano-Agugliaro, et al., 2015).

Designers of buildings have always tried to achieve an optimal comfort level within interior spaces. In history, vernacular architecture used passive building techniques to mitigate negative and utilize positive effects of the local climate (Olgyay, 2015). But since the Industrial Revolution, comfort in modern buildings has been regulated by devices that constantly consume energy and have a high environmental footprint. Since then, building design has focused mainly on protecting building from the environmental factors and regulating the climate through installations.

It was around the 1980's that environmental awareness increased and the need for sustainable building design got more recognition. During current times of rapid urbanization and sustainability awareness, it makes sense to practice sustainable ecological design. Bioclimatic design fits well within this context. Bioclimatic design of buildings serves four main objectives (Benessaia, 2011):

- Save conventional energy
- Use available natural resources
- Protection from the environment
- Improve thermal comfort and air quality

As the objectives illustrate, bioclimatic design depends on the building location potential. Based on the location's dry-bulb air temperature and relative humidity, the most promising passive design strategies can be chosen (Pajek & Košir, 2018). Bioclimatic building design comprises several strategies: careful allocation and

orientation of the building, smart building envelope design, passive shading, planting of trees near the building, protection from the wind, energy storage in the thermal mass, using natural lighting as much as possible and improving the microclimate around the building.

2.3 Human health and comfort

In the two previous paragraphs the global issues of urbanization and building energy use were discussed. These issues received global attention partly due to their negative impact on human well-being. Human well-being is often described in terms of health, comfort and happiness and these aspects are evidently interrelated (Steemers & Manchanda, 2010). For example unhappiness and discomfort can influence health. In this context health is not merely the absence of disease, but more along the lines of the World Health Organization definition.

"Health is a state of complete physical, mental and social well-being and not merely the absence of disease or infirmity." (World Health Organization, 2014)

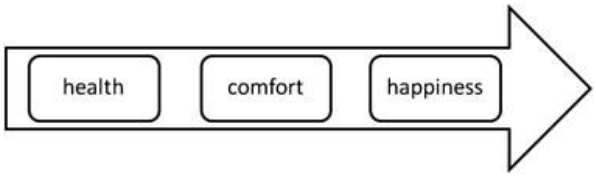

Figure 9: Well-being spectrum from measurable (left) to qualitative (right) (Steemers & Manchanda, 2010)

But in comparison to comfort and happiness, health is most easily measurable as the well-being spectrum illustrates (Figure 9). Comfort factors are also measurable, but comfort is significantly influenced by the amount of personal control that users can exert over climatic conditions (Gou, et al., 2013). Psychological factors can also influence the experience of comfort. Happiness is the most difficult parameter to quantify and can only effectively be determined by surveying people.

In this research the focus is on the measurable aspects health and comfort in relation to the urban microclimate and buildings.

2.3.1 Health and comfort in the urban microclimate

There is growing evidence that the warming trend over recent decades has already contributed to an increased morbidity and mortality (Patz, et al., 2005). This is most noticeable in sprawling cities where the UHI amplifies heat wave implications. Climate projections suggest an increase of the global mean temperature and also of extreme weather events such as heat waves (IPCC, 2014). Extreme ambient air temperatures contribute directly to deaths of cardiovascular and respiratory diseases, especially among vulnerable groups such as elderly people. For example in the heat wave during the summer of 2003 in Europe, 70.000 more deaths were recorded (Robine, et al., 2008).

But warming in cities also indirectly influences human health. The storm water runoff temperatures are elevated and this thermal pollution leads to a decrease in water quality, which strongly associates with water-borne diseases. The higher air temperatures also lead to an increase of the rate of ground-level ozone formation which worsens cardiovascular and respiratory disease. Additionally, pollen and other aeroallergen levels surge which can trigger asthma attacks (Noyes, et al., 2009).

An urban microclimate is the distinctive climate in a small-scale urban area and constitutes the influence of the built environment on large scale climatic conditions. These local conditions can deviate greatly from larger scale climatic conditions. The design of a city influences the microclimate directly, so careful design of the urban environment could contribute significantly to the physical well-being of the people in it. According to the WHO urban design is an important contributor to healthy cities (World Health Organization, 2014).

1.1.1 Health and comfort in buildings

Surveys show that humans spend approximately 88% of their time indoors (Robinson & Nelson, 1995), so health and comfort in buildings is an important topic. According to Bluyssen there are four factors that influence our perception of the

indoor environment (Bluyssen, et al., 2007):

- Lighting quality
- Acoustical quality
- Air quality
- Thermal comfort

While all these factors influence the health and comfort of building occupants to some extent, the last few decades there has been an increasing concern about the impact of air quality on health. Changes in building design that improve the energy efficiency require the building to be more airtight. As a result there is less infiltration and natural ventilation in the building and we rely more on mechanical ventilation. Additionally, we use more synthetic building materials. Even though our buildings are more comfortable and energy efficient, they also provide an environment where contaminants are easily produced and have higher concentrations (Jones, 1999). Poor indoor air quality can lead to a range of vague symptoms from building users, often referred to as Sick Building Syndrome.

Bluyssen proposed a framework to improve health and comfort in buildings (Figure 10). According to this framework a healthy and comfortable building requires consideration of the human being, the building envelope, control strategies and end-user requirements (Bluyssen, et al., 2007).

2.4 Conclusions problem context

In conclusion, there lies a challenge in providing a healthy and comfortable environment in cities in a sustainable way. Urban areas have to deal with heat stress, air pollution, traffic noise and amplified wind effects. Green balconies could potentially address these problems by improving the local microclimate and therefore diminish building energy use within the limited space of an urban environment.

Figure 10: Framework for health and comfort in buildings (Bluyssen, et al., 2007)

3 Research Definition

In the previous chapter the problem context of this research project was described. This problem context leads to a research objective, research questions and research outline.

3.1 Research objective

Green balconies are a relatively new method to integrate vegetation with the building design. While green balconies are predominantly placed because of their aesthetic appeal, the vegetation also has a direct effect on the microclimate of the balcony and indirectly influences the heat transfer through the building envelope and the urban environment. A limited amount of research has been done on the microclimatic effects of green balconies. This research aims to expand the knowledge on this topic.

Some effects of vegetation are more qualitative in nature, but this research focuses on the quantitative effects. Psychological and ecological effects of greenery will therefore not be evaluated explicitly. The scope is limited to the physical processes of heat and moisture transfer between green balcony vegetation and the surroundings.

By quantifying the effects of green balconies on the physical environment, it is possible to predict to what extent green balconies contribute to a better climate in an urban environment. This could make the case for vertical forests as a means to mitigate climate change effects in the urban context. Also a better understanding of the heat and moisture transfer will lead to guidelines for designing green balconies that benefit the microclimate.

3.2 Research questions

The main research question is:

What is the impact of green balconies on the microclimate by solar shading, evapotranspiration and wind flow change?

In relation to this main question, the following sub-questions can be formulated.

1. *How does building integrated vegetation influence the microclimate?*
2. *What are the mechanisms of heat and moisture transfer for trees?*
3. *How can the microclimatic effects of green balconies be modelled?*
4. *How does the environment and design of a vertical forest influence the microclimate?*

3.3 Research outline

The research outline is summarized in Figure 11. In Part I vertical forests and green balconies are introduced. Then the problem context of urbanization and climate change are described. This first exploration leads to the research definition and research questions.

In Part II the theoretical framework is presented that forms the background of the research project. A literature study is done on the history of building integrated vegetation. Also a literature study is done on the effects of other forms of building integrated vegetation such as green roofs and green facades. Then the relevant mechanisms of heat and moisture transfer for trees are described.

In Part III the knowledge from the theoretical framework is applied on a small scale by setting up green balcony simulations. The project Bosco Verticale in Milan is used as a reference, since these buildings are already constructed and therefore it was possible to perform measurements there. In the second chapter of Part III a simple thermal network model is made in MATLAB to describe the heat and moisture transfer mechanisms at work on a green balcony. Then a more extensive model of a green balcony situation is setup in microclimate software ENVI-

met which also includes turbulent wind effects. The purpose of the ENVI-met model is to examine how parameters such as temperature, balcony orientation and wind direction influence the impact of the balcony greenery on the microclimate.

Finally, in Part IV the discussion, conclusions and recommendations form the final remarks and provide an answer to the research questions.

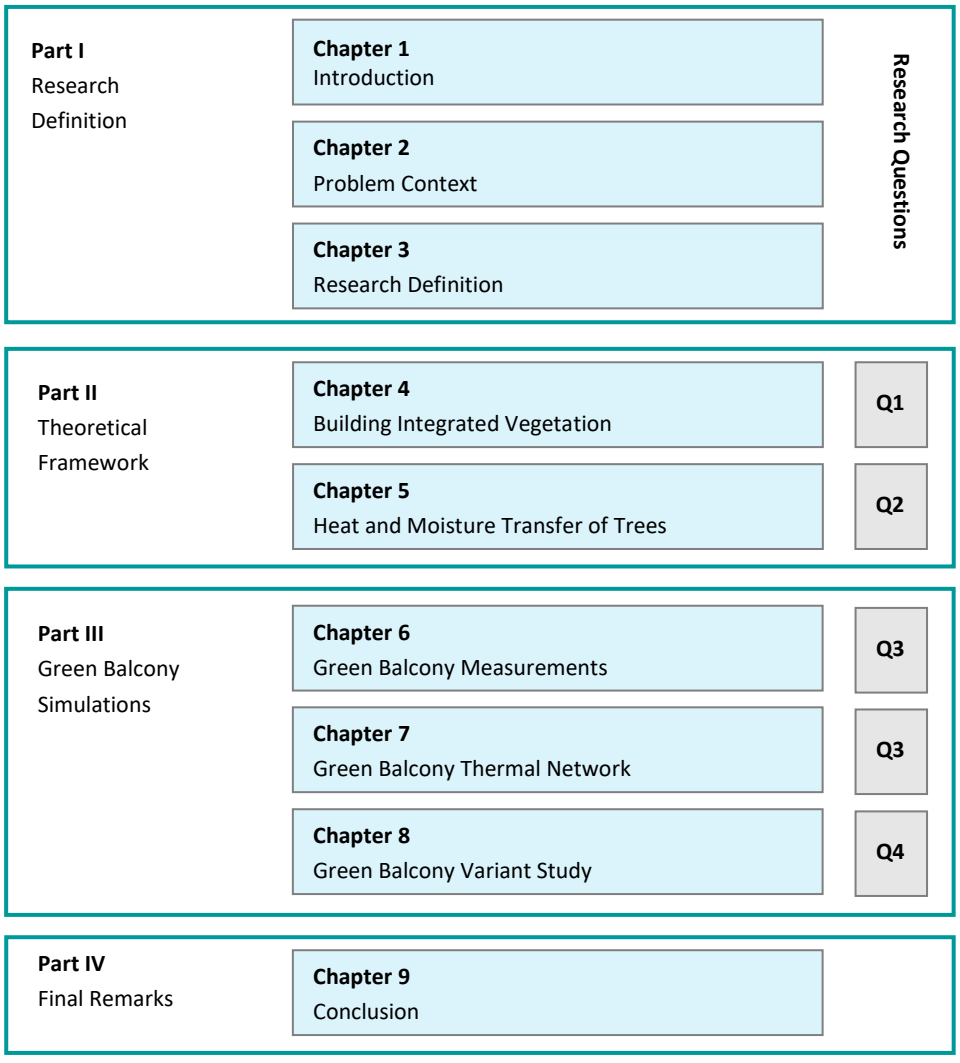

Figure 11: Research setup overview

Trudo Vertical Forest Eindhoven, Stefano Boeri

Part II

Theoretical Framework

4 Building Integrated Vegetation

In this chapter a literature study is performed on vegetation that is integrated in building design. The first paragraph describes the history of building integrated vegetation. In the second paragraph an overview is given of common building greening system typologies such as green roofs and green facades. In the third paragraph the effects of trees near the building envelope are considered. This leads to the concluding paragraph which summarizes the potential benefits of green balconies.

4.1 History of building integrated vegetation

The integration of vegetation with buildings is not a new concept. In this paragraph the history of building-integrated vegetation will be described.

4.1.1 Ancient times

Greek and Roman texts paint a vivid picture of the luxurious Hanging Gardens of Babylon. This was the first widespread account of building-integrated vegetation and one of the Seven Wonders of the Ancient World. According to the descriptions lush vegetation cascaded down the terraces of the grand palace, creating an oasis of green amidst the arid desert-like environment of ancient Babylon (located in present-day Iraq). The Garden contained a wide variety of trees, shrubs and vines that dazzled the eye (Klein, 2013).

According to the legend written down in 290 B.C., the King Nebuchadnezzar II of Babylon constructed the Hanging Gardens around 600 B.C. as a gift to his wife Amytis. She had been missing the green hills and valleys of her homeland Media (modern-day Iran). To provide the garden with irrigation, a system of cisterns, pumps and waterwheels was employed to raise water from the nearby Euphrates River to the top of Hanging Gardens (Dalley, 2013).

The origins of green roofs can also be found in ancient times. Especially humans living in a harsh climate needed weather-proof enclosures in order to survive. In Neolithic times shelters were built by earth daubing and then nature's seed rain naturally created a vegetative cover. When the shelters turned evolved into separate walls and roofs, innovations were needed to increase weather-proofing and durability. Mat-like sods were cut from natural meadows, with the roots of the plants preventing erosion in the early construction stage. These shelters can be seen as the precursor of the modern-day green roof (Jim, 2017).

About two thousand years ago, vine trees gained popularity in Med iterranean countries. They were used to provide shade for the facades, evaporative cooling and economic benefits through the production of fruits. They were one of the earliest accounts of vertical greening systems (Medl & Florineth, 2017).

4.1.2 Early modern architecture

Fast-forwarding in time, the work of Le Corbusier played an important role in promoting building-integrated vegetation in modern architecture. A significant early work related to this topic was l'Esprit Nouveau Pavilion built in 1925 for the Paris International Exhibition of Modern Decorative and Industrial Arts. The Pavilion was built around a tree that emerged through a hole in the rooftop (Figure 12). The pavilion represented a future urban housing unit. It was

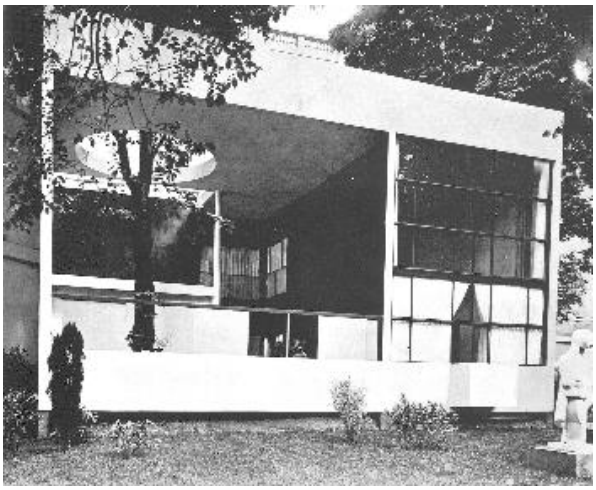

Figure 12: l'Esprit Noveau Pavilion by Le Corbusier, 1925 (Difford, 2009)

part of his provocative idea to reconstruct six hundred acres of central Paris with sixty-story apartment towers and park-like green spaces surrounding it (Difford, 2009).

Le Corbusier's writing and pavilion attracted a significant amount of attention, resulting in commissions for residential building designs. In 1931 Villa Savoye was delivered, one of his most notorious buildings. It marked a subtle shift in incorporating nature by placing the landscape on top of the building rather than next to it. This building showcased Corbusier's five points of architecture, that he described in the essay *Five Points Toward a New Architecture*. His architectural vision describes a design with ground-level pilotis to elevate the building, a free floor plan relieved from load-bearing walls, long windows, freely-designed facades and a roof garden (Corbusier & Jeanneret, 1926). On the roof garden Le Corbusier elaborated:

"Roof gardens will display highly luxuriant vegetation. Shrubs and even small trees up to 3 or 4 metres tall can be planted. In this way the roof garden will become the most favoured place in the building. In general, roof gardens mean to a city the recovery of all the built-up area." (Corbusier & Jeanneret, 1926)

4.1.3 Greening incentive programs

According to Köhler and Ksiazek-Mikenas (2018), Berlin was likely the first city to adopt policies stimulating building-integrated vegetation. Green roofs have a long history in Berlin, between 1880 and 1914 around two thousand green roofs were installed, but unfortunately only a few of those survived both World Wars.

In 1984 the Landscape Program for Berlin was initiated, aiming to redevelop the city with integration of nature in the form of green roofs, green facades and community gardens. Environmental concerns formed the basis to stimulate the installation of green roofs, especially the enhanced insulation and temperature buffering properties were considered of importance. A prime example is the Paul-Lincke-Ufer building that was retrofitted in 1985 with a green roof. This was one of the first projects with relatively thin vegetation layers resulting from the technology of ready-made turf mats that is widely applied nowadays (Köhler & Ksiazek-Mikenas, 2018).

Through the Landscape program approximately 65.750 m^2 of extensive green roofs were subsidized. About half of green roof installation costs were subsidized by the government. Berlin had to end the program due to deficits, but continues to stimulate building-integrated greenery with fees and regulations. In 1983 at least 24 German cities had incentive programs to support urban greening projects. Later, German national and local legislation and policies were adjusted to recognize the environmental benefits of green roofs. Comparable greening incentive programs were later adopted by cities abroad (Köhler & Poll, 2010).

4.1.4 Garden atria in office buildings

The first large office building in the United States to devote a substantial proportion of the building to vegetation, was the Ford Foundation Building in New York City. It was designed by Kevin Roche and John Dinkeloo and completed in 1968. The building features a publicly accessible atrium garden that was purposed to provide urban greenspace year round (Figure 13). The building was recognized by the Architectural Record as "a new kind of urban space", since it was highly unusual at the time to provide greenery in this form (Jones, 2013).

Not long after the completion of Ford Foundation, the oil crisis of 1973 marked a key moment in the history of building design. In reaction to an oil embargo by Arab countries, the European Union set out a new energy policy strategy to stimulate energy savings within the building sector. The aim of these policies was to reduce the growth of internal energy consumption by using energy in a rational way. In 1993 the first Directive of the EU on the energy performance of buildings was published (Fokaides, et al., 2017). The oil crisis did not only affect Europe, but also overseas the demand for energy-conscious buildings increased.

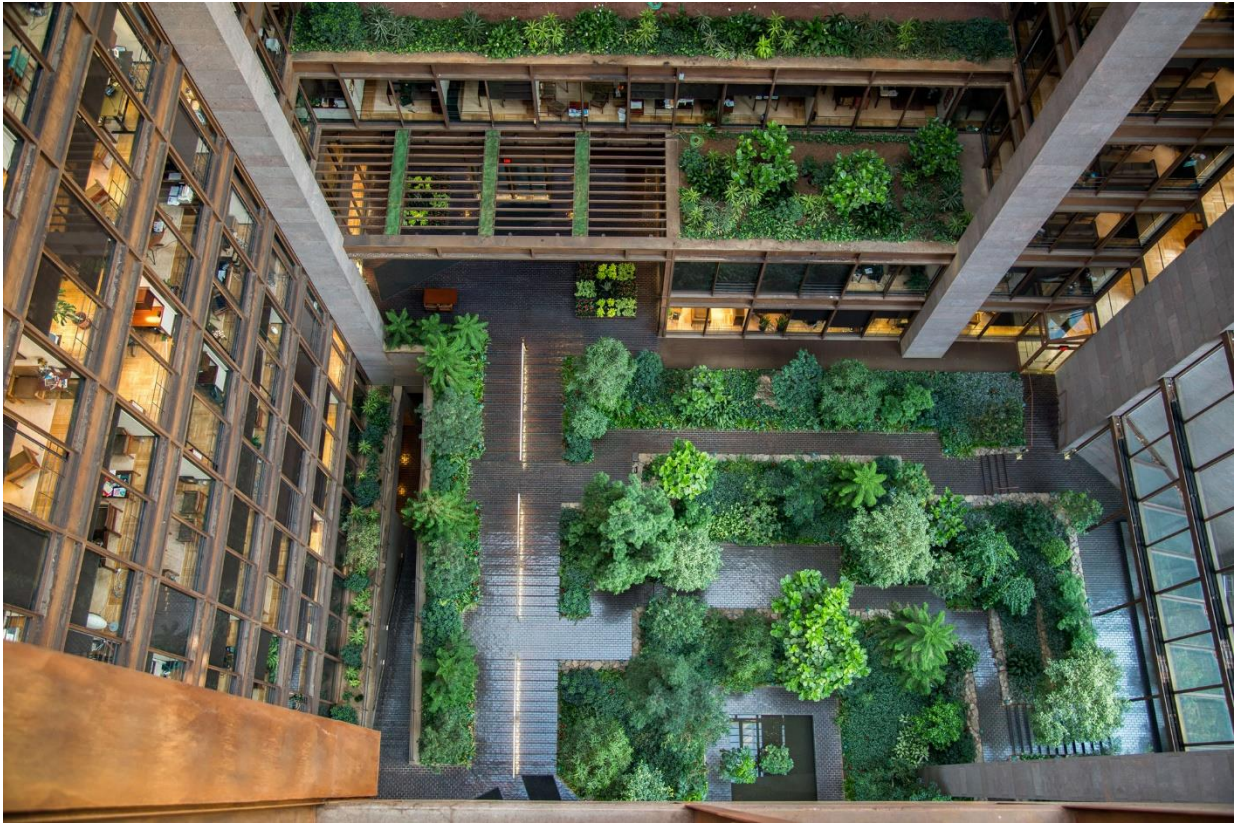

Figure 13: Ford Foundation Building by Roche & Dinkeloo in New York City, 1968 (Larry Lederman, Monacelli Press)

Norman Foster was one of the pioneers in this new approach of sustainable building design (Powell, 2011). After experimenting with natural concepts in the HSBC Building, his firm Foster & Partners designed the Commerzbank Tower in Frankfurt which was delivered in 1997 (Foster & Partners, 2018). Aside from being the tallest building in Europe at the time of completion, it was also an innovative skyscraper from a sustainability perspective. The project explores possibilities of integrating vegetation and makes use of natural systems for lighting and ventilation. The triangular shaped building features a central atrium with winter gardens spiraling around it on nine different levels. The greenery in the sky gardens were selected from North American, Asian or Mediterranean origin, depending on the microclimate resulting from the façade orientation. The central atrium acts as a ventilation chimney and allows offices to be naturally ventilated 85% of the year. Also every office has access to natural daylight reducing the need for electrical lighting.

4.1.5 The ecological skyscraper

Ken Yeang is one of the leading architects in the field of ecological buildings in dense urban areas. The topics of skyscraper design and environmental responsibility seem an unlikely match, but the theory of the ecological skyscraper aims to contradict this. This field has notably been shaped by Yeang's works *The Skycraper, Bioclimatically Considered* (1996) and *The Green Skyscraper* (1999) (Yeang & Yeang, 2008). In his books he proposes interconnecting measures regarding the use of energy, water and light. He also relates these concepts the local climate, ecology and function of the building. In this way plants can play a vital role for energy conservation in the building as well as improve the living quality of vertical cities (Yeang, 1996).

The Minara Mesiniaga tower by Hamzah and Yeang was the first realization of his bioclimatic design principles in 1992. The cylindrical building features a spiral of vegetated sky courts that provides a connection to nature on all levels and promotes natural ventilation (Douglass-Jaimes, 2015). Yeang and Hamzah's 1998 proposal for the EDITT tower in Singapore also showed extensive vegetation on the outside of the building. Even though the building has not been realized, it was featured in several international publications because of its distinctive design (Figure 14) (Fulcher, 2011).

Just like Yeang, the French architect Jean Nouvel also aims to design buildings that are in harmony with their environment. In his most recent works, he collaborated with botanist Patrick Blanc to feature ecology as an integral part of the building architecture (Riley, 2017). Noteworthy collaborative projects include the Musée du Quai Branly in Paris (2006) and One Central Park in

Sydney (2015). The latter combines an extensive green façade with a cantilevered assembly of mirrors. The mirrors are motorized for optimized positioning to capture sunlight and direct it down to the gardens (Nouvel & Beissel, 2014).

The search for sustainable design solutions in high-rise building has lead architects towards biomimicry concepts (Mirniazmandan & Rahimianzarif, 2017). Biomimicry uses the ideas from nature and can offer optimal solutions for conflicts between nature and human activities. Since all organisms are looking for more efficiency and less energy and material use, nature is an exemplary model for sustainable engineering. The Dragonfly project by Vincent Callebaut Architectures is an example of a biomimicry high-rise building. The light glass and steel wings of the building are structured to mimic the membranous wings of a dragonfly. And not only the building structure is inspired by nature. Like a true living organism, the tower is also self-sufficient in water, energy and biofertilization, featuring a metabolic farm for urban agriculture (Vincent Callebaut Architectures, 2009).

4.1.6 The garden city movement

The phrase 'garden city' was coined by Ebenezer Howard, who published *Garden Cities of Tomorrow* in 1902 to spread his vision on urban planning in response to the overcrowded industrialized cities in the UK (Hall, 2016). While his ideas were first criticized as being utopian, the garden city model was realized in several suburban areas, resulting in detached and semi-detached homes surrounded by spacious gardens and landscapes. The garden city movement eventually gained following throughout Europe, North America and other global urban developments (Allmond, 2017).

The city-state of Singapore shows how the garden city concept can be implemented in a high-density high-rise environment. The first Singaporean tree planting campaigns started in 1963 and policies to promote urban greenery have continued throughout the last five decades of the city's rapid urbanization. Singapore's nickname 'garden city' can be attributed to a strong governmental

Figure 14: Rendering of the EDITT Tower by Hamzah & Yeang, 1998 (Fulcher, 2011)

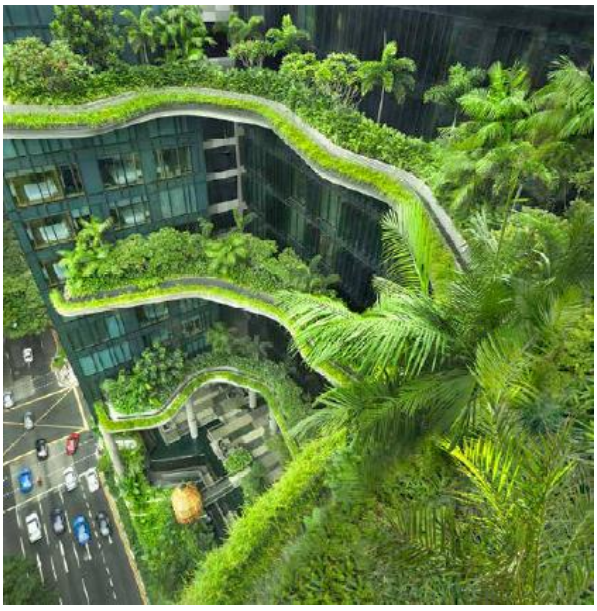

Figure 15: PARKROYAL on Pickering by WOHA, 2013 (WOHA, 2018)

commitment to greenery, which is reflected in the allocation of land and financial resources (Tan, et al., 2013). An exemplary programme is the Skyrise Greenery Incentive Scheme which encourages the installation of greenery on existing buildings. Already 110 buildings have been retrofitted with greenery and they plan to achieve 200 ha of skyrise greenery by 2030 (National Parks Board, 2018).

The architectural firm WOHA contributed to the development of the garden city Singapore by experimenting with natural vegetation as a building element. New ecological high-rise typologies were introduced in the Oasis hotel (2016) and PARKROYAL on Pickering (2013) (Figure 15). In 2016 the firm published *Garden City Mega City* and opened the homonymous exhibition, to promote garden city solutions as a strategy to combat climate change issues in mega cities (WOHA, 2018).

4.1.7 Vertical forests

In this research a vertical forest is defined as a building that features balconies with built-in tree planters containing full-sized trees of at least three meters height along the majority of the façade area.

The MVRDV pavilion at the Expo 2000 in Hannover could be considered a predecessor of the vertical forest concept. It explored the possibility of incorporating trees and nature into architecture. The theme of the World Fair was "man, nature and technology" and MVRDV interpreted this in an open-air building with a distinct ecosystem on six separate levels. It showcased how the densely populated country of the Netherlands might have to create space in the future by expanding in the vertical direction. The pavilion shows the make-ability of nature through a multi-level park featuring dunes, agriculture, a forest with full-sized trees and a rooftop lake (MVDRV, 2018).

In 2014 Stefano Boeri Architetti brought the term 'vertical forest' under the attention of a worldwide audience with their project Bosco Verticale. The project continued the exploration

Figure 16: Vertical cross section and typical floorplan of Bosco Verticale (Giacomello & Valagussa, 2015)

of vertical densification of nature in two residential towers of respectively 116 and 85 meters in height. The buildings incorporate over 700 trees and 5.000 bushes along their facades (Figure 16), featuring full-sized trees of up to 6 meters in height on the balconies. Bosco Verticale was part of an urban redevelopment program in the heavily polluted neighborhood Porta Nuova in Milan. The trees were not only placed to provide a new ecosystem in the city, but also to improve the quality of the environment and microclimate. The trees were expected to absorb dust, reduce pollution, sequester carbon, mitigate air temperature and increase air humidity (Giacomello, 2015).

Figure 17: Rendering of Liuzhou Forest City (Stefano Boeri Architetti, 2018)

The realization of Bosco Verticale was specifically challenging from a structural design point of view. To determine the structural loads a 1:100 scale-model with pressure sensors was subjected to a wind-tunnel tests to determine wind forces, moments and aerodynamic coefficients. Also full-scale trees were subjected to a wind tunnel test at the maximum wind speed of 67 m/s to determine the aerodynamic coefficients more accurately (Mousaad, et al., 2013).

Since the completion of Bosco Verticale, Stefano Boeri Architetti has been commissioned for several international vertical forest projects. In Nanjing and Lausanne vertical forests are currently in construction. In the Netherlands, Wonderwoods is planned to be constructed in Utrecht and Trudo Vertical Forest will be the first social housing vertical forest and located in Eindhoven. Both of these projects are still in the design phase (Stefano Boeri Architetti, 2018). Also MVRDV's Winy Maas recently applied green balconies in The Valley, which is currently under construction in Amsterdam (MVRDV, 2018).

In the south of China urban development plans aim to take the vertical forest concept to the next level. Stefano Boeri Architetti has been commissioned to design Liuzhou Forest City in the north of Liuzhou. The green city will host 30.000 people and 40.000 trees, in an area that covers 175 hectare along the Liujiang river (Figure 17). In 2017 the masterplan was approved by the municipality, works are planned to start in 2020 (Stefano Boeri Architetti, 2018). In Malaysia near the border of Singapore another mega-project is currently under construction. Forest City Johor will span ten square kilometers and includes 250.000 residential units. The design by Sasaki Associates features vertical greenery, sky gardens and rooftop gardens to generate a forest-like environment. The first phase is currently for sale and the total project is set to be completed in 2040 (Country Garden, 2018).

4.2 Building integrated vegetation typologies

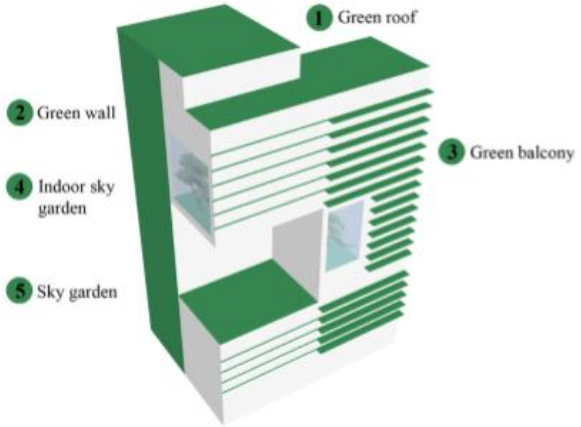

Figure 18: Building integrated vegetation typologies (Raji, et al., 2015)

The term building integrated vegetation can also be referred to as building greening systems. The

five most common building integrated vegetation typologies are shown in Figure 18 (Raji, et al., 2015). In this paragraph the green roof, green wall, indoor sky garden, sky garden and green balcony systems will be described.

4.2.1 Green roof

The most widely applied greening system is the green roof. A green roof is a roof with a vegetated surface and substrate layer (Oberndorfer, et al., 2007). Roofs can represent up to 32% of horizontal surfaces in the built environment (Fraser, 2005). So especially in urban areas with limited availability of space, rooftops can provide a large surface area for possible integration of greenery. The main functions of a traditional rooftop are to act as the thermal shell of the building and as a barrier to rainwater, but a green rooftop can also provide additional benefits.

In urban areas rainwater run-off can pose a serious issue due to the high amount of impervious surfaces. The water-retaining capacity of the green roof substrate can play an important role in storm water management (Mentens, et al., 2006). Green roofs also impact the micro climate of cities, which in turn impacts the macro climate. The vegetation and substrate layer protects the roof from incoming solar radiation and vegetation has a higher albedo than common black roofing materials. Therefore a green roof can mitigate the urban heat island effect (Dwivedi & Mohan, 2018). An additional benefit is that green roofs can reduce the summer cooling load. A study on an eight-story building in Madrid showed that the installation of a green roof reduced summer cooling load with 6% and reductions in peak hour cooling load in the upper floors could reach 25% (Saiz, et al., 2006). Similar energy consumption reductions could be achieved with a white roof and additional insulation, but green roofs also provide aesthetics, purify air, absorb sound pollution and protect biodiversity (Oberndorfer, et al., 2007).

A distinction is made between intensive and extensive green roofs. An intensive roof can be characterized with a deep stratum layer and includes a wide variety of plant species. An extensive green roof has a thin soil layer, vegetation usually includes herbs, grasses and mosses and it requires relatively little maintenance (Spala, et al., 2008). Green roofs can be applied as an integrated system, modular system or pre-cultivated vegetation blanket that is rolled onto an existing rooftop (Banting, et al., 2005). Green roof technology usually does not only include the vegetation layer and substrate, but also a drainage layer, root barrier and waterproofing (Figure 19). Plant selection is a critical factor in determining the success of the green roof, since not all plants can survive the harsh living conditions with strong wind and intensive solar radiation that are inherent to a rooftop environment. Extensive green rooftops are typically planted with sedums, which are drought tolerant species that perform well in a shallow substrate layer. Intensive green roofs can include a wider variety of plants due to the thick substrate layer. Intensive green roofs can be named roof gardens when they include shrubs, trees and recreational space (Afrin, 2009).

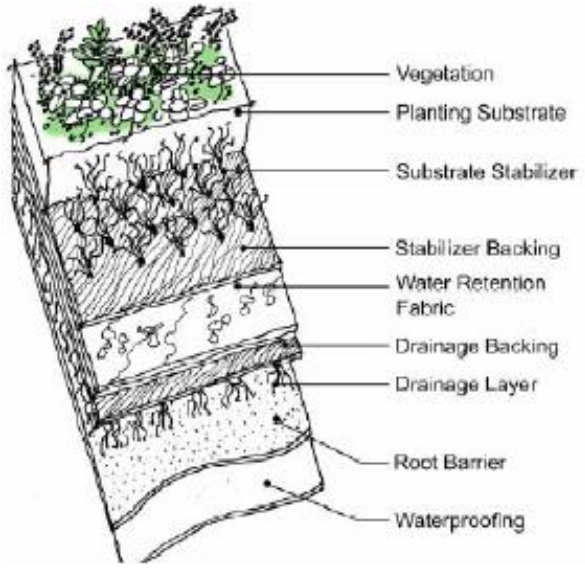

Figure 19: XeroFlor green roof system (Banting, et al., 2005)

4.2.2 Green wall

A green wall has controlled growth of vegetation integrated into the vertical surface of the building. Greenery in the vertical direction is sometimes referred to with the term ‘vertical garden’. A green wall could be placed inside or outside the building. Typically green wall systems include an

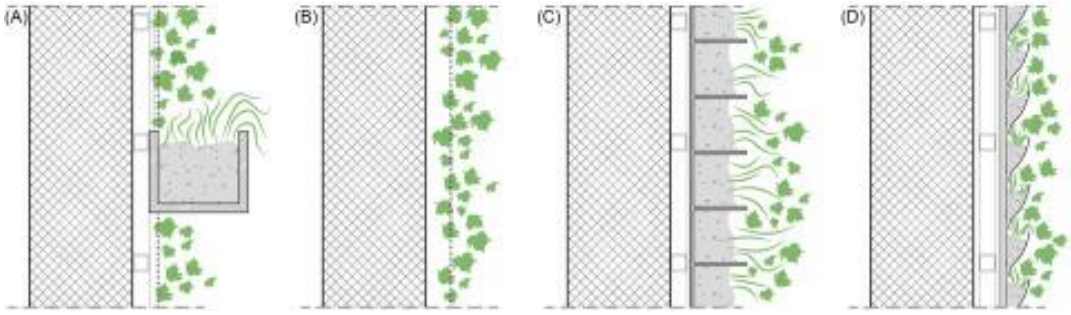

Figure 20: (A) Green facade with planter boxes, (B) Green facade direct greening, (C) Living wall soil cell system, (D) Living wall hydroponic system (Fernández-Cañero, et al., 2018)

irrigation system for easy maintenance. Two main categories of vertical greening systems can be distinguished according to the growing method: green façades and living walls (Köhler, 2008). Green facades are mostly made of climbing and hanging plants (e.g. Hedera Helix) that attach to a support structure. The green façade could directly adhere to the building exterior or grow on a secondary support structure such as stainless steel cables or modular trellises. The plants are typically rooted at the base of the structure or in planter boxes (Hondel & Alibaba, 2016).

Living wall systems are more intensive and can support a wider range of species: epiphytic plants, lithophilic plants, bromeliads, ferns, succulents and herbaceous plants (Fernández-Cañero, et al., 2018). The two main types of living walls are soil-cell systems and hydroponic systems. Soil-cell systems have several soil compartments grouped on a panel which can be attached to a supporting frame. This modular potted system is typically heavier than a hydroponic system, but can support a wider variety of species. Hydroponic systems use a mat of felt-like material as the growing medium and are continuously hydrated with nutrient-enriched water (Riley, 2017). An overview of green wall typologies is given in Figure 20. It is also possible to apply these vertical greening systems in the cavity of a double skin façade, which provides protection to vegetation from external climate factors such as direct solar radiation and strong winds. In this configuration the plants can directly influence the indoor building environment (Stec, 2006).

The environmental benefits related to a green wall can act on the urban scale, building scale and microclimate scale. The benefits of a green wall on the building scale are mainly related to lowering the energy demand for cooling and the improvement of insulative properties (Perini & Magliocco, 2012). The cooling effect of vegetation is twofold: the leaves provide shading and stomata show evapotranspiration. In addition, dense foliage will decrease the wind flow around the building creating a layer of stagnant air that adds an extra insulating layer in front of the building envelope. Since wind can decrease the energy efficiency of a building by 50% wind reduction could positively influence building energy performance (Ottelé, 2011).

Measurements comparing a vegetated and bare section on the same façade in a Mediterranean climate showed that the surface temperature could be up to 10,8 °C lower behind a green wall (Eumorfopoulou & Kontoleon, 2009). Aside from the impact on heat transfer, green walls also have an aesthetic function, increase biodiversity and can slow down deterioration of building envelope materials by reducing the amount of UV light received (Giacomello & Valagussa, 2015).

4.2.3 Sky garden

The term sky garden has several meanings, but in this research it is defined as the green space on the rooftop or on intermediate floors of a high-rise building. When the garden is situated on an intermediate level it is also called a podium garden and on top of the building the term roof garden is often used (Tian & Jim, 2012). A podium garden usually encompasses several levels of the

building. The effects of a sky garden are similar to that of other building greening systems, but due to more extensive planting of vegetation the effects are also noticeable on a larger scale. The vegetation in the sky garden can provide shading, improve air quality, reduce noise pollution and store rain water (Ong, 2003).

Even though the benefits of a sky garden show similarities with green roofs and green walls, a sky garden is usually constructed with a different purpose. Sky gardens are designed for active usage as a recreational place and to promote social interaction (Samant & Hsi-En, 2017). In comparison to an intensive green roof, the water bearing capacity of a sky garden is more significant due to the greater substrate layer depth. Recently the interest in rain water harvesting systems has increased and rooftop sky gardens can serve as a catchment area for rain water collection as well as a storm water management system (Mun, et al., 2012).

4.2.4 Indoor sky garden

An indoor sky garden can also be called a winter garden or green atrium. In comparison to an outdoor sky garden it has the advantage of providing a comfortable environment independent of the outdoor climatic conditions. But the function is often similar to that of the outdoor sky garden and is focused on recreation and social interaction.

Placing greenery inside the building has the advantage of directly influencing the indoor environmental quality. On average people spend 88% of their time indoors (Robinson & Nelson, 1995), so if indoor air quality is poor this could be detrimental to health. Symptoms caused by indoor air pollutants are referred to as 'sick building syndrome'. Airborne pollutants can not only affect health, but also indoor comfort and worker performance in offices (Wolkoff, 2013).

Research on vegetated atria shows that the vegetation in an office environment could lead to an improvement of worker productivity by 10-15% and also positively impacts occupant thermal comfort (Mangone, 2015). Indoor vegetation is often mentioned as a passive measure to reduce pollutants. However, the results of air quality improvement found in literature are typically small but still significant (Abbass, et al., 2017).

4.2.5 Green balcony

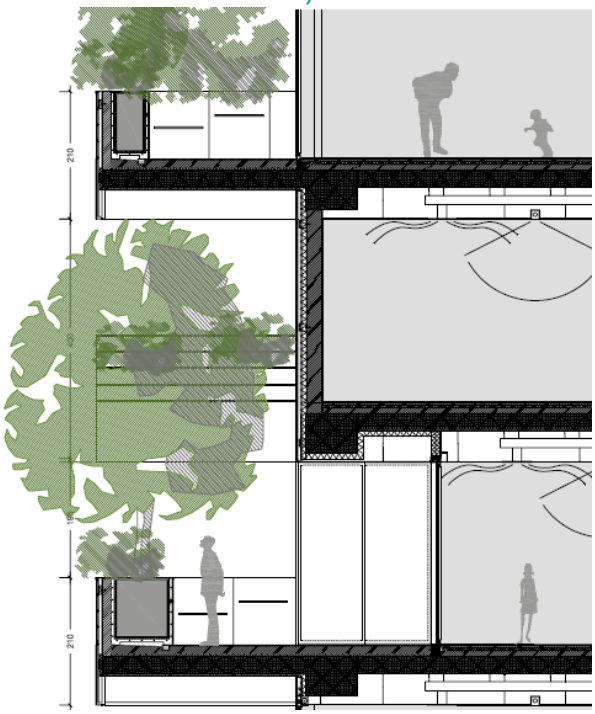

Figure 21: Vertical cross section of green balcony Bosco Verticale (Stefano Boeri Architetti, 2018)

A balcony is defined as a platform that projects from the wall of a building and is enclosed by a parapet or railing (Merriam-Webster, 2018). The term terrace is sometimes used to refer to a balcony, but the term is rather ambiguous since it could also refer to a flat roof or paved area on the ground level. When the term green balcony or balcony garden is used in scientific literature, it usually refers to the placement of a greening module or potted plants on a balcony. Because these type of plants are limited in size, the effects on the microclimate are also limited.

The effects of small-scale balcony greening of approximately 4 meters in length were studied in Panzihua City, China for a balcony with an adjacent semi-open living room. In comparison to a regular balcony, the indoor relative humidity increased with 0,1-3,5% and temperature decreased with 0,1-1,0 °C by adding the plants. On average the relative humidity was 1-2% higher

and the ambient temperature 0,4 °C lower. The indoor formaldehyde concentration decreased by 0,026 mg/m^3 (Sun, et al., 2015).

Use of geopolymers for pre-cultivation of trees within a limited space and development of post-tensioned reinforced concrete have made it possible to not only include smaller plants, but also full-sized trees on balconies. In this research, the term green balcony is used to refer to balconies with trees planted on them (Figure 21). A green balcony is defined as a balcony with a built-in container that features a substrate layer and one or more full-sized trees.

Bosco Verticale in Milan has green balconies along all building façades. The balconies are cantilevered 3,3 meters from the building façade and have to support trees ranging from 3 to 9 meters in height. The trees were pre-cultivated and then hoisted onto the construction with a crane. The trees are planted in substrate containers of 1,1 meters in depth and width. To minimize construction costs it was crucial to accurately determine the dynamic loads on the building. For this purpose 1:100 scale building models with pressure sensors were tested with the surrounding urban area in a wind tunnel. Additionally, wind tunnel tests were performed on four full-sized trees for wind speeds up to 53 m/s (Mousaad, et al., 2013).

For safety reasons and to ensure upright tree growth, each tree is fixed with three elastic binds

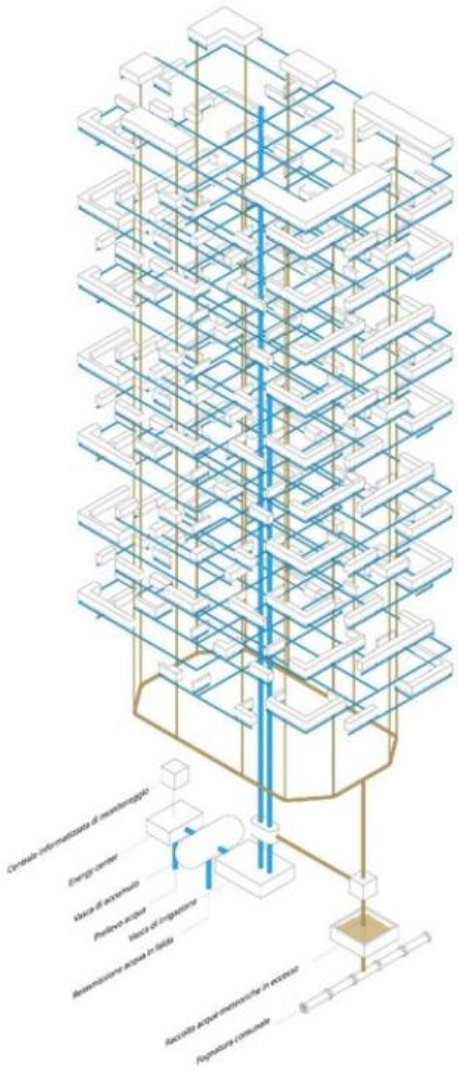

Figure 22: Bosco Verticale irrigation system (Stefano Boeri Architetti, 2018)

Figure 23: Pre-cultivated tree being hoisted in place (Giacomello & Valagussa, 2015); elastic binds on tree connected to steel support cable (Giacomello, 2015); external pruning of green balconies by alpinist (Barber & Putalik, 2018)

to a steel cable that is anchored to the balcony above. The plant containers are also designed with extra safety measures. First the container is lined with bituminous waterproofing materials, then a protective sheeting is placed to prevent root penetration. On top of that is the drainage layer, made of two synthetic filters which support the outflow of water. An additional welded steel net anchors the roots of the trees in place. Finally, the container is filled with the substrate which mainly consists of volcanic lapilli (Giacomello, 2015).

The CTBUH Vertical Greenery publication by Giacomello & Valagussa (2015) elaborately described the technology and maintenance at Bosco Verticale. The maintenance of the green balconies is done by the building management, so residents are not allowed to make alterations to the greenery. The green balconies are maintained by building management in two ways. Firstly, the terraces are accessed via the apartments six times a year for control and diagnostics. During the visits in winter, spring and at the end of summer internal pruning will be done. Secondly, there is a basket lift attached to a telescoping arm on the rooftop of the building which allows external pruning and façade cleaning to be performed one time a year in winter (Figure 23). The pruning of the trees is of great importance because the trees are dimensionally constrained and there are great consequences if branches were to break and fall off from the top of the building.

Aside from pruning, the trees also require watering and fertilization which is provided through an irrigation system (Figure 22). The irrigation system uses groundwater and contains 280 valves that are electronically operated. Each plant container has a control group that consists of a solenoid valve, filtration unit and pressure regulator which allows for different irrigation flows for every container. A drip system further transports irrigation along the surface of the planter substrate. Each planter also features two humidity sensors to ensure the efficient distribution of water (Giacomello & Valagussa, 2015).

Giacemello and Valagussa also studied the health of the trees right after placement in the balcony containers, but no significant tree health implications were found at the time. Simulations of the building in EnergyPlus by Giacomello showed that balconies impact the building cooling load more significantly than the addition of trees. Both configurations with and without trees decrease the yearly electricity consumption for cooling and heating with 7,5%. Additionally, the effect of tree shading increases the heating demand in winter with 37,3% and decreases the summer cooling needs by 68% when compared to a configuration without trees, see Table 1. The influence of the terraces and trees on the yearly energy consumption was also considered by modelling the electric energy consumed by the heat pumps and chillers. The Coefficient of Performance (COP) of the heat pump was chosen as 2,5 and the Seasonal Energy Efficiency Rating (SEER) of the chiller as 3,5, leading to the yearly electricity consumption as in Table 1.

Table 1: Simulated yearly energy consumption Bosco Verticale (Giacomello & Valagussa, 2015)

Variant	Winter heating demand	Summer cooling demand	Electricity consumption heat/cool
	23,2 kWh/m²/y **+37,3%**	7,0 kWh/m²/y **-68%**	12,7 kWh/m²/y
	18,6 kWh/m²/y **+10,6%**	11,8 kWh/m²/y **-42,2%**	12,7 kWh/m²/y
	16,9 kWh/m²/y **100%**	22,0 kWh/m²/y **100%**	13,7 kWh/m²/y

It must be noted that this research was conducted during the construction of Bosco Verticale in 2013 and 2014. The results from energy simulations were not validated. No research has been done on the actual energy consumption of the building now it has been in use for several years.

4.3 Trees near the building envelope

In the previous paragraphs the history and typologies of building integrated vegetation were described. This was done because there is limited research on green balconies, but there is a

substantial amount about other forms of building integrated vegetation. Also a noteworthy amount of research was done on the effects of trees near the building envelope. Most efforts were geared towards the energy reduction potential of trees near the building envelope. Three relevant studies found on this topic will be discussed in this paragraph.

4.3.1 Effect of tree shading and transpiration on building cooling energy use

Hsieh, Li, Zhang and Schwegler (2018) did research on the cooling effect of trees around buildings and the influence of tree characteristics by doing urban microclimate field measurements and measurements of the sap flow rate of trees in subtropical Nanjing City in China. Four scenarios of trees near the building envelope were developed on a typical summer day to evaluate the different effects. The main factors considered were shading and transpiration. Climatic measurements were done on one building without trees and one building with trees. The maximum transpiration rate from the tree sap flow meter was found in the period from 10:00 to 14:00. The climatic measurements were used as input for the energy simulations in EnergyPlus. In comparison to the scenario without trees, the building showed a 10,3% decrease in cooling load due to tree shading and transpiration (Hsieh, et al., 2018).

4.3.2 Effect of tree shading on solar irradiance and building surface temperature

Berry et al. (2013) measured and modelled the effect of tree shading on a building wall for a potted Fraxinus tree of 2,9 meter and an Angophora tree of 3,8 meter of height at a distance of 1,1-2,1 meter from the building envelope. The study was conducted in summer in Melbourne, which is characterized by an oceanic climate. Using an infra-red temperature sensor, wall surface temperature was determined and solar irradiance on the wall was measured simultaneously with wall-mounted pyranometers. Tree shade coverage turned out to be the best predictor of wall surface temperatures, addition of ambient air temperature, relative humidity and wind speed as variables in the model did not lead to a better prediction. Small trees and trees further away from the building did little to reduce the temperature. But trees with a dense canopy close to the building reduced the wall surface temperatures by up to 9 °C. Also the air temperature between the tree and the building reduced by up to 1 °C (Berry, et al., 2013).

4.3.3 Optimal tree position around a building to reduce cooling energy consumption

Calcerano and Martinelli (2016) made a model to optimize the energy consumption reduction potential of a typical energy consuming stand-alone building in Italy. They considered several possible tree locations around the building as depicted in Figure 24. To reduce run time trees at the north location were not considered since this is known by experts to have the least beneficial shading effect.

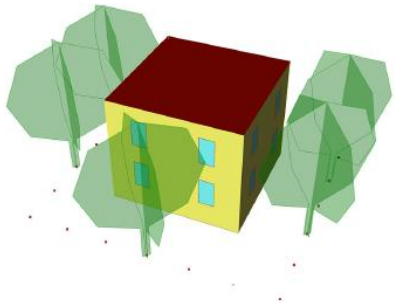

Figure 24: Possible positions of trees around typical Italian building (Calcerano & Martinelli, 2016)

Ladybug was used to compute the sunshine duration in the urban environment and Honeybee to evaluate the indoor mean radiant temperature based on the EnergyPlus simulation results. Evapotranspiration or wind effects were not included in the model. An optimal configuration was calculated using Galapagos for the Energy Reduction Potential for five possible scenario's ranging from one to five shading trees. This was done for both a single level and double level building. According to the simulations the positioning of the trees on the east and west side of the building obstruct solar radiation in summer without reducing desirable solar gains in winter

like a southern orientation. A reduction in solar gain of 50-70% could be achieved and especially solar radiation obstruction on the roof was effective. The energy consumption reduction by trees decreases as the amount of trees is increased as a result of overlapping shade. Therefore the placement of only two trees can already lead to a significant overall energy consumption reduction of 20% (Calcerano & Martinelli, 2016).

4.4 Conclusion: potential benefits of green balconies

In this chapter a literature study was performed on the history and applications of building integrated vegetation. Finally the effect of trees near the building envelope was considered. The amount of research found on green balconies was limited, but a considerable amount of research has been done on other types of building greening systems such as green roofs and green facades. Green balcony vegetation has a larger distance from the building envelope than the vegetation of green roofs and green facades. So the effects of the vegetation on the building such as insulation, shading and façade protection are expected to be less direct for green balconies. However, trees generally have a wider leaf area density profile. A higher leaf area density could be beneficial to both the heating and cooling performance of a building (Poddar, et al., 2017). Potential benefits that have a correlation with the leaf area such as evapotranspiration and air pollutant removal could therefore be more significant for a full-sized tree when compared to an extensive green roof or wall.

Taking these differences into account and considering the research done by others on trees near the building envelope, the literature study in this chapter can be summarized by providing an overview of the potential benefits of green balconies. This is graphically displayed in Figure 25. Effects are not quantified, since the size of the effect depends greatly on the microclimate and tree properties. But in general green balconies could provide cooling, reduce wind velocities, improve air quality, enhance human well-being, increase urban biodiversity and reduce noise.

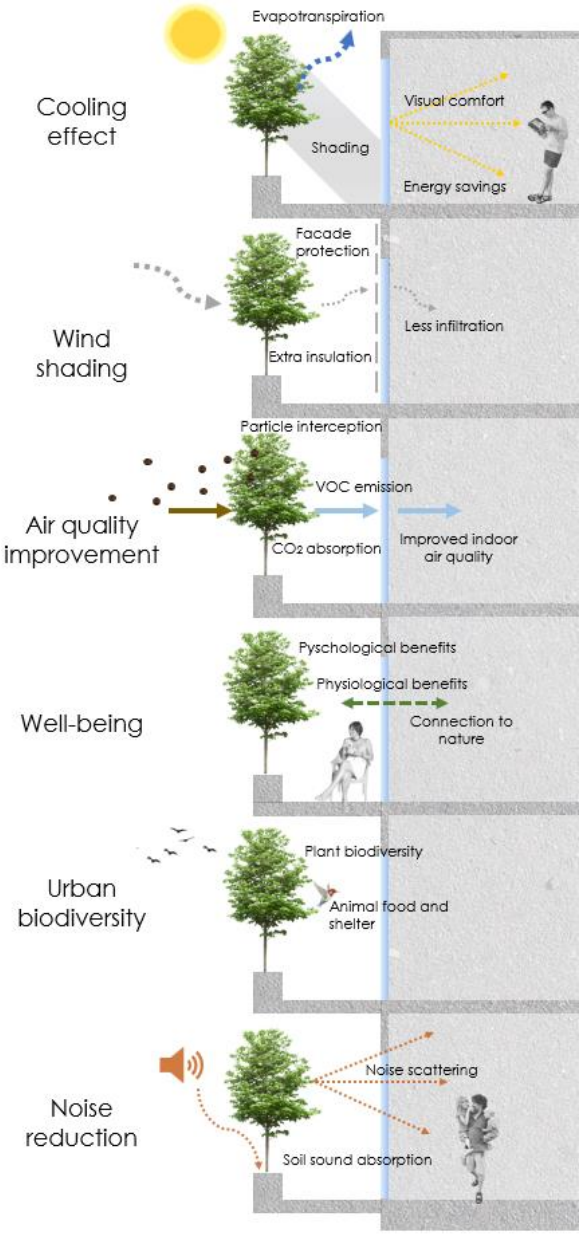

Figure 25: Potential benefits of green balconies (illustration by author)

It must be noted that some of these potential benefits could also have a negative impact. For example an increase in relative humidity could negatively influence thermal comfort in a wet climate. The shading effect of trees could be a disadvantage in winter. Also the increase in urban biodiversity might lead to nuisance by birds and insects for the residents.

Even though there are several potential benefits of green balconies as Figure 25 illustrates, this research focuses on the cooling effect and wind shading by trees. In the next chapter these potential benefits will be described into more detail as the heat and moisture transfer of trees is evaluated.

5 Heat and Moisture Transfer of Trees

Heat and moisture transfer between trees and their environment could provide environment-friendly benefits at both the building and urban scale (Poddar, et al., 2017). In heat and moisture transfer of trees several different fluxes of energy are of importance. According to the conservation of energy, the equation of the energy balance of a tree may be written as (Villalobos, et al., 2016):

$$R_n - G - LH - SH = 0 \qquad (5.1)$$

Where R_n is the net radiation (W/m^2), *LH* is the latent heat flux (W/m^2), S*H* is the sensible heat flux (W/m^2) and *G* is the soil heat flux (W/m^2). As can be seen in Figure 26, the dominant form of energy transfer in a humid environment is determined by latent heat transfer, followed by sensible heat transfer and finally heat absorbed by the ground (Stec, 2006). Since the impact of the soil heat flux is limited it will not be considered in this research. Especially on green balconies where trees are grown in dimensionally constrained containers, the ground heat transfer area and therefore effect is expected to be minimal. Also, the energy consumed by photosynthesis and stored in the plant biomass are not part of the energy balance equation since these are negligible compared to other factors.

In paragraph 5.1 sensible heat transfer of trees will be treated. In paragraph 5.2 latent heat transfer will be considered. Finally, in paragraph 5.3 wind flow will be considered, since this also plays an important role in heat and moisture transfer of trees to their environment.

5.1 Sensible heat transfer

Sensible heat transfer describes a different type of energy transport than latent heat transfer, since the first directly influences the air temperature whereas the second involves a phase change such as water vaporization. According to de Wit (2008), in general for sensible heat transfer (J):

$$Q_{sensible} = mc\Delta T \qquad (5.2)$$

With *m* the body mass, *c* the specific heat capacity and *ΔT* the change in temperature. Sensible heat flux encompasses radiation, conduction and convection. Convection will be treated in paragraph 5.3 since this is related to wind flow.

5.1.1 Incoming solar radiation

The solar radiation reaching the earth at the top of the atmosphere is on average is 1370 W/m^2. This value is also known as the solar constant (Duffie & Beckman, 2013). But not all this solar radiation reaches the earth surface as part of it is absorbed into the atmosphere and part of it is reflected back into space. The fraction of the solar constant reaching a surface on earth is also dependent on the angle of incidence of the solar beam. According to Lambert's cosine law the angle of incidence of a ray of light is related to the irradiance of the surface (*I*) according to:

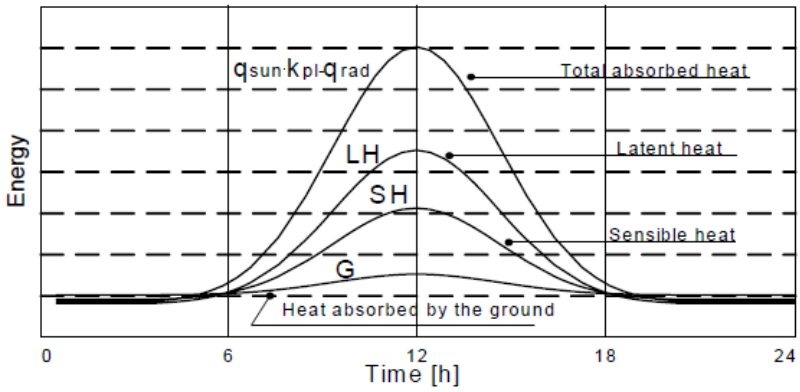

Figure 26: Energy arriving/leaving the surface of a plant over time (Stec, 2006)

$$I = I_p \cos\theta \qquad (5.3)$$

Where θ is the zenith angle (the angle between the radiant beam and the vertical).

To describe the geometric relationship between a plane relative to the earth at any time and the incoming solar beam radiation, the position of the sun can be described in terms of several angles as illustrated in Figure 27 . The zenith angle (ϑ_z) is the angle between the vertical and the line to the sun, the solar altitude angle (α_s) is the angle between the horizontal and the line to the sun complementary to the zenith angle and the solar azimuth angle (γ_s) is the displacement from the south of the projection of the beam on the horizontal plane with the east displacements negative and west displacements positive. When the azimuth angle is given in only positive degrees in the range from 0 to 360°, it represents the displacement from the north.

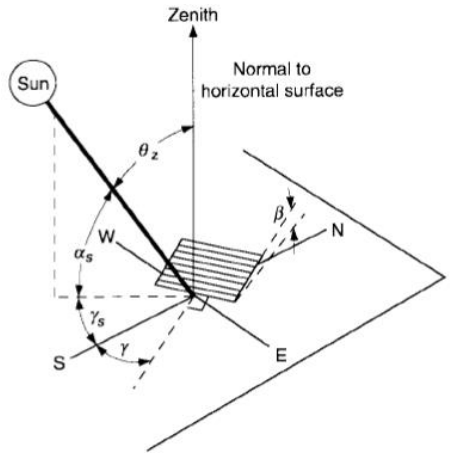

Figure 27: Zenith angle (θ_z), solar altitude angle (α_s) and solar azimuth angle (γ_s) (Duffie & Beckman, 2013)

Solar radiation reaching the surface of the earth reaches a maximum of around 75% the solar constant, due to absorption and scattering of the radiation in the atmosphere. The beam radiation coming directly from the sun is called direct solar radiation and the remaining part is diffuse solar radiation that reaches the surface from the entire sky due to scattering. The sum of direct and diffuse solar radiation on a horizontal surface is called global radiation.

5.1.2 Solar radiation on a leaf

Figure 28 shows what happens to the incoming solar radiation at a leaf (Kong, et al., 2017) . Incoming solar radiation consists of two parts: short-wave radiation (in the visible spectrum) and long-wave radiation (in the infrared spectrum). The amount of radiation that is reflected depends on the albedo of the leaf. Light colored leaves will have a higher albedo than darker leaves. Around 10% of the visible light is reflected by the corolla structure of the tree and about 50% of the infrared radiation is reflected. Leaves of plants can also transmit light. Around 10% of visible light is transmitted and 30% of infrared. Finally, part of the solar radiation is absorbed. Around 80% of visible light is absorbed and around 20% of the infrared.

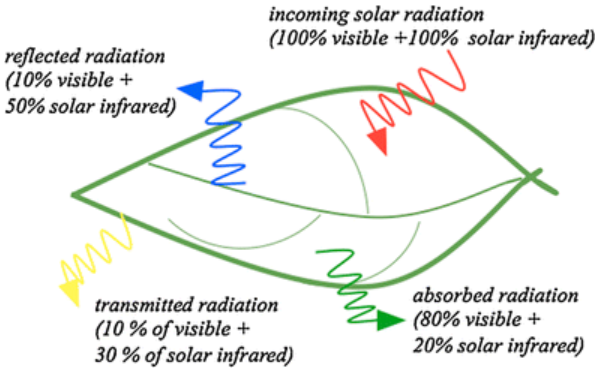

Figure 28: Incoming solar radiation on a leaf (Kong, et al., 2017)

The solar radiation that is transmitted through the canopy of a plant is dependent on the Leaf Area Index (LAI). The LAI is the ratio between the total green leaf surface area on one side per unit ground surface area (m^2/m^2). Since the repeated interception of light by leaves leads to a reduced brightness of light, the light that reaches the soil beneath the leaf canopy can be calculated according to Beert-Lambert's law of light extinction (Monsi & Saeki, 1953):

$$I = I_0\, e^{-k\,LAI} \qquad (5.4)$$

Where I_o and I are the flux densities above and below the tree canopy and k is the extinction coefficient. There is a linear relationship between the logarithm of the light intensity as a percentage of the incoming light and the leaf area index as a denser leaf area will lead to faster light

extinction. In the study by Monsi & Saeki extinction coefficients between 0,7-1,5 were found for broad-leafed plants. The extinction coefficient depends both on leaf size and the angle of the leaves. As is visible in Figure 29, the extinction coefficient decreases as the angle of inclination of the leaf increases.

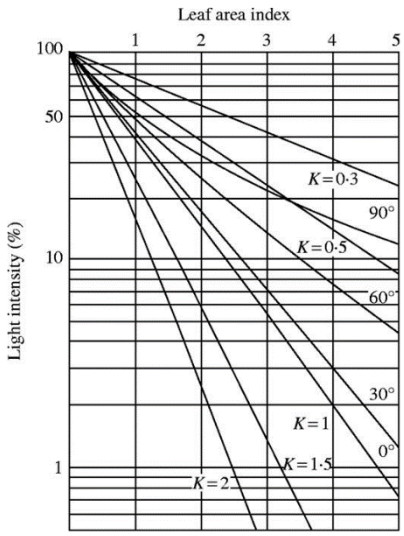

Figure 29: Light intensity percentage of above canopy, leaf angles and extinction coefficient (K) (Monsi & Saeki, 1953)

5.2 Latent heat transfer

Latent heat transfer is the release or absorption of energy during a constant temperature process. This process is associated with the evaporation and transpiration of water. According to de Wit (2008) in general specific latent heat (kJ) can be determined by:

$$Q_{latent} = mL \qquad (5.5)$$

Where *m* is the mass of the substance (kg) and *L* is the specific latent heat for the substance (kJ/kg).

Latent heat transfer between trees and their environment happens through a process called evapotranspiration. Evapotranspiration is the combination of evaporation from water from the soil surface and transpiration of water from the plant. The mechanisms of evapotranspiration will be explained in this paragraph.

5.2.1 Air temperature and humidity

The air temperature and humidity are key factors in determining the rate of evapotranspiration. Some basic principles of air temperature and humidity will be described according to the Wit 2008).

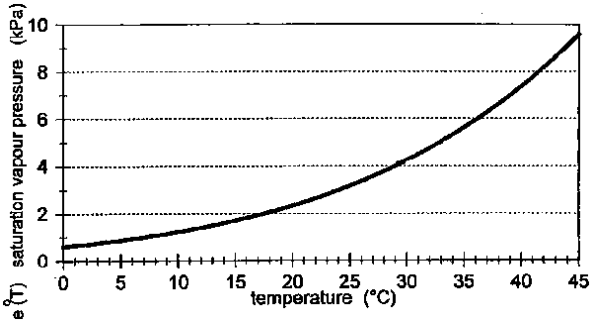

Figure 30: Saturation vapour pressure curve (Allen, et al., 1998)

The saturation vapor pressure e_s (kPa) is the pressure at which the air is saturated and depends on the air temperature. The relation as depicted in Figure 30 is:

$$e_s = 0{,}61078e^{\left(\frac{17{,}27T}{237{,}3+T}\right)} \qquad (5.6)$$

With temperature *T* in °C. But usually the air is not fully saturated, with the relative humidity (%) indicating the degree of saturation as:

$$RH = 100\frac{e_a}{e_s} \qquad (5.7)$$

With e_a the partial vapor pressure (kPa). But another way to express the humidity of air is the vapor pressure deficit (VPD) which is the difference between e_s-e_a which gives an indication of the drying power of the atmosphere which is an important factor in determining the rate of evaporation and transpiration. A third way to express the humidity of air is with the dew point temperature (T_d) which is the temperature required for a parcel of air at constant pressure and constant water vapor content to reach saturation. Below the dew point temperature condensation will occur. The drier the air, the larger the difference between the air temperature and dew point temperature.

There is also a ratio to how much water vapor is available per unit dry air and this mixing ratio (g/kg) can be calculated according to:

$$X_v = 622 \frac{e_a}{P_{at} - e_a} \qquad (5.8)$$

With P_{at} is the atmospheric pressure (kPa). Finally, the humidity can also be expressed as absolute humidity which is the mass of water vapor per volume air (g/m^3):

$$\rho_v = \frac{1000 e_a}{0{,}4615 T} \qquad (5.9)$$

With T is the air temperature (K).

5.2.2 Evaporation

Firstly, evaporation is the process in which liquid water is converted to water vapor and removed from the evaporating surface. Changing water from liquid to vapor requires 2,45 MJ/kg (Monteith & Unsworth, 1990). Water evaporates from various surfaces such as lakes, rivers and wet vegetation. Energy is required to change the state of water molecules form liquid to vapor. Direct solar radiation and to a limited extent ambient temperature provide this energy. The driving force in evaporation is the difference in water vapor pressure between the atmosphere and the evaporating surface. The replacement of saturated air with drier air is greatly dependent upon wind speed. So important factors in determining the evaporation are the climate factors solar radiation, air temperature, air humidity and wind speed (Allen, et al., 1998).

5.2.3 Transpiration

Transpiration is the vaporization of liquid water from plant tissues and the movement of vapor to the atmosphere. Transpiration occurs mainly through the stomata of plants. These can be compared to the pores of the human skin, as a stoma is a small opening through which vapor and gas exchange between the plant and its surroundings can take place. The pore is bordered by guard cells that are responsible for regulating the opening and closing of the stoma (Figure 31). The response of the guard cells depends on the plant environmental conditions such as light intensity, humidity and carbon dioxide concentration (Allen, et al., 1998).

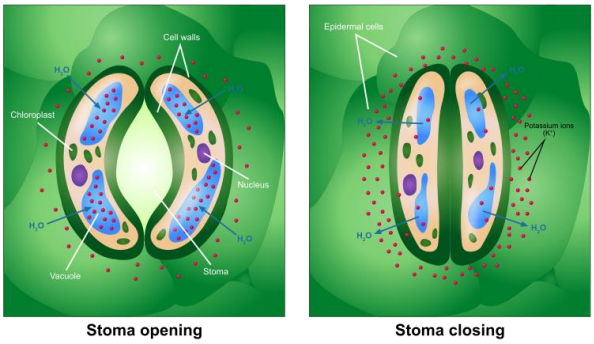

Figure 31: Opening and closing of a stoma (Reece & Wasserman, 2016)

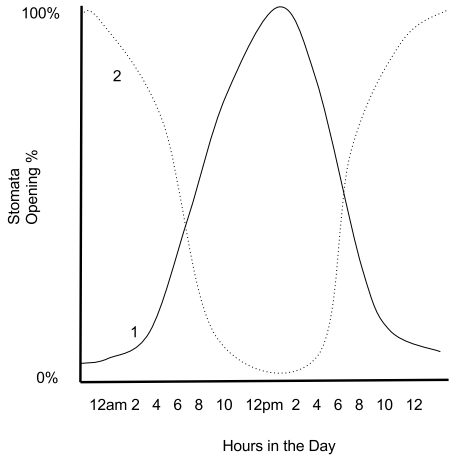

Figure 32: Percentage stomata opening throughout the day for CAM plants (1) and C3 and C4 plants (2)

Plants can be categorized according to their carbon concentrating mechanisms. Based on carbon fixation there are three categories of plants: CAM plants, C_4 plants and C_3 plants. CAM plants are mostly desert plants and typically open their stomata at night when water evaporates more slowly. C_3 and C_4 plants open their stomata during daytime in response to climatic conditions, see Figure 32. The large majority of plants is of the type C_3 which has the highest carbon dioxide compensation. The opening of the stomata for carbon dioxide exchange as part of photosynthesis will also release water vapor from the air spaces in the leaf. Therefore, carbon dioxide fixation will occur simultaneously with the loss of water vapor (Zeiger, et al., 1987).

5.2.4 Evapotranspiration

Evapotranspiration (*ET*) is the sum of evaporation from the soil surface (E_s) plant transpiration (E_p) and evaporation from plant surfaces (E_{ps}). If the leaf canopy is dry there will be no evaporation from the plant surface and it can be assumed (Allen, et al., 1998):

$$ET = E_s + E_p \qquad (5.10)$$

Since evaporation and transpiration occur simultaneously it is difficult to make a distinction between the two. When a plant is small, water is predominantly lost by soil evaporation, whereas larger plants have more shade across the soil and a larger leaf area so therefore water loss through transpiration becomes dominant. Maximum transpiration will occur when sufficient soil water is available to not limit the root water uptake.

The rate of evapotranspiration mainly depends on radiation, vapor pressure, temperature and wind speed. It will also depend on the vegetation properties such as crown area, leaf area index, height of the leaves, stomatal conductance and hydraulic resistance at the shoot and root. Finally, the rate of evapotranspiration also depends on the soil properties such as dryness, compaction and hydraulic conductivity (Gkatsopoulosa, 2017).

5.2.5 Penman-Monteith equation

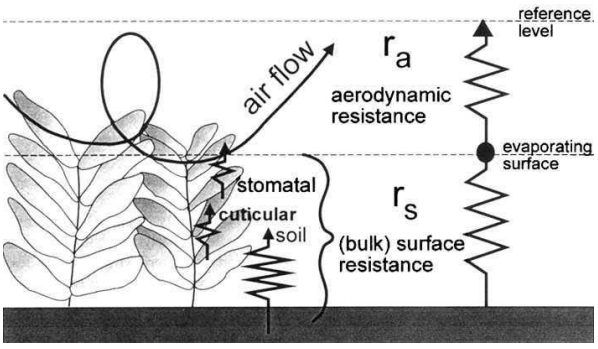

Figure 33: Aerodynamic resistance and bulk surface resistance of plants (Allen, et al., 1998)

The first equation to calculate evaporation was proposed by Penman in 1948 combining latent and sensible heat fluxes. Monteith first introduced the concept of surface resistance integrated into this evaporation equation. The resistance element is key to distinguish evapotranspiration from regular evaporation. The surface resistance r_s describes the bulk surface resistance of vegetation upwards which is a combination of the soil, stomatal and cuticle resistance of the plant. This resistance is in series with the aerodynamic resistance r_a. Both resistances are depicted in Figure 33.

The Penman-Monteith equation is dependent on both the surface and aerodynamic resistances and consists of a latent heat flux and sensible heat flux part (Monteith, 1965). For the latent heat flux *LH* of evapotranspiration:

$$LH = \frac{\rho C_p}{\gamma} \frac{(e_{sc} - e_a)}{(r_s + r_a)} \qquad (5.11)$$

Where ρ is the density of air (g/m^3), C_p is the specific heat of air at constant pressure and γ is the psychrometric constant (±0,067 kPa/K), e_{sc} is the saturation vapor pressure at canopy temperature (kPa) and e_a is the vapor pressure (kPa), r_s is the surface resistance (s/m) and r_a is the aerodynamic resistance to water vapor flow. The positive flux moves from the plant to the air above. Typical values for r_s are 100-200 s/m for trees with a good water supply. In a water deficit situation this value could become much higher (Villalobos, et al., 2016).

The sensible heat flux component of the Penman-Monteith equation differs from latent heat flux in that it can be detected directly as a change in air temperature. The sensible heat transfer (*SH*) between the canopy and atmosphere can be calculated as (Monteith, 1965):

$$SH = \rho C_p \frac{T_c - T_a}{r_a} \qquad (5.12)$$

Where ρ is the density of air (g/m^3), C_p is the specific heat of air at constant pressure (J/g/K), T_c and T_a are the canopy and air temperature respectively (K) and r_a is the aerodynamic resistance for heat transport (s/m). Solving both equations for *LH* and taking into account the incoming solar radiation, this leads to the Penman-Monteith equation (Monteith, 1965):

$$LE = \frac{\Delta(R_n - G) + \rho C_p \frac{VPD}{r_a}}{\Delta + \gamma\left(1 + \frac{r_s}{r_a}\right)} \quad (5.13)$$

Where R_n is the net radiation, G the ground flux, the Vapor Pressure Deficit (*VPD*) which is an indication for the evaporative capacity of the air is calculated as e_s-e_a and Δ is the slope of the saturation vapor pressure curve (kPa/°C) calculated as follows:

$$\Delta = \frac{4098\left[0{,}6108exp\left(\frac{17{,}27T}{T+237{,}3}\right)\right]}{(T+237{,}3)^2} \quad (5.14)$$

Where T is the air temperature (°C).

The Penman-Monteith equation shows that tree evapotranspiration depends on both meteorological factors (solar radiation, temperature, humidity and wind speed) and plant factors (r_s). The aerodynamic resistance (r_a) depends on both the canopy characteristics (height, leaf area) as the meteorology (wind speed). One of the drawbacks of using the Penman-Monteith equation is that the canopy resistance in itself is also dependent on environmental factors such as temperature, radiation and the VPD. But for most species it is found that the canopy resistance is proportional to the VPD.

The Penman-Monteith equation clearly illustrates the concepts of evapotranspiration. For example when the VPD approaches zero as it would in extremely humid conditions and the canopy resistance is small, the evaporation will correspond to only radiation and temperature. The opposite case of a rough canopy in windy conditions such as an isolated tree with small leaves will depend mostly on the VPD and canopy resistance.

5.2.6 FAO Penman-Monteith equation

Especially in the agricultural sector it is of importance to accurately predict the rate of evapotranspiration for plants, since this makes it possible to accurately predict water use. Since the Penman-Monteith equation requires specific data for different plant types which are not easily measurable, the United Nations' Food and Agriculture Organization (FOA) proposed a simplified method to determine the evapotranspiration rate of a well-watered grass reference crop ET_0 (mm/day). This FOA Penman Monteith equation is as follows (Allen, et al., 1998):

$$ET_0 = \frac{0{,}408\Delta(R_n - G) + \gamma\frac{900}{T+273}u_2(e_s - e_a)}{\Delta + \gamma(1 + 0{,}34u_2)} \quad (5.15)$$

With R_n is net radiation (MJ/m^2/day), G is the soil heat flux density (MJ/m^2/day), γ is the psychrometric constant (kPa/°C), T is the mean daily temperature at 2 meters height (°C), u_2 is the wind speed measured at 2 meters height (m/s), e_s and e_a are the saturation and actual vapor pressure (kPa) and Δ is the slope of the saturation vapor pressure curve (kPa/°C).

The three-dimensional shape of plants is also an important determinant for the evapotranspiration rate as it influences the canopy conductance. Grasses close to the ground for example have low conductance because of the still air. Isolated trees on the other hand, catch a lot of wind and have high conductance. The crop evapotranspiration ET_C (mm/day) of several species can be calculated by multiplying the reference evapotranspiration of grass with the crop factor:

$$ET_c = K_c \cdot ET_0 \quad (5.16)$$

Where the crop factor K_c incorporates crop characteristics and soil evaporation effects and ET_0 describes climatic factors according to the FAO Penman-Monteith equation. For most plants the crop factor is smaller than 1 because of stomatal resistance. The crop factor also changes depending on the growth of the crop. Standard values for different phenological stages are given in the FAO Irrigation and Drainage papers.

But the crop factors K_c are given for well-watered crops. Drought reduces evapotranspiration and leads to a lower crop factor because the stomata shut down to limit water use. So to account for soil water stress, the crop coefficient should be

lowered further by multiplying with the water stress coefficient K_s. This depends on the level of moisture deficit and soil salinity. Higher soil salinity leads to a lower water stress. And as depicted in Figure 34, the evapotranspiration when corrected for water stress will usually be lower than the crop evapotranspiration.

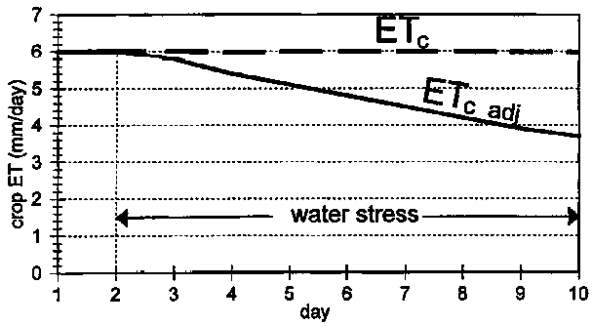

Figure 34: Crop evapotranspiration and adjusted crop evapotranspiration over time (Allen, et al., 1998)

The adjusted crop evapotranspiration with incorporation of water and environmental stress can be calculated as:

$$ET_{c\,adj} = K_c \cdot K_s \cdot ET_0 \qquad (5.17)$$

Where K_s describes the effect of water stress on crop transpiration. When there is no soil water stress $K_s = 1$.

The process of determining the evapotranspiration of crops according to the United Nations FOA is summarized in Figure 35. First the reference evapotranspiration ET_0 for a grass reference crop with a certain climate is calculated with the radiation, temperature, wind speed and humidity measurements as input. Then the standard evapotranspiration is adjusted with the crop factor K_c to determine the crop evapotranspiration ET_c for a well-watered crop in optimal conditions. A list of crop factors for commonly used agricultural crops is given in the paper. Finally, the water and environmental stress can be incorporated by multiplying the crop evapotranspiration with the environmental stress factor K_s to obtain the adjusted crop evapotranspiration $ET_{c\,adj}$.

5.2.7 Landscape evapotranspiration

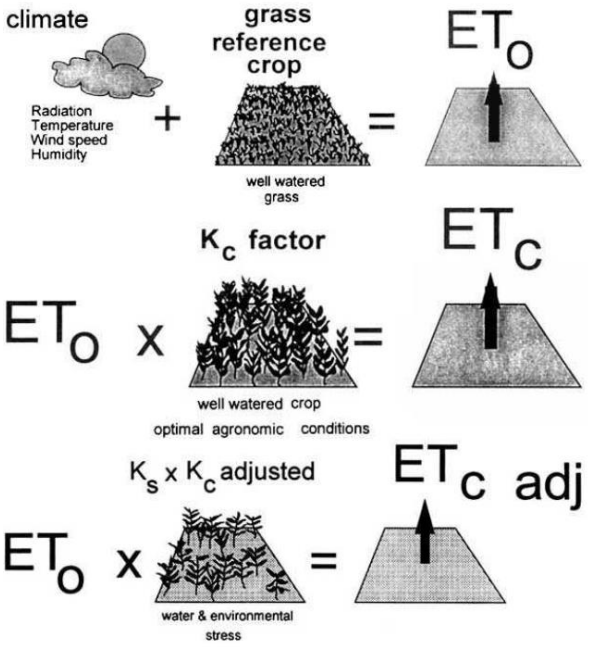

Figure 35: FAO method for determining crop evapotranspiration (Allen, et al., 1998)

The FAO method for determining evapotranspiration as described in the previous subparagraph was designed for agricultural purposes. For plants in a landscape that have primarily an aesthetic function, the Water Use Classification of Landscape Species (WUCOLS) was initiated. It was drafted by the California Department of Water Resources to stimulate water use efficiency while maintaining landscape health and appearance (DWR, 2000).

Table 2: Factors influencing landscape evapotranspiration (DWR, 2000)

	High	Moderate	Low	Very Low
K_s (species)	0,7-0,9	0,4-0,6	0,1=0,3	<0,1
K_d (density)	1,1-1,3	1,0	0,5-0,9	
K_{mc} (microclimate)	1,1-1,4	1,0	0,5-0,9	

The method is based on the FAO Drainage and Irrigation papers, but instead of using the crop factor which describes agricultural grasses and turfs, a landscape factor is used. The landscape factor depends on three parameters: the species factor k_s, density k_d and microclimate k_{mc}. The ranges of these parameters are given in Table 2.

5.2.8 Evapotranspiration of individual trees

To determine the evapotranspiration of individual trees, the Penman-Monteith equation must be adjusted. The amount of absorbed radiation for a tree is smaller than for the reference crop grass, since only part of the tree will absorb solar radiation and the other part of the tree receives limited solar radiation due to shading of the canopy. To calculate evapotranspiration the tree canopy can be assumed as a single leaf (Caspari, et al., 1993):

$$R_{n,tree} \approx R_n L_p \qquad (5.18)$$

Where L_p is the projected ground area covered by the canopy. For the Leaf Area Index it is known that LAI = L/L_p. This big leaf model assumes that the amount of radiation absorbed is the same as the horizontal plane projected to the ground. Sap flow measurements by Zhang et al (1997) showed that the net radiation absorbed per unit leaf area for trees is close to half the incoming solar radiation on the horizontal plane. Therefore it can be assumed that $L_p \approx 0{,}5$ (Zhang, et al., 1997).

5.3 Wind flow

Trees have an impact on the behavior of wind turbulence and speed and additionally wind influences the evapotranspiration of trees. These relations are discussed in this paragraph.

5.3.1 Wind flow in an urban environment

Generally wind moves from areas with high air pressure to areas with low air pressure. Near the earth surface wind speeds are lower due to the friction caused by obstacles blocking wind flow. In the free atmosphere (more than 100m from the earth surface) geostrophic wind relationships are used. But in the lower 100m of the atmosphere both the log wind profile and wind profile law can be used to describe the vertical distribution of horizontal mean wind speed. In a flat terrain the log wind profile equation can be used to estimate the wind speed *U* (m/s) at a certain height of *z* (m) above the ground as follows (Wieringa, 1998):

$$\mathrm{U(z)} = \frac{U^*}{\kappa} \ln\left(\frac{z-d}{z_0}\right) \qquad (5.19)$$

Where U^* is the friction velocity (m/s), κ is the Von Kármán constant (~0,41), *d* is the zero-plane displacement (m), *z* (m) is the height above the surface and z_0 is the surface roughness (m). The friction velocity U^* is the fictional velocity depending on the friction wind undergoes near the ground surface:

$$U^* = \sqrt{\frac{T_w}{\rho}} \qquad (5.20)$$

Where T_w is the shear stress (Pa) and ρ is the air density (kg/m^3). In the case of wind near the ground surface, the shear stress is often assumed independent of height and approximates the square of the mean wind velocity. So in this case the friction velocity would equal the value for which the square law would be valid (Sutton, 1953).

In the equation above the zero-plane displacement *d* is the height above the ground at which zero wind speed is achieved as a result of flow obstacles such as trees or buildings. It can be approximated with ¾ or ⅔ of the obstacle height in the case that the density of the obstacles is greater than approximately 25% of the total surface. For example if estimating winds over a forest canopy which covers more than 25% of the total surface and has an average 30 m height, the zero-plane displacement could be estimated at 20 m.

The roughness length is a corrective measure to account for the roughness of a surface on the wind flow and depends on the terrain. This is the height at which the log wind speed profile would become zero when it would be extrapolated downward through the surface layer. As an approximation the roughness length can be assumed one-tenth of the height of the surface roughness elements. For example short grass of 0,01 m has a roughness length of approximately 0,001 m. Rougher surfaces have a greater roughness length. Some characteristic roughness lengths are given in Table 3.

Table 3: Roughness lengths of different landscapes (Wieringa, 1998)

Landscape	Roughness length z_0 (m)
Open sea	0,0002
Mud flats, snow; no vegetation, no obstacles	0,005
Open flat terrain; grass, few isolated obstacles	0,03
Low crops; occasional large obstacles	0,10
High crops; scattered obstacles	0,25
Parkland, bushes; numerous obstacles	0,5
Regular large obstacle coverage (suburb, forest)	1,0
City centre with high- and low-rise buildings	≥ 2

In weather stations the wind speeds are usually registered with an anemometer and typically weather stations are situated on a flat terrain with a roughness length of 0,03 m (Bronsema, 2013). The wind speed registered at a weather station can be referred to as the potential wind speed. With the logarithmic wind profile equation the potential wind speed can be transformed to the actual wind speed at a certain height.

The Beaufort wind force scale is often used to classify wind speeds based on observed conditions. Originally the scale was designed to standardize observed wind conditions on a ship, but later the scale was adjusted to also include land observations. Nowadays the weather conditions can be accurately measured, but the Beaufort scale is still used to give weather warnings to the public. The classes are given in Table 4. The classification ranges from a calm wind with a speed lower than 0,3 m/s (scale 0) to a hurricane force of more than 32,7 m/s (scale 12) (WMO, 2012).

But the behavior of wind does not only relate to the wind speed. The wind direction and turbulence are also of importance. The atmospheric stability classes by Pasquill can be used to categorize atmospheric turbulence (Pasquill, 1961). It contains six stability classes that are featured in Table 5.

Table 4: International Beaufort scale (WMO, 2012)

Class	Description	Wind speed (m/s)
0	Calm	< 0,3
1	Light air	0,3 – 1,5
2	Light breeze	1,6 – 3,3
3	Gentle breeze	3,4 – 5,5
4	Moderate breeze	5,5 – 7,9
5	Fresh breeze	8,0 – 10,7
6	Strong breeze	10,8 – 13,8
7	Moderate gake	13,9 – 17,1
8	Fresh gale	17,2 – 20,7
9	Strong gale	20,8 – 24,4
10	Storm	24,5 – 28,4
11	Violent storm	28,5 – 32,6
12	Hurricane	≥ 32,7

Table 5: Atmospheric stability classes (Pasquill, 1961)

Stability class	Definition
A	Very unstable
B	Unstable
C	Slightly unstable
D	Neutral
E	Slightly stable
F	Stable

Table 6: Meteorological conditions that define stability classes (Pasquill, 1961)

Windspeed	Daytime incoming solar radiation			Nighttime cloud cover	
m/s	> 700 W/m²	350-700 W/m²	< 350 W/m²	> 50%	< 50%
< 2	A	A-B	B	E	F
2-3	A-B	B	C	E	F
3-5	B	B-C	C	D	E
5-6	C	C-D	D	D	D
> 6	C	D	D	D	D

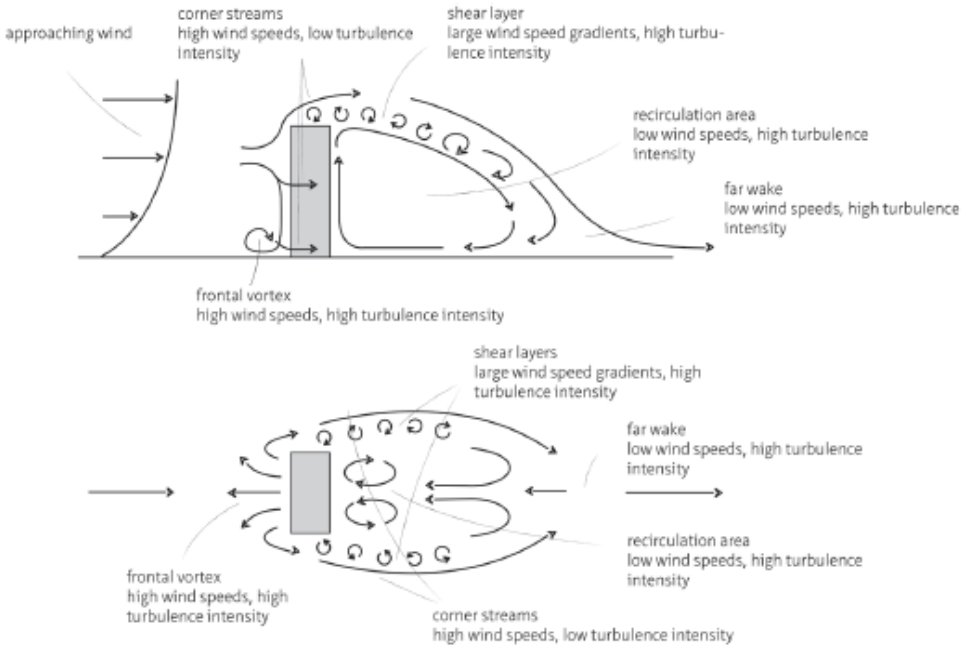

Figure 36: Wind flow around a single building (Pijpers-van Esch, 2015)

The meteorological conditions that define the classes are displayed in Table 6. Pasquill's stability classes illustrate some key concepts linking meteorology to wind turbulence. An increase in solar radiation increases the atmospheric instability, because the earth surface is heated and warm air near the surface rises up to create vertical mixing. Clear nights with a low percentage of cloud cover are stable because the ground cools faster. Higher wind speeds lead to an increase of vertical mixing and destabilize stratification leading to more turbulence.

5.3.2 Wind flow around buildings

It is difficult to accurately predict the wind pattern around a building. As described in the previous subparagraph, the incoming wind speed perpendicular to the building increases as the distance from the ground surface increases according to the log wind profile. As a result of the wind being blocked by the building, the air pressure at the wind-facing side of the building also increases with height. The highest air pressure usually develops at 70-80% of the height of the building. As the air pressure increases, the wind is forced down along the façade of the building in the frontal vortex. This create high wind speeds with high turbulence at the frontal vortex, which is often a cause of wind discomfort. Part of the wind moves upwards along the top of the building. This creates overpressure at the wind facing side and under pressure at the downwind side. Along the corners of the building high wind speeds with low turbulence occur. But on the downwind side the turbulence intensity increases and causes a large recirculation area (Pijpers-van Esch, 2015). Typical wind flow around a single building is depicted in Figure 36.

5.3.3 Wind flow around trees

Trees have been used for many years to influence wind speed in the direct environment. For example planned trees in a wind corridor shape will positively affect thermal comfort in warm climates, whereas wind speed reduction in intensive use areas will cause an undesirable temperature increase (Kong, et al., 2017).

The aerodynamic impact depends mainly on the height and the porosity of the tree. Trees with a low leaf area density have a high optical porosity and therefore are less effective in decreasing the wind speed. The optical porosity strongly depends on the phenological stage of the tree.

Stredova et al (2012) modeled the relationship between the optical porosity of trees and the wind speed reduction at the leeward side for different distances from the windbreaking trees (Stredova, et al., 2012). Li et al (2007) also considered the effect of tree porosity on wind speed reduction but specifically in an urban environment. With a porosity of 20-30% and at a distance of one tree height the maximum wind speed reduction was 80%. With a porosity of 50% and a distance of twice the tree height the maximum wind speed reduction was 70% (Li, et al., 2007).

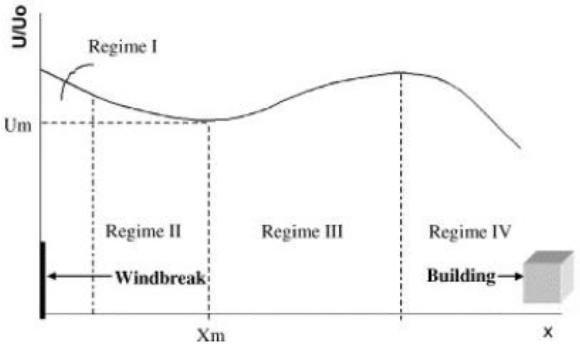

Figure 37: Different wind flow regimes between a porous windbreak and building (Li, et al., 2007)

But Li et al (2007) also considered the sheltering effects of trees as windbreaks in the case that the tree is located in proximity to a building. Wind tunnel modelling and CFD simulations showed that the addition of a building changes the shape of the mean wind speed curve and especially the position of the minimum wind speed. In this case the distance between the building and the tree is of more significant influence than the optical porosity of the tree (Figure 37) (Li, et al., 2007).

5.3.4 Effect of wind speed on evapotranspiration

When water is vaporized from the canopy of a tree the air above the tree becomes more saturated. If this air is not replaced with drier air, the driving force of water vapor removal and the evapotranspiration rate decreases. Therefore wind flow and air turbulence plays an important role in determining evapotranspiration (Allen, et al., 1998).

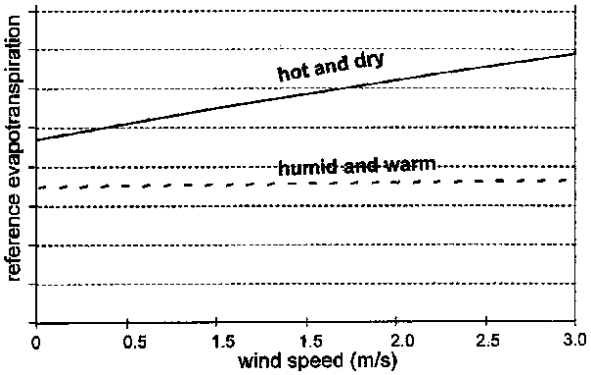

Figure 38: The effect of wind speed on evapotranspiration in hot-dry and humid-warm weather conditions (Allen, et al., 1998)

For two different climates the effect of wind speed on reference evapotranspiration is visualized in Figure 38. In hot and dry weather the evapotranspiration rate will be high due to a large amount of energy coming from solar radiation and the dryness of the air that can store a significant amount of moisture. In humid and warm weather on the other hand, there is a high humidity and less solar radiation, so a lower rate of evapotranspiration. The effect of wind on evapotranspiration is different for both climates. In the humid climate the wind can only replace saturated air with slightly less saturated air, so the effect is limited. In a drier climate the wind speed will affect evapotranspiration to a far greater extent and higher wind speeds will lead to an increased rate of evapotranspiration.

6 Green Balcony Measurements

In the previous chapters, the theoretical framework of green balconies was explored. In this chapter, actual measurements are done to in the field to explore the effect of trees on the microclimate near buildings. These measurements are done to validate later simulations in ENVI-met.

In Paragraph 6.1 measurements were conducted to quantify the impact of the tree canopy on the surface temperature. For this purpose thermal images are taken of five different trees standing close to a building envelope. In Paragraph 6.2 measurements were conducted on eleven actual green balconies on a Bosco Verticale building in Milan. The four microclimatic factors air temperature, relative humidity, wind speed and solar radiation were measured. In Paragraph 6.3 the ENVI-met model of the same building with green balconies is described. In Paragraph 6.4 the results from the green balcony measurements and model are discussed. Finally, in Paragraph 6.5 this leads to conclusions about the reliability of the microclimate model in ENVI-met.

6.1 Measurements of trees near the building envelope

The literature study in the previous chapters showed that the increase in thermal comfort by trees can be largely attributed to the shading effect by the leaves in the canopy. But the amount of shading is largely dependent on the tree properties and location. At Bosco Verticale, the trees are approximately 6 meters in height and located at a distance of 2 meters from the building envelope. Based on these parameters, a measurement location was found with similar conditions to the reference green balcony situation.

Five trees were selected for evaluation. The trees are located near the west façade of the Applied Physics building on the campus of Delft University of Technology in Delft, the Netherlands and are evenly spaced along the building facade (Figure 40).

Pictures were taken around 15:00 on the sunny and cloudless 6th of June 2018. The hourly climate data at this time was retrieved from KNMI for the nearest meteorological station of Rotterdam, given in Table 7 (KNMI, 2018).

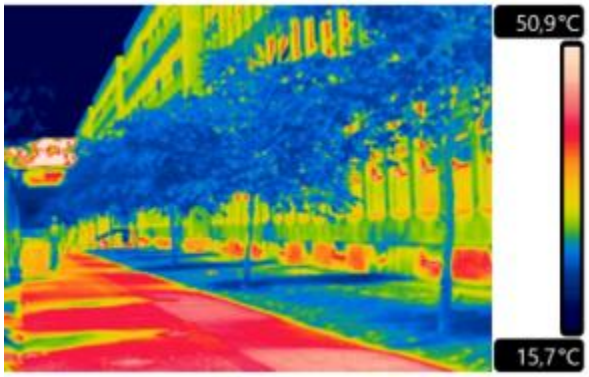

Figure 40: Thermal image of the studied trees at the faculty of Applied Physics at Delft University of Technology

Table 7: Climate data at 15:00 on 6-6-2018 (KNMI, 2018)

Temperature at 1,50m	25,9 °C
Dew point temperature at 1,50m	16,0 °C
Relative humidity at 1,50m	54%
Global radiation past hour	254 J/cm^2 = 706 W/m^2
Cloud cover	0

Thermal images were taken with a FLIR T420bx camera. It is important to note that the infrared radiation measured by the camera does not directly measure the emitted radiation from the object surcace. The infrared radiation measured by the camera also contains disturbances, such as radiation emitted by the surroundings and radiation reflected by the objects. And even

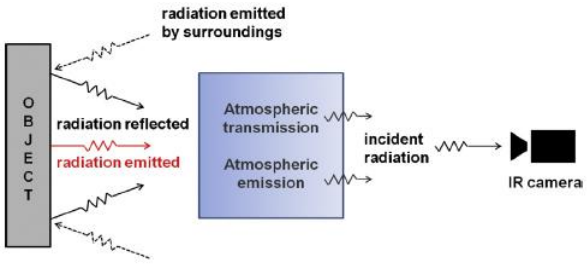

Figure 39: Components of incident infrared radiation (Taylor, et al., 2014)

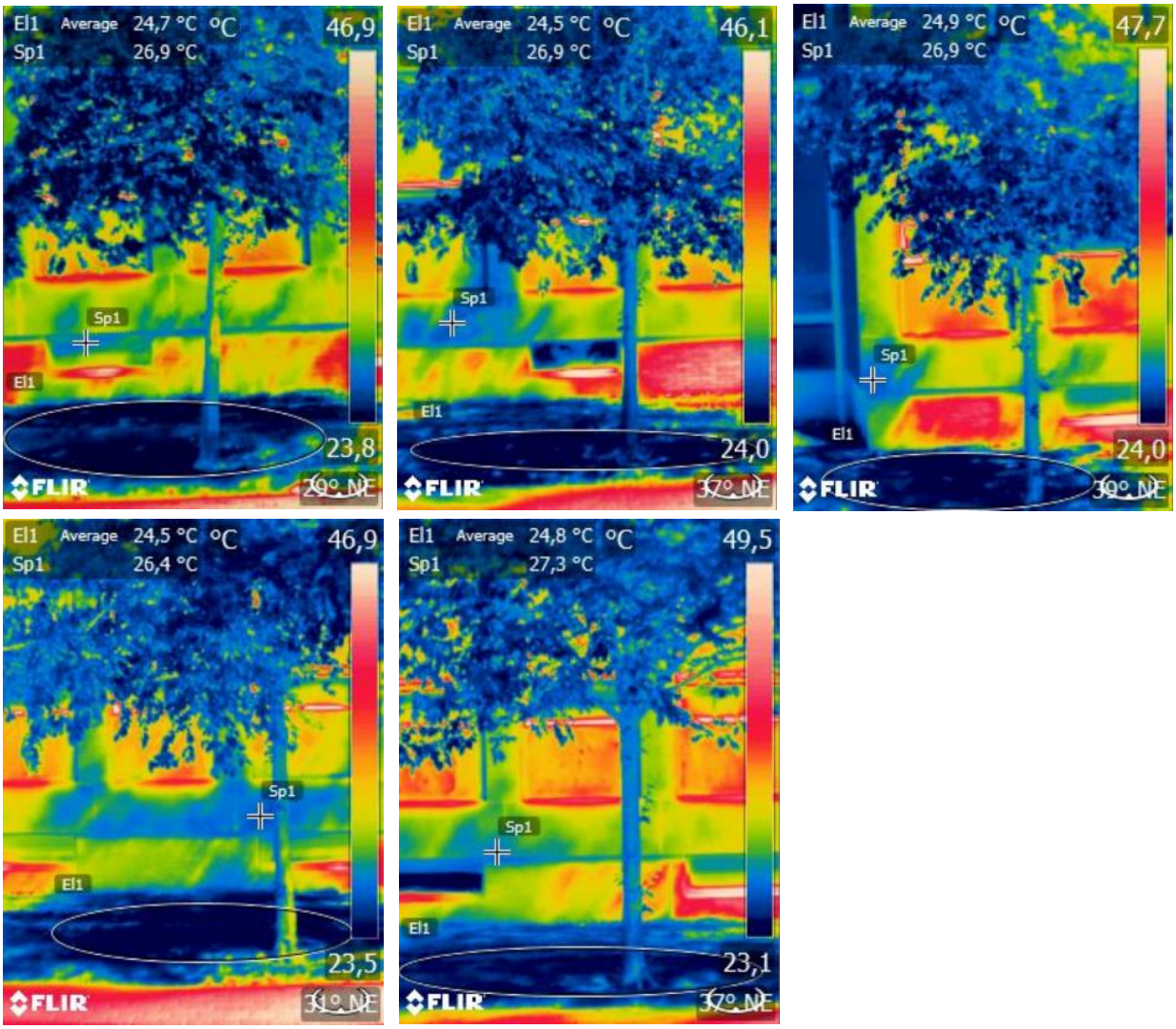

Figure 41: Thermal images of five trees with average temperature of directly shaded area (el) and spot temperature measurement of partially shaded area (sp1)

though the thermal heat storage capacity of the atmosphere is limited, it does have the ability to absorb and emit radiation and can therefore influence the output of the thermal images. A schematic diagram of the factors influence the reception of the infrared camera are given in Figure 39.

To calibrate the thermal images with radiometric parameters the software FLIR Tools was used. The atmospheric temperature and relative humidity were set according to the climate data in Table 7. To adjust for atmospheric emissivity the distance from the object was noted. The effective temperature of the surroundings can be determined by measuring the average temperature of the surrounding surfaces with the IR camera taking into account the view factors (Taylor, et al., 2014). The average temperature of the surfaces surrounding the tree is taken as 30 °C (Figure 40). The emissivity of the concrete facade is 0,94 (de Wit, 2017) and the average emissivity of a tree is 0,98 (Rubio, et al., 1997). Therefore the emissivity for the thermal image is set at the average value of 0,96.

The thermal image results from the infrared camera are given in Figure 41. The most significant temperature reduction is visible in the direct shading of the tree. The average temperature of this elliptical area on the grass surface directly beneath the tree crown is

calculated and labeled *El1*. In calculating the average value of the elliptical area underneath the tree, it is inevitable that part of the tree trunk blocking the shadow is included. Since this temperature is slightly higher than that of the directly shaded area, it slightly brings down the average cooling effect. Also FLIR Tools software is limited to calculating an area with an elliptical shape, whereas the actual shadow is not perfectly elliptical. So this will also lead to a degree of inaccuracy. The average temperature of the grass was determined for all five trees and was found to be 27,6 °C on average whilst the average temperature in the direct shade of the tree was found to be 24,7 °C. This means the average cooling of the surface temperature by direct shading for this case is 2,9 °C.

Napoli et al. (2016) also researched the effect of tree shade on ground surface temperatures for different tree species in Florence, Italy (Napoli, et al., 2016). Surface temperature data on asphalt and grass were collected for ten different tree species. On asphalt the surface temperature reduction ranged from 13,8 to 22,8 °C. On grass the negative relationship between the Leaf Area Index and surface temperature was found to be weaker probably due to the combined effect of shade and grass evapotranspiration. For the grass surface the temperature reduction in the shade ranged from 6,9 to 9,4 °C. When comparing this to own measurements, the cooling effect measured by Napoli et al. is more than double.

The differences in ambient temperature cannot explain these differences. A larger cooling effect is expected at higher ambient temperature. With an average temperature of 25,9 °C in Delft and 23,3 °C in Florence this does not rationalize these discrepancies in the cooling effect. However, when taking a closer look at the range of total tree heights (3,5-17,2 m) and the range of average crown diameter (2,3-17,2 m) it is clearly visible that these are of a different magnitude than the trees studied in Delft. The difference in cooling effect can therefore be mainly attributed to the larger tree crowns in Florence which result in a greater shading capacity.

6.2 Measurements on green balconies

Even though there are several vertical forest projects currently in construction, the project Bosco Verticale in Milan is one of the very few vertical forest projects that is already completed and in use. This is why Bosco Verticale was selected to conduct microclimate measurements.

6.2.1 Location of measurements

The project Bosco Verticale consists of two buildings: Tower D (78 m height and 18 levels) and Tower E (111 m height and 27 levels) which were both delivered in 2014 and have been in use since. Stefano Boeri Architetti were contacted and via the architectural firm contact with the buildings owner was made. The building owner did not see possibilities to measure on the private balconies within a reasonable time frame, so this was unfortunately not possible. Also an effort to cooperate with researcher Elena Giacomello did not result in possibilities for measurements. Also due to the strict security regulations to protect the privacy of the residents in Bosco Verticale on both buildings it was not permitted to go door by door and ask residents for cooperation in the research.

Therefore, the choice was made to post flyers in the mail boxes to directly address the residents of the building to evaluate if they were open to cooperation. All residents of Tower D and E received a flyer in their mail in which they were asked for their cooperation for measuring the microclimate on their balconies for research purposes, with an elaborate explanation of the research team and the purpose of the research. The flyers were posted during the summer holiday and therefore many residents were not present in the building. This partially explains why there was only one positive response to the request for cooperation.

During the visit of this respondent in tower D, it was discovered that there are balconies on both Bosco Verticale buildings that do not belong to any of the residents. The vegetation containers on these balconies are all lined with sensors and this makes it possible to measure the water use accurately for every container. Every measurable

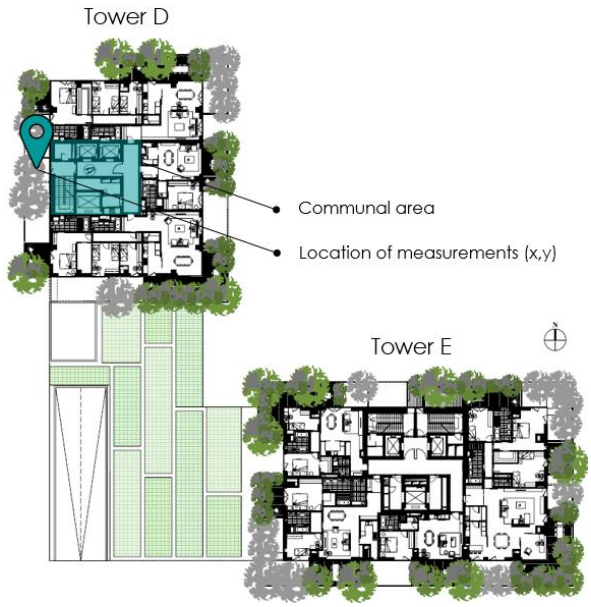

Figure 42: Location of measurements (x,y)

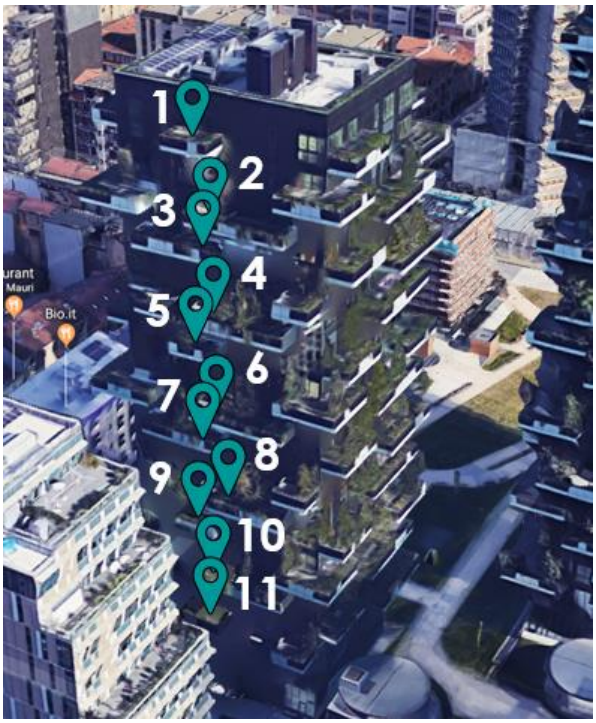

Figure 43: Location of measurements (x,y,z)

plant container is a control group and they are used to predict the water use of the other similar plant containers on the building, which are not lined with humidity sensors. These control group balconies can be accessed from the communal areas of the building where the elevators and staircases are located. In tower D the communal area is situated on the west side of the building and the balconies are also oriented towards the west. The layout of the communal area is duplicated on every level and therefore the door leading to the balconies for measurements is also located on the exact same location for every level (Figure 42). In total there are eleven communal balconies. Measurements were done on the center of all eleven communal balconies of Tower D. The measurement locations along the façade of the building are depicted in Figure 43. As is clearly visible from the figure, even though the entrance to these balconies is on the same location at every level, the size of the balcony varies as well as the location of the center of the balcony along the width of the building. These differences are described in Table 13. Also for every level the height of the balcony platform was determined from architectural drawings and rounded off to whole meters since this is also the modelling accuracy. Then the measurement height was calculated by adding the 1,5 meters at which the measurement devices were set up. The balcony widths were determined in similar fashion. The y-coordinate in Table 8 assumes the south west corner of Tower D as coordinate (0,0) and x and y axis in the standard directions (pointing east and north respectively). Since the data was recorded at the center of the balcony and some balconies have different sizes, the y-coordinates of measurements are also slightly different.

Table 8: Measurements locations data

ID	Building level	Height (m)	Balcony width (m)	Y-coordinate
1	18	76,5	5	15
2	16	68,5	5	13
3	15	64,5	3	14
4	13	56,5	5	13
5	12	52,5	5	15
6	10	44,5	5	13
7	9	40,5	3	14
8	7	32,5	5	13
9	6	28,5	5	15
10	4	20,5	5	13
11	3	16,5	3	14

6.2.2 Climate conditions at time of measurements

Figure 44: Cloudless sky and sunny conditions on the day of measuring (picture by author)

Measurements were conducted on August 10th 2018 between 11:00 and 13:45 in intervals of 15 minutes. During measurements the sky was clear and no clouds were present as is visible in Figure 44 which is picture of the Bosco Verticale towers and sky on the day of measuring. The climate data of this day was retrieved from the Italian meteorological institute ARPA Lombardia. In Figure 45 the weather stations near Bosco Verticale are depicted.

Figure 45: Weather stations in the vicinity of Bosco Verticale

The station Via Rosellini is located closest to Bosco Verticale, but unfortunately this station only measures precipitation and not temperature, humidity, wind and global radiation. The stations Viale Marche and Via Brera do measure these four factors. Viale Marche is in closer proximity to Bosco Verticale than Via Brera, but the difference in distance is not significant. But the weather station Via Brera is located in an urban area with high density, which better represents the environment of the Bosco Verticale towers. Viale Marche is located in a less dense urban area, therefore it might be possible that this weather station does not accurately approximate the weather conditions at the Bosco Verticale site. To determine which weather station data to use, the microclimate measurements conducted at the Bosco Verticale location were compared to the climate measurements at the two weather stations Viale Marche and Via Brera. This comparison is visible in the graph of Figure 46.

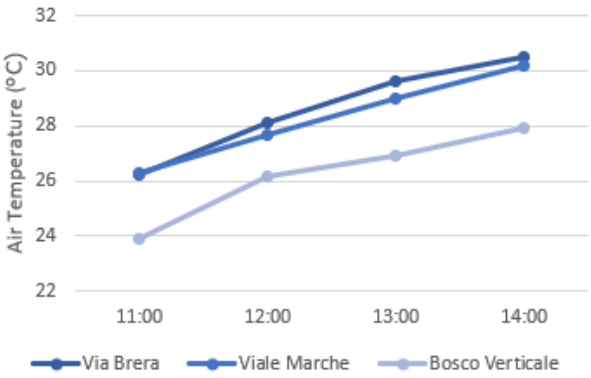

Figure 46: Measured air temperature on August 10th 2018 at different locations

The differences in temperature between Via Brera and Viale Marche turned out to be relatively small, with the Viale Marche temperatures most similar to Bosco Verticale measurements. Therefore the station Milano Viale Marche was chosen as the most representative weather station at a distance of 1,16 km of Bosco Verticale. At the time of measurements between 11:00 and 14:00 the temperature at this weather station ranged between 26,3 and 30,2 °C, the relative humidity range between 44,3 and 56,8 %, global radiation between 609,1 and 904,2 W/m^2 and the wind speed between 1,0 and 1,4 m/s.

6.2.3 Measuring equipment

In Chapter 5 a literature study was done on the heat and moisture transfer of trees. From this study the most relevant microclimate factors that

were found to be influenced by vegetation are the air temperature, humidity, radiation and wind speed. To validate microclimate models, these four factors must be measured.

Air temperature and humidity

The air temperature and humidity were measured using a HOBO U12-012 Temp/RH/Light/External Data Logger from Onset. The data logger can gather 43,000 measurements with 12-bit resolution. The device is conveniently linked to HOBOware software that provides direct possibilities for setup, graphing and analysis. The device can register temperatures between -20° and 70°C and relative humidity between 5% and 95%, which is both sufficient for the microclimate ranges in Milan. The accuracy of the temperature measurements between the common range of 0° to 50°C is ± 0,35°C. The accuracy of the relative humidity measurements between typical values of 10% to 90% is ±2,5%. Data can be read out from the device by inserting it with a USB cable to the computer.

Figure 47: HOBO Onset U12-012 Data Logger (Onset)

Wind speed

The HOBO Onset data logger also has the possibility of attaching an external channel. With a wire inserted to the right side of the HOBO data logger, a Mjolnir Vaavud wind speed meter was attached and data was automatically logged onto the HOBO device set to units m/s. The Vaavud wind speed meter can be attached to the jack of a mobile phone to easily measure the wind speed with the corresponding free mobile application. The correct functioning of the device was tested with this mobile app and results were compared to a handheld anemometer. One of the advantages of using this device as opposed to a handheld anemometer is that the wind speed measurement does not depend on the wind direction because the cup-anemometer catches wind from every direction. The operating range of the wind speed meter is 1-25 m/s and the accuracy is ±4%.

Figure 48: Vaavud Mjolnir cup-anemometer (Vaavud)

Solar radiation

To measure the incoming solar radiation on the horizontal surface, a VOLTCRAFT solar-datalogger DL-131 LUX was used. The measurement data is stored on the device itself and it can be directly inserted into the computer with a USB connection. Accuracy of the measuring device was tested by comparing the results to a globe radiation meter. The measurement range of the solar logger is between 1-1999 W/m^2. It measures the solar intensity at an accuracy of ±10 W/m^2. The device can be mounted to a camera tripod with a similar connection. Voltsoft software can be used to analyze the data.

Figure 49: VOLTCRAFT solar-datalogger DL-131 LUX (Conrad)

Measurement devices setup

All three measurement devices were mounted to a tripod which was set to a height of 1,5 meters. The solar datalogger was mounted to the top of the tripod and put level with the plumb rule on the tripod to ensure the exact horizontal level measurement of the W/m^2. The temperature and humidity measuring device was attached to the tripod with Velcro stickers at the side facing away from the building. Especially for the cup-anemometer it was important to make sure the measurement device is entirely level so it will not experience friction and therefore register lower wind speeds. The tripod was featured with plumb rules in all three dimensions and adjustability to ensure the measurement devices are level. The

Figure 50: Setup of solar radiation, temperature/humidity and wind meters on balcony

wind meter was attached to the tripod with a plastic extension tube and fixed in place with tie wraps. The complete setup on a balcony on the east façade of Tower D is visible in Figure 50.

6.2.4 Classification of vegetation

It is difficult to simplify vegetation for modelling purposes. But the vegetative canopy is an important factor in determining the exchange of energy between the plant and the atmosphere. The most common way of expressing the leaf area density of a single tree is by giving the Leaf Area Index (LAI). The Leaf Area Index is the leaf area of the tree (m^2) in comparison to the ground area (m^2) so this is given in m^2/m^2. Since the Leaf Area Index is difficult to determine and can only be accurately determined with a plant canopy analyzer tool, an average value for the leaf area density was based on measurements done on Bosco Verticale by Giacomello (Giacomello & Valagussa, 2015). This gives the Lea14f Area Index averages as displayed in Table 9.

This Leaf Area Index is distributed along the height of the tree according to the vertical distribution function Leaf Area Density (LAD) which is given in m^2/m^3. The LAD depends on the shape of the tree. Different models can be used to estimate the leaf area vertical distribution. The most common way to model the vertical distribution of the foliage area of the individual stem is with a normal distribution (Lechner, 2014), so this distribution has also been applied to the trees in this case.

Table 9: Average measured LAI's per tree type on Bosco Verticale (Giacomello & Valagussa, 2015)

Querces ilex	Fagus sylvatica
	
Average LAI = 5,40 m^2/m^2	Average LAI = 5,75 m^2/m^2
Prunus subhirtella	**Corylus colurna**
	
Average LAI = 3,16 m^2/m^2	Average LAI = 1,15 m^2/m^2

The height of the vegetation was determined with the similar triangle method, depicted in Figure 52. A geometrical triangle with a straight angle is held

level and a finger is placed where the sight line intersects the vertical side of the triangle to find the height *h*. Then by similar triangles it is known that (Lechner, 2014):

$$H = D \times \frac{h}{d} \qquad (6.1)$$

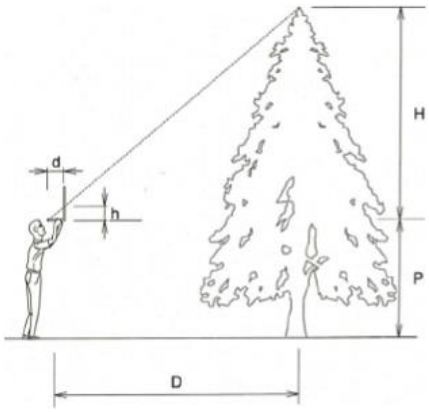

Figure 52: Similar triangle method to determine height of tree (Lechner, 2014)

Then the length of the person that measured *P* (1,63 m) is added to the measured tree height *H* to obtain the total measurement height from the top of the tree to the balcony platform. Finally the height of the plant container (1,1 m) must be subtracted from this number to obtain the actual height of the tree. Since the smallest resolution to define a 3D tree in Albero is 1 meter and this method of measurement is prone to error by sight, the measurements of the vegetation height are rounded off to whole meters. Pictures documenting the vegetation on all green balconies that were measured can be found in Appendix B.

6.2.5 Measurement data statistical analysis

Measurements of temperature, humidity, incoming solar radiation and wind speed were done continuously at an interval of 1 minute between 11:00 and 13:45. All measurements can be found in Appendix A.1. However, every 15 minutes the location of measuring was changed and the measuring equipment was moved to a different floor. During this period of moving the measuring equipment the data logging continued. To eliminate outliers of the measurements due to movement of the equipment or other measuring deficiencies, a statistical analysis of the measurements is done.

One method for visualizing the measurement data is with a box-and-whisker plot or briefly a boxplot (Figure 51). The box of the graph displays the lower to the upper quartile. This is the 25th empirical percentile until the 75th empirical percentile. The distance between the quartiles is called the interquartile range or IQR. This range is the middle half of the dataset and is a robust measurement of the variability among the dataset. Up from the upper quartile and down from the lower quartile at a maximum distance of 1,5 times the IQR the maximum value is determined. At these two points the horizontal lines of the whisker are drawn. All observations beyond the whiskers are marked with an open circle and are outliers (Dekking, et al., 2005).

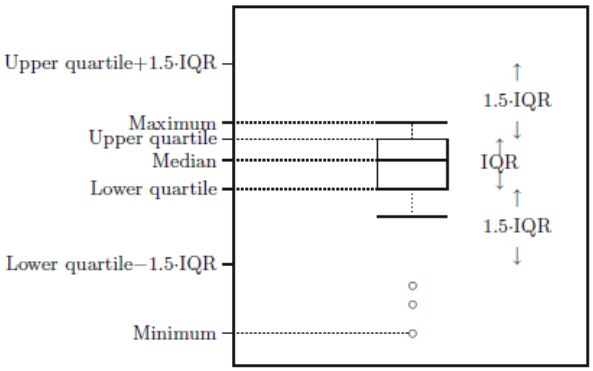

Figure 51: Box-and-whisker plot (Dekking, et al., 2005)

A boxplot was made of all types of microclimate measurements (temperature, relative humidity, solar radiation and wind speed) and the measurements are grouped per 15 minutes time interval. The boxplots of all the measurements can be found in . The boxplots of the temperature (Appendix A.2) and relative humidity (Appendix A.3) show no outliers that reach beyond the whiskers. When comparing the temperature and relative humidity charts it is notable that the levels with a wider range of temperature measurements are in accordance with the wider range of relative humidity. These results were expected, since the ambient temperature and relative humidity are known to interact. This has to do with the saturation vapor pressure which

increases as the ambient temperature increases. Other than that it is notable that the temperature increases as the height of the measurement decreases and the time increases. This behavior is to be expected as the solar radiation increases over time and the temperature more near to the ground level is expected to be higher because of lower direct solar radiation, more reflected radiation and lower wind speeds. The humidity box plots show the exact opposite trend over time as opposed to the temperature, which is expected behavior. As a result of a lower air pressure at increasing height, the relative humidity is expected to . At higher altitudes the air can therefore hold relatively more water vapor than at a lower level.

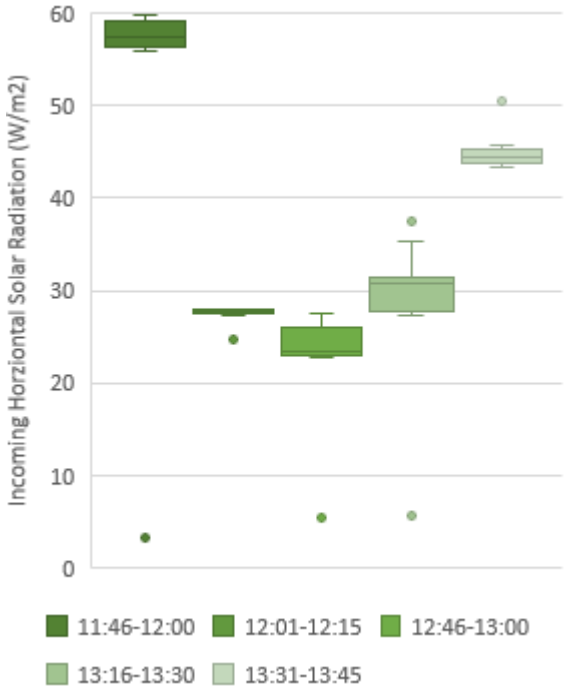

Figure 54: Measured solar radiation box plots grouped per 15 minute time interval with outliers

The solar radiation box plots (Appendix A.4) do not show a trend over the time since the amount of solar radiation received on the balcony mainly depends on the amount of solar shading by the plants and surrounding balconies, so this differs strongly per location. The five time intervals with outliers are depicted in Figure 54. All outliers occurred either at the beginning or the end of the measuring period, which means the difference in measured solar radiation is caused by the movement of the measuring equipment to a different location. Inaccuracy in the timing of moving the equipment could mean that the solar radiation in the first or last minute recorded the incoming solar radiation inside the building or of the previous or next measurement location. Therefore the outlier measurement points are disregarded in further analysis and will not be included in determining the average value of the incoming solar radiation per 15 minute time interval.

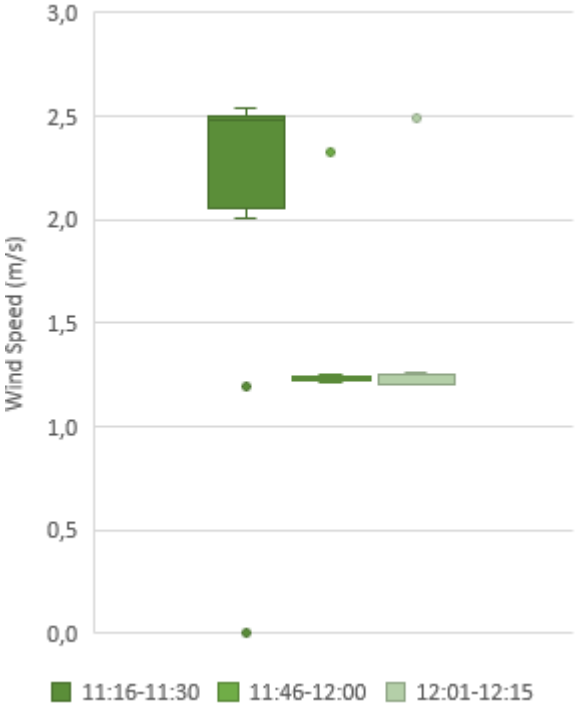

Figure 53: Measured wind speed boxplots grouped per 15 minute time interval with outliers

The wind speed box plots (Appendix A.5) do show a trend as the time and height of measurements changes. As is to be expected according to the log-wind profile the wind speed is larger at greater distance from the ground level. The wind speed measurements largely follow a decreasing trend with decreasing height, with some variability probably caused by the plants interfering with the wind and the natural variability of wind speed. At the last two measurement points closest to the ground level, the wind speed slows down even to an extent that it reaches 0 m/s. The wind meter is expected to be largely influenced by the movement of the measuring devices as the wind

meter shows very different results when positioned not exactly level. During movement the wind meter is slightly tilted and this could lead to distortion of the wind speed. Again the outliers are found at the beginning and the end of the 15 minute measuring period, indicating that the outliers are most likely caused by movement of the wind speed meter. The outliers occurred in three different time intervals and there are four outliers, as depicted in Figure 53. Like the outliers of the solar radiation measurements, the outliers of the wind speed measurements are disregarded in further analysis.

After removing the outliers the average values for every 15 minutes of measurements are calculated for all four types of microclimate measurements (temperature, humidity, solar radiation and wind speed). These values will later be compared to the microclimate model results.

6.3 Modelling of green balconies

To accurately predict the behavior of green balconies on the microclimate without having to conduct measurements, it is useful to make a microclimate model. This paragraph discusses first the choice for a certain microclimate software. Then the three-dimensional model and model input are discussed.

6.3.1 ENVI-met microclimate modelling

From Chapter 5 the most relevant factors to be included in microclimate modelling of a green balcony were found to be radiation, wind, evapotranspiration and shading.

To model the most relevant microclimate effects ENVI-met software is used (Figure 55). ENVI-met has been mostly applied for scientific studies on the effects of vegetation in an urban environment. It is a three-dimensional non-hydrostatic model for the simulation of surface-plant-air interactions. The typical resolution is 0,5-10 m and a typical time frame is 24-48 hours with time steps of 1-5 seconds. Therefore it allows the analysis of small-scale interactions between buildings, surfaces and plants (ENVI-met, 2017). In this research ENVI-met V4.3.1 is used with a Science and Education License and the BioMet module. ENVI-met includes a three-dimensional computational fluid dynamics (CFD) model that solves turbulent wind flow. A disadvantage of modelling turbulent wind behavior is that it requires large computing power. But this aspect is especially relevant for the green balcony case, since wind around a tree behaves predominantly turbulent. ENVI-met uses Reynolds-averaged Navier-Stokes (RANS) equations to model turbulence. The Boussinesq approach is used to

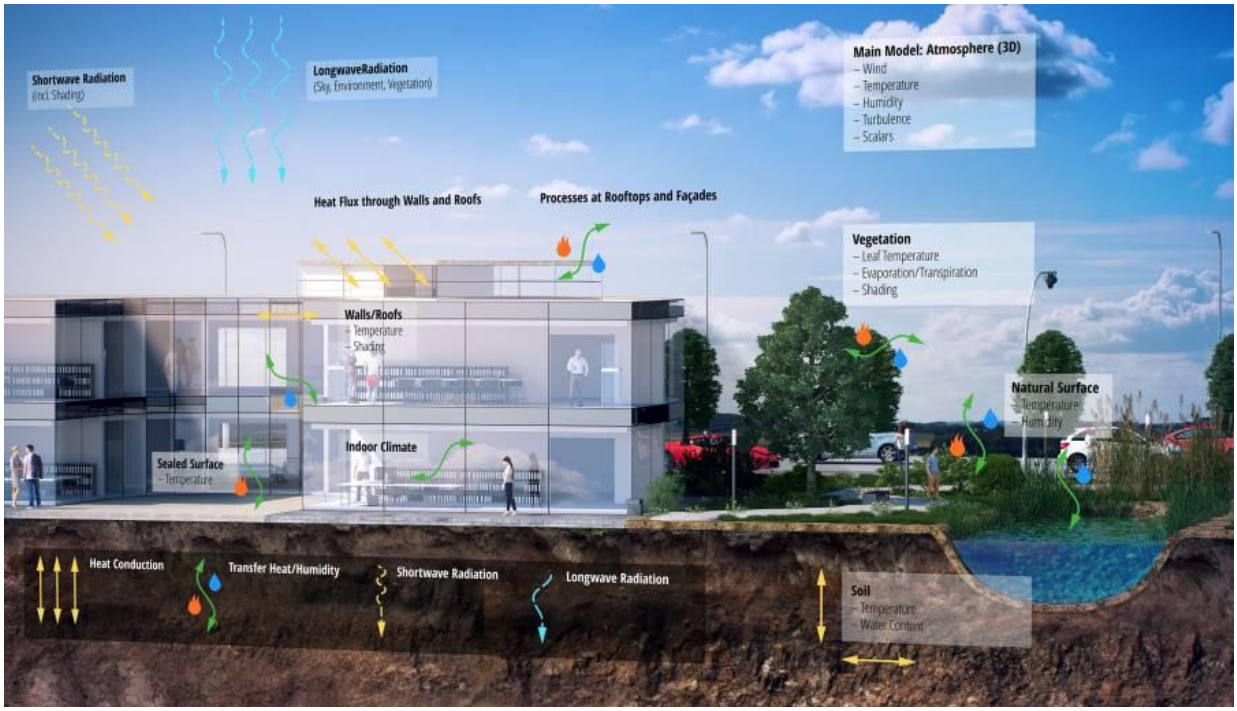

Figure 55: Aspects that are included in ENVI-met microclimate software (ENVI-met, 2017)

determine turbulent viscosity and solve transport equations for every grid cell within a given timestep. In ENVI-met a one-dimensional model of 2500 m is used to accurately model the inflow wind profile. The model lateral boundary conditions can be chosen as open, force or cyclic. ENVI-met also contains a soil model that reaches a depth of 2 meter and is one-dimensional.

Other CFD software such as ANSYS Fluent, OpenFOAM or PHOENICS, were also considered for green balcony modelling. While it is possible to use these types of software, this would provide an unnecessary level of detail which is not needed in this project. Also ENVI-met has the advantage of having the built-in three-dimensional plant editor Albero. So compared to other models ENVI-met is considered most suitable for this research project.

To setup the model simulation in ENVI-met two input files are needed. The model input file contains the model space and the simulation input file contains modelling configurations such as meteorology and time steps. The input will be described in the next two subparagraphs.

6.3.2 Model input

The main model area contains all the buildings directly surrounding Tower D (Figure 56) and is 130 x 130 x 136 (x, y, z) with a grid cell size of 1 meter in every direction. The grid cell size is in accordance with the smallest grid cell size for 3D

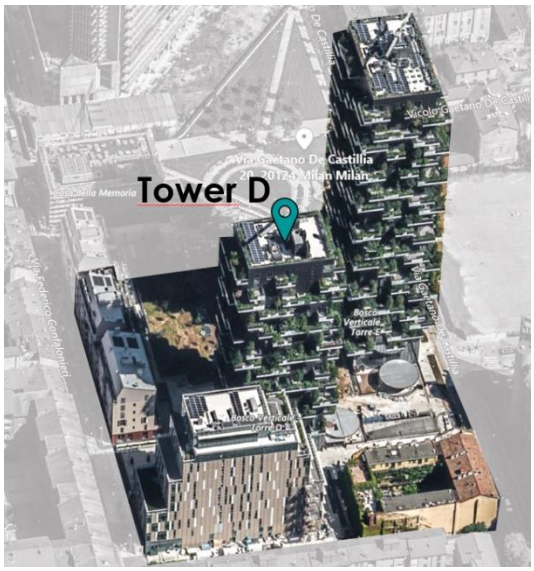

Figure 56: Bird's eye view of main model area (Bing)

Figure 57: Underlayer used in SPACES (osm.org)

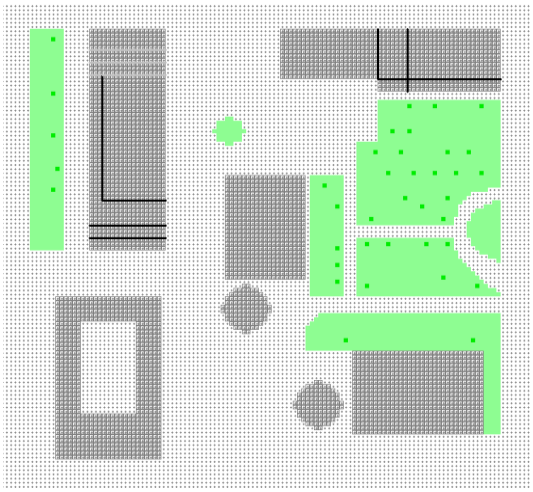

Figure 58: Top view from of vegetation in SPACES

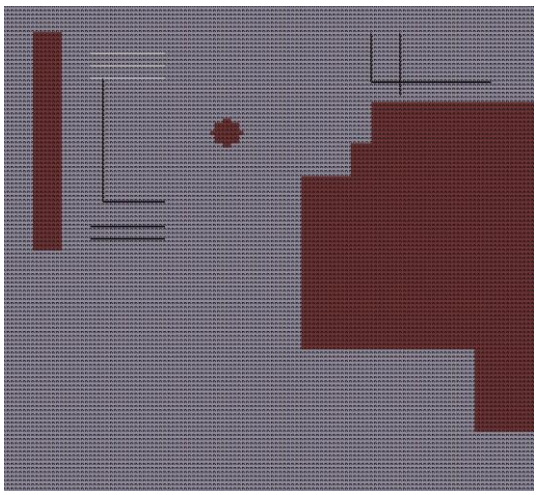

Figure 59: Top view of soil and pavement in SPACES

tree adjustments in Albero. The model height is chosen as twice the height of the highest building (Tower E with 111 m) and 20 nesting grids are placed in all directions around the main model area to prevent wind flow issues. The distance between the nesting grids increases as the distance from the nesting grid to the main model area increases. Nesting grid soil profiles used are concrete pavement and loamy soil. To prevent issues with the wind flow, the model area should be large in enough in the z-direction. To minimize run time and maximize height, the vertical grid is generated with a telescoping factor of 10% starting at a height of 78 meter which is above the top of the building of Tower D. The location is set to Milan, Italy with latitude 45,49 and longitude 9,19 with reference longitude 15. The time zone is CET/GMT+1, so when interpreting output from ENVI-met the time must be corrected for Daylight Savings Time. Model rotation out of grid north is 351° and reference level above sea level is 103 m for DEM = 0. An underlayer from OpenStreetMap was used (Figure 57) to draw in the buildings in the area. In the tab vegetation (Figure 58) the one-dimensional vegetation is modelled. For the park areas short grass is implemented and simple trees are placed. The location of the trees was deducted from satellite images from Google Maps.

Soil and surface

In the tab 'Soil and Surface' loamy soil was defined underneath the park area and used concrete pavement at other locations (Figure 59). In ENVI-met the interaction with the soil is also simulated one dimensionally up to a depth of 2 m. The simulated soil profile for used concrete is given in Figure 60. From the surface the first 4 cm are concrete, followed by 2 cm sand and the remaining profile up to a depth of 2 meters is loam. The material properties of the different layers are given in Table 10.

Receptors

Receptors are placed at a distance of 1 meter from the building and at the eastern façade at three different locations (Figure 61). This is necessary because measurements were conducted at the center of every balcony, but the

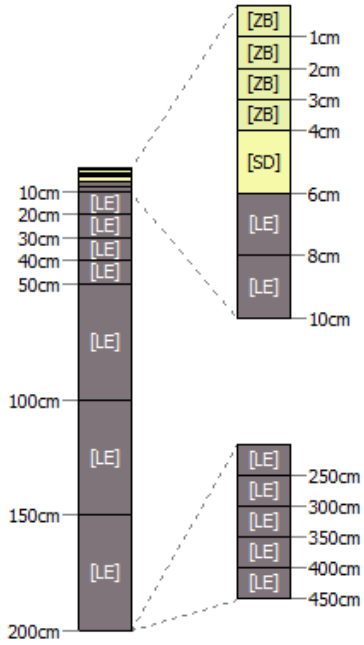

Figure 60: Soil profile of main model area

Table 10: Soil properties

Parameter	Value
[ZB] Concrete	
Volumetric heat capacity Heat conductivity	2,083 E6 J/(m³K) 1,63 W/(mK)
[SD] Sand	
Volumetric heat capacity Water content at saturation Hydraulic conductivity	1,46 E6 J/(m³K) 0,395 m³ water / m³ soil 176 E-6 m/s
[LE] Loam	
Volumetric heat capacity Water content at saturation Hydraulic conductivity	1,21 E6 J/(m³K) 0,451 m³ water / m³ soil 7 E-6 m/s

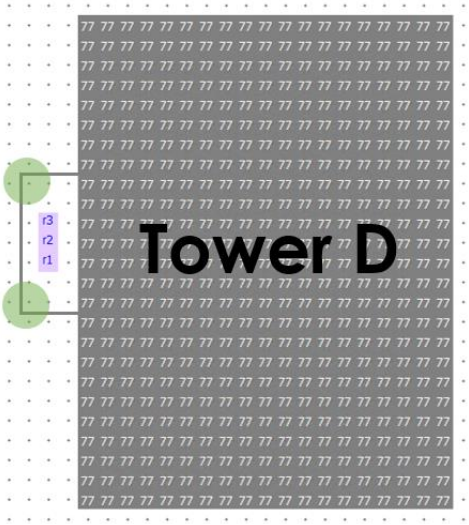

Figure 61: Top view of tower D with locations of receptors 1, 2 and 3 in SPACES

balconies differed in width so the y-location changed (see Figure 43).

Building

The building envelope is made of 20 cm aerated brick, 10 cm insulation and 2 cm stone cladding (Figure 63). In reality the building envelope of Bosco Verticale also has an air cavity of 3 cm between the stone cladding and insulation, but this is not modelled because ENVI-met wall configurations are restricted to a maximum of three material layers.

The construction of the service roof has the same insulation and brick layer as the construction of the building envelope. Only the top layer is different featuring roof cladding of 2 cm thickness, see Figure 62. Material properties are given in Table 11.

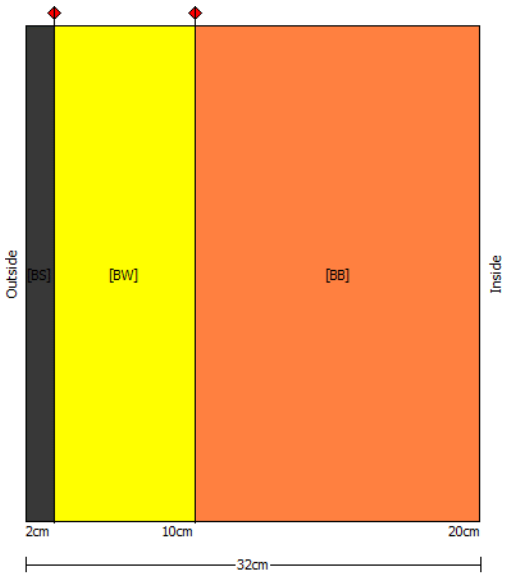

Figure 63: Construction of building envelope

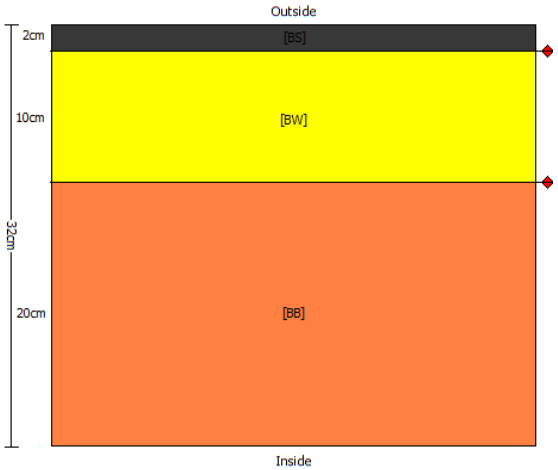

Figure 62: Construction of roof

The balcony platforms cantilever from the building to a depth of 3 meters and differ in width. The balconies are modelled by using single walls attached to the building. These single walls are made up of reinforced concrete with the material properties as defined in Table 11. The thickness of the balcony platform is 30 cm and the thickness of the parapet 20 cm.

Table 11: Material properties building

Parameter	Value
[BS] Stone cladding	
Thickness	0,02 m
Absorption	0,7
Specific heat capacity	840 J/(kgK)
Thermal conductivity	0,9 W/(mK)
Density	1850 kg/m^3
[BW] Mineral wool insulation	
Thickness	0,10 m
Specific heat capacity	1030 J/(kgK)
Thermal conductivity	0,045 W/(mK)
Density	20 kg/m^3
[BB] Aerated brick	
Thickness	0,20 m
Specific heat capacity	840 J/(kgK)
Thermal conductivity	0,3 W/(mK)
Density	1000 kg/m^3
[BR] Roof cladding	
Thickness	0,02 m
Absorption	0,95
Specific heat capacity	1470 J/(kgK)
Thermal conductivity	0,2 W/(mK)
Density	1050 kg/m^3
[BC] Concrete	
Absorption	0,7
Specific heat capacity	840 J/(kgK)
Thermal conductivity	1,4 W/(mK)
Density	2300 kg/m^3

Vegetation
The measurements of vegetation LAI and dimensions were described in subparagraph 6.2.4 and pictures of the balcony vegetation can be found in Appendix B. When the LAI and vegetation dimensions are known, the vegetation can be modeled in Albero.

6.3.3 *Simulation input*
In the Configuration Wizard the following simulation input was used.

Time and date
The simulation start date is 10th of August 2018 and the simulation needs to initialize before the sun comes up. The sun comes up after 6:00 in Daylight Savings Time which is 5:00 in ENVI-met standard time. The measurements stopped at 13:45 Daylight Savings Time, so the ENVI-met run can end at 13:00. Simple forcing is used to set the temperature and humidity at 2 meters for every hour according to the climate conditions measured at the weather station nearby.

Meteorology
For the measurement period 11:00-14:00 the weather station Viale Marche gives an average wind speed of 1,2 m/s and wind direction of 216° (where 0° is from the north and 180° from the south), so these are used as basic settings.

The temperature and relative humidity is input as simple forcing according to the observational data from the weather station (again corrected for the Daylight Savings Time). The course of the temperature and humidity over the day at 2 m is depicted in Figure 64. As these two factors are correlated they follow an opposing trend.

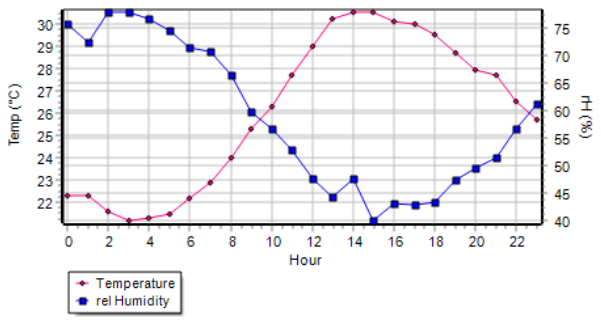

Figure 64: Simple forcing of temperature and relative humidity

Solar radiation
In ENVI-met a standard graph of the incoming solar radiation is determined through standard formulas combining information about the location on the earth and time of the year. The amount of incoming solar radiation can only be adjusted by giving a solar adjustment factor by which all values of the solar radiation will be multiplied. This correction enables more accurate approximation of the actual incoming solar radiation at a certain location. To determine the solar adjustment factor, the standard solar radiation curve of Milan on the 10th of August is compared to the measured global radiation from the weather station Viale Marche. The data from the weather station is given in Milan Daylight-Saving Time (GMT+2) whereas the data from ENVI-met does not take into account the change of the clock and is therefore in standard time (GMT+1). To still be able to compare the two, the solar radiation data from ENVI-met has an extra hour added to it, so both data is given in Daylight-Saving Time in Figure 65.

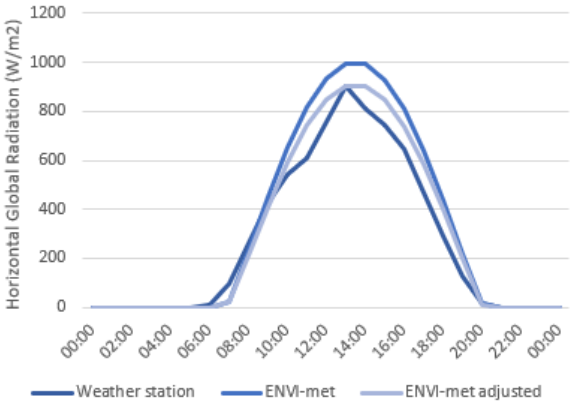

Figure 65: Global radiation at weather station, in ENVI-met and in ENVI-met with solar adjustment factor 0,91

Both the global radiation from the weather station and from ENVI-met show the maximum value at 13:00. But the maximum global radiation in ENVI-met is higher with 994 W/m^2 in comparison to 904 W/m^2 at the weather station. To make the maxima of ENVI-met fit with the actual measurements an adjustment factor of

0,91 is applied suffices. The adjusted ENVI-met global radiation is also given in Figure 65. In comparison to the measurements, the ENVI-met model still slightly overestimates the amount of horizontal global radiation since it follows a perfect curve. The global radiation is made up of direct and diffuse radiation in ENVI-met according to the graph depicted in Figure 66.

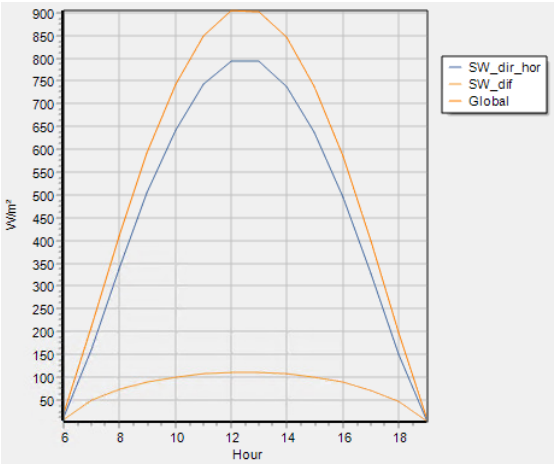

Figure 66: Direct, diffuse and global radiation in ENVI-met

Model timing

Dynamic time step management makes it possible to decrease the running time of the model by increasing the number of seconds per time step. But when there is a lot of solar radiation there is a larger chance of instability in the system and therefore it is desirable to have a smaller time step when the solar angle is large (higher solar intensity). To accommodate this behavior there are three different time steps defined as in Figure 67.

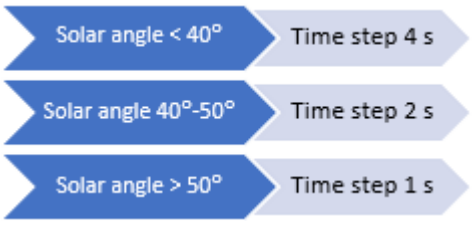

Figure 67: Dynamic time step management

6.4 Results

In this paragraph the results from both the measurements and the simulation are discussed and compared. All results are displayed in Figure 68 and these graphs will be discussed below. When interpreting the results from the graph it is important to keep in mind that the measurements were not only done at different time intervals of 15 minutes as the graphs clearly show, but also at different locations. The height of every measurement location is given in Table 8. This also explains why there is no line between the markers in the graph, since there is not continuation of measurements at the same location. Also it must be noted that the markers in the graph indicate the average measurements of the time period fifteen minutes before, corrected for outliers. For example the marker at 12:30 in the first graph is actually the average value of the period from 12:16-12:30 with outliers removed from the data.

The first graphs shows the air temperature. The air temperature measurements have an accuracy of ± 3,5°C and this is displayed with a vertical error bar in the graph. The temperature in the model shows a steady trend and the temperature increases as the distance from the ground level becomes lower. The differences between the model and the measurements only seem to be significant at the first four measurements more towards the top of the building. At the top of the building wind effects are more noticeable as well as the impact of solar radiation. At the lower levels there is another building facing the east façade of Bosco Verticale Tower D partially protecting this part of the building.

The relative humidity measurements (accuracy ±2,5%) and model simulations follow a similar trend which is opposite to the behavior of the air temperature as is to be expected. When air temperature is higher the air can hold more moisture so relative humidity will decrease. Also the density of air is higher towards the earth surface due to gravitational forces. Therefore the relative humidity is higher at the top of the building and the beginning of the day, but decreases as the measurement height decreases. Again the model shows a steady trend which seems more dependent on the height and location than on the building vegetation, which only slightly influences the relative humidity. In reality around 12:15 the balcony has a lot of vegetation which might explain the high relative

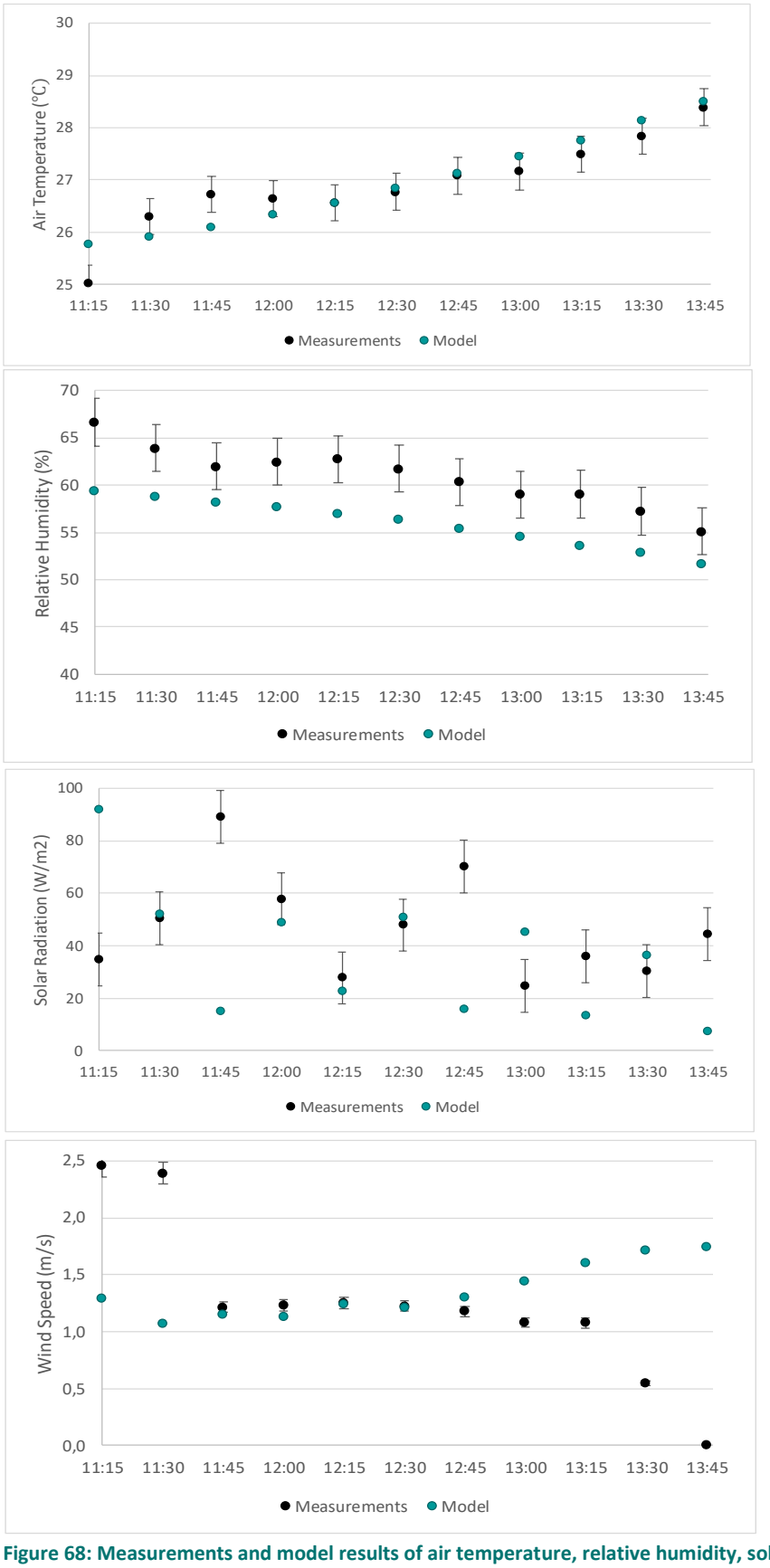

Figure 68: Measurements and model results of air temperature, relative humidity, solar radiation and wind speed

humidity that is measured. The model steadily underestimates the relative humidity with approximately 6%.

The amount of solar radiation that is measured shows no clear trend depending on height. This factor is first and foremost influenced by whether a balcony above the measurement balcony is present and casting a direct shadow. Second there is also the influence of vegetation that can cause a partial shading of the measurement area. Only four out of eleven measurements show no significant error (at the measurement accuracy of 10 W/m^2) between the model and the measurements. It is known to be difficult to estimate the solar radiation, researchers Marc Ottelé and Elena Giacomello both conducted solar radiation measurements on greenery and ran into similar issues of inaccurate measurements in comparison to modelling results. And even with the solar adjustment factor given in ENVI-met already the incoming solar radiation shows a slight error and then the most significant differences are probably caused by the differences in vegetative shadow casting.

Finally, the wind speed measuring device (error of ±1%) shows a decreasing trend over time as the height of the measuring decreases. According to the log-wind profile this is to be expected. Surprisingly, ENVI-met model simulation shows an opposing trend as the wind speed slightly increases as the height of the building decreases. It must be noted however, that the incoming wind in ENVI-met has a fixed direction and flows in layered, whereas wind in reality does not flow in this way and especially in an urban area already shows an irregular pattern due to local air pressure differences and obstructions by buildings further away than is modelled here in ENVI-met. But on average the measured wind speed and the modeled wind speed show similarities.

6.5 Conclusion and discussion

The measurements done on eleven balconies within this limited time frame of course has its limitations. However, some conclusions can still be drawn. In the case of Bosco Verticale ENVI-met seems well capable in predicting the air temperature at different locations and also the trend of the relative humidity, but relative humidity measured was around 7% higher on average than the simulation predicted. Measurements of solar radiation showed some similarities where there was not too much vegetation present on the balcony, but because it is hard to define the shading properties of trees most results from the model significantly differed from reality. The wind speed in general from different locations can be predicted by the model, but because the exact local wind conditions are unknown and constantly changing, it is almost impossible to predict the exact wind speed at a certain time through modelling.

7 Green Balcony Thermal Network

In the previous chapters the heat and moisture transfer of trees was evaluated with a literature study. No example models could be found specifically for a green balcony situation. To get a basic understanding of the heat and moisture transfer on a green balcony, a simplified thermal network model will be presented in this chapter.

7.1 Methodology

The purpose of the thermal network model is to make a simplified representation of a green balcony and the factors that influence the microclimate.

The most simplified model would only contain a building wall and a balcony platform with a tree on it. As discussed in the previous chapters, trees can influence the microclimate by shading, evapotranspiration and wind protection. Since the wind speed in an urban environment is expected to be very low, especially near the buildin2g envelope, the effect of wind is neglected in this thermal network model. Radiation however is expected to be an important factor as the shading of the trees can provide a change in the amount of solar radiation received at both the balcony platform and building façade. Also latent heat transfer should be modeled, since the tree releases moisture which could influence the balcony microclimate. Since most building materials have a high heat storage capacity, the thermal storage of nodes is also modelled.

Assumptions

The radiation from the pavement on the ground level is not taken into account as the balcony is assumed to be on a higher level of the building. The radiation from the higher levels of the building is also not taken into account, as it has a large distance to the balcony. Only the radiation from the building façade directly next to the balcony platform is considered. For simplification, multiple reflections between objects and heat conduction through the building façade and balcony platform are not taken into account. The atmosphere is assumed to have a constant temperature. Also the building wall and balcony parapet are assumed adiabatic, so no heat transfer is conducted through these objects. An overview of the thermal network model is given in Figure 69.

7.2 Model description

This paragraph describes the input, setup and calculation of the thermal network model that was implemented in MATLAB and Simulink.

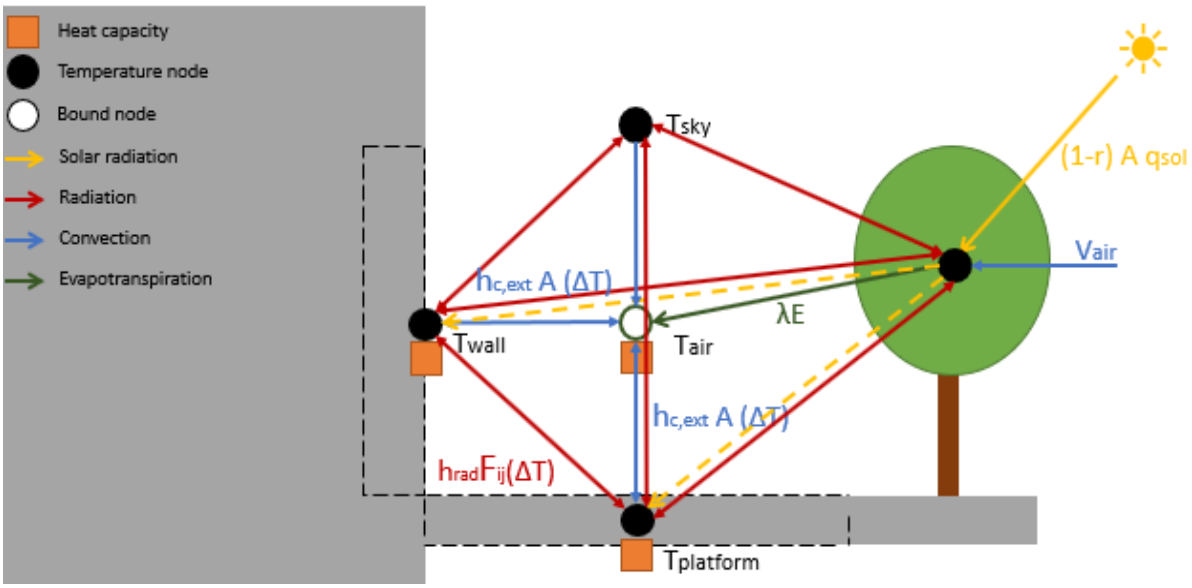

Figure 69: Thermal network model green balcony (illustration by author)

7.2.1 Model input

The following input values were used in MATLAB.

Penetration depth

Instead of calculating the transient heat transfer in the building wall and balcony parapet, an analytical solution is used to determine the penetration depth. For a cyclic surface temperature variation of a semi-infinite thick slab the penetration depth *d** (m) can be calculated according to de Wit (2017):

$$d^* = \sqrt{\frac{a\, t_0}{\pi}} \qquad (7.1)$$

Where *a* is the thermal diffusivity of the material (m^2/s) and t_0 is the time (s). The thermal diffusivity is λ/ρc, which for the material properties of concrete mentioned below yields $6{,}94 \cdot 10^{-7}$ m^2/s. If a daily cyclic temperature variation is considered t_0 is 24 * 3600 seconds. For the concrete in this case that leads to a penetration depth of 0,14 m. This is used as the effective thickness of the wall and balcony platform.

Material properties

1: Building wall

V_{wall} = x * y * z = 0,14 x 8 x 3 = 3,36 m^3
ρ_{wall} = 2400 kg/m^3
c_{wall} = 840 J/(kgK)
λ_{wall} = 1,4 W/(mK)
ε_{wall} = 0,9
Albedo = 0,3

2: Balcony platform

$V_{platform}$ = x * y * z = 3 x 8 x 0,14 = 3,36 m^3
$\rho_{platform}$ = 2400 kg/m^3
$c_{platform}$ = 840 J/(kgK)
$\lambda_{platform}$ = 1,4 W/(mK)
$\varepsilon_{platform}$ = 0,9
Albedo = 0,3

3: Air

V_{air} = x * y * z = 3 x 8 x 3 = 72 m^3
ρ_{air} = 1,2 kg/m^3
c_{air} = 1000 J/(kgK)

Heat transfer coefficients

The convective heat exchange between the exterior of the building surface and the external environment is usually calculated based on the convective heat transfer coefficient $h_{c,ext}$. The convective heat transfer coefficient (W/m^2K) is defined as (de Wit, 2017):

$$h_{c,ext} = \frac{q_c}{T_s - T_a} \qquad (7.2)$$

Where q_c is the convective heat flux, T_s is the surface temperature and T_a is the air temperature. The convective heat transfer coefficient is dependent on several factors such as building geometry, surroundings, surface roughness and wind speed. Analytical, numerical and experimental methods can be used to determine $h_{c,ext}$. Analytical methods are only suitable for simple geometries, numerical methods such as Computational Fluid Dynamics require large computational power and therefore experimental methods are most commonly used. The model by McAdams is often used in building simulation software (Mirsadeghi, et al., 2013):

$$h_{c,ext} = 5{,}678 \left[m + n \left(\frac{V_f}{0{,}3048}\right)^p\right] \qquad (7.3)$$

Where V_f is the free stream wind velocity (m/s), *m*, *n* and *p* are roughness parameters for smooth and rough surfaces as given in Table 12.

Table 12: Parameters in McAdams model (Mirsadeghi, et al., 2013)

V_f < 4,88 m/s			
Surface type	*m*	*n*	*p*
Smooth	0,99	0,21	1
Rough	1,09	0,23	1
4,88 m/s < V_f < 30,48 m/s			
Surface type	*m*	*n*	*p*
Smooth	0	0,50	0,78
Rough	0	0,53	0,78

For a free wind speed of 1,3 m/s (derived from EnergyPlus climate data for Milan) and a rough surface, the model by McAdams leads to a convective heat transfer coefficient of 11,8 W/m^2K.

For radiation it is known that the net rate of heat flow q_{rad} is (Marín, 2009):

$$q_{rad} = \sigma A \varepsilon (T_2^4 - T_1^4) \qquad (7.4)$$

Where σ is the Stefan-Boltzmann constant (5,67 · 10^8 W/m^{2}K^4), A is the surface area of the radiating object (m^2) and ε is the total emissivity of the surface with absolute temperature T_2 (K). If the temperature difference T_2-T_1 is small, then it could be expanded as a Taylor series around T_1 to obtain the linear relationship:

$$q_{rad} = 4\sigma A \varepsilon T_1^3 (T_2 - T_1) \qquad (7.5)$$

Where the radiation heat transfer coefficient $h_{rad} = 4\sigma A \varepsilon T_1^3$.

View factors

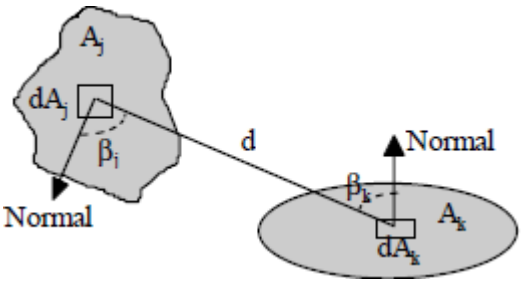

Figure 70: View factor from surface j to k (Jóhannesson, 2006)

The view factor between two diffuse surfaces is equally distributed in all directions from a plane surface *j*. The amount of radiation that reaches the remote surface *k* is determined by the proportion of the hemisphere that is covered by the projection of this surface (see Figure 70). This geometrical quantity can be expressed in the view factor (Jóhannesson, 2006):

$$F_{jk} = \frac{1}{A_j} \int_{A_j} \int_{A_k} \frac{cos\beta_j \cdot cos\beta_k}{\pi \cdot d^2} dA_j dA_k \qquad (7.6)$$

Solving the integral above for two adjacent rectangular plates of equal size at an angle of 90° (Howell, 1982):

$$F_{1-2} = \frac{1}{\pi L}\left(L \tan^{-1}\left(\frac{1}{L}\right) + N \tan^{-1}\left(\frac{1}{N}\right) - \sqrt{N^2 + L^2} \tan^{-1}\left(\frac{1}{\sqrt{N^2+L^2}}\right) + \frac{1}{4}\left\{\ln\left[\frac{(1+L^2)(1+N^2)}{1+L^2+N^2}\right] + L^2 \ln\left[\frac{L^2(1+N^2+L^2)}{(1+L^2)(1+N^2)}\right] + N^2 \ln\left[\frac{N^2(1+N^2+L^2)}{(1+N^2)(N^2+L^2)}\right]\right\}\right) \qquad (7.7)$$

Where $N = c/b$ and $L = a/b$ (see Figure 71). In this model a = 3, b = 8 and c = 3. Therefore $N = L$ = 0,375. This results in a view factor of 0,211 between the balcony platform and building wall.

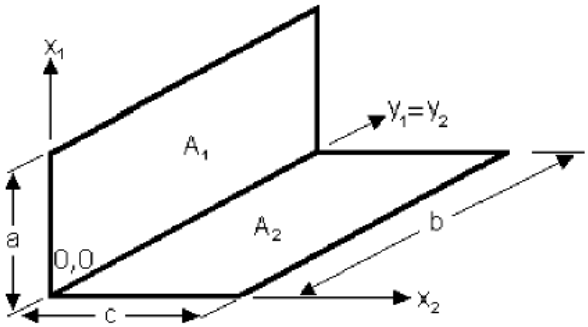

Figure 71: Two orthogonal surfaces with one common edge (Howell, 1982)

Urban climatologists usually use the Sky View Factor (SVF) as a geometric measure that expresses the openness of a point to the sky and therefore the capability to emit and receive longwave radiation to and from the sky. The Liu-Jordan model is one of the most widely used models to obtain the solar view factor (Rehman & Uzair, 2017):

$$SVF = \frac{1 + \cos\beta}{2} \qquad (7.8)$$

Where β is the tilt angle of the plane measured from the horizonal plane. For a vertical façade that is unobstructed by its surroundings the SVF has a maximum value of 0,5 as it can only be seen by half of the sky (Chatzipoulka, et al., 2018). For the horizontal plane of the balcony platform it is more difficult to determine the SVF as the path to the sky vault is partially obstructed by the adjacent wall of the building. But since it is known that the sum of all view factors form a surface has to equal unity (Jóhannesson, 2006):

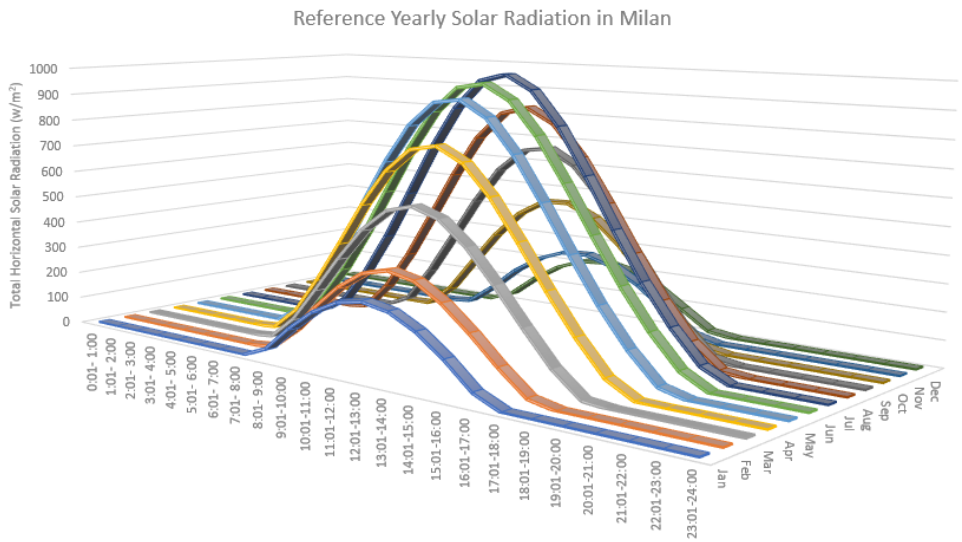

Figure 72: Reference incoming horizontal solar radiation in Milan over a year (image by author)

$$\sum_{j=1}^{n} F_{kj} = 1 \qquad (7.9)$$

Therefore the view factor from the balcony platform to the sky can be assumed 0,789.

Climate data

The reference climate data based on thirty years of measurements in Milan is retrieved from EnergyPlus (EnergyPlus, 2018). The initial temperature is set to 17,8 °C base on the climate data. The yearly solar radiation of Milan was evaluated and the highest amount of solar radiation is received in July (Figure 72) so this data was used as input in the model.

Air temperature

The sky temperature is assumed as dependent on the air temperature. The relation between the air temperature and sky temperature is derived from Straube & Burnett (Straube & Burnett, 2005):

$$T_{sky} = T_{air}\left[0{,}8 + \left(T_{dewpoint} - 273\right) \div 250\right]^{0{,}25} \qquad (7.10)$$

Evapotranspiration

The latent heat exchange from a tree can be represented by the 'big leaf' model. This depends largely on the Leaf Area Index (LAI) of the tree. The latent heat exchange can be represented by the following equation (Graamans, et al., 2016):

$$\lambda E = LAI \cdot \lambda \cdot \frac{\chi_s - \chi_a}{r_s + r_a} \qquad (7.11)$$

Where χ_s is the vapour concentration at the transpiring surface (derived from the Penman-Monteith equation) and χ_a in the surrounding air, r_s is the stomatal resistance and r_a is the aerodynamic resistance.

7.2.2 Mass matrix

The mass matrix indicates the thermal heat mass capacity in Joules/Kelvin by multiplying the mass with the specific heat capacity.

7.2.3 Stiffness matrix

The stiffness matrix defines the thermal coupling between the nodes such as convection, radiation and latent heat transfer. The heat balance in the case of radiative heat transfer is:

$$S_{1,2} = \alpha_{rad}\, A\, F_{1,2} \begin{pmatrix} 1 & -1 \\ -1 & 1 \end{pmatrix} \text{ or } S_{1,2} = \alpha_{rad}\, A\, F_{2,1} \begin{pmatrix} 1 & -1 \\ -1 & 1 \end{pmatrix}$$

The heat balance for convection between air and a surface is described below.

$$S_{1,2} = \alpha_{conv}\, A \begin{pmatrix} 1 & -1 \\ -1 & 1 \end{pmatrix}$$

And the heat balance for advection in the case of two nodes without mass and a known rate of air exchange working both ways:

$$S_{1,2} = \rho\, c\, A\, v \begin{pmatrix} 1 & -1 \\ -1 & 1 \end{pmatrix}$$

7.2.4 Load vector

The load vector Q is determined by the solar gain and the convection coming from the atmosphere. We assume the solar gain is not absorbed entirely, but part is reflected depending on the albedo of the material. The assumed albedo for concrete is 0,3. The hourly q_{sol} in W/m2 data is retrieved from the ENVI-met database of incoming solar radiation for Milan.

7.2.5 Solving the heat balances

Now we can derive the temperature by solving the matrix equations:

M * T(dt) + S * T = Q
T(dt) = M^{-1} * (Q - S * T)
T(t) = $\int_0^t M^{-1}(Q - S * T)dt$

7.3 Results

The simple air temperature model of MATLAB is compared to the simulation results in ENVI-met. The results are shown in the figure below. Since the sky temperature is bound, the air temperature on the balcony shows the same gradient over time. However, the air temperature on the balcony also interacts with the latent heat transfer from the tree and with the surfaces. The surfaces in ENVI-met have a much larger surface temperature than they would get in the MATLAB model. Possible explanation for this is that the ENVI-met model also has an interaction with the wind and might have a different active part of the wall than is calculated here. The walls in ENVI-met are namely also connected to inside the building where an initial temperature is set and then during the simulation there is conduction between the indoor and outdoor air. Also in ENVI-met multiple reflections are considered which could heat the surface temperatures up further. Another uncertainty is the evapotranspiration. In MATLAB it is modelled quite simply, whereas ENVI-met uses the A-gs model.

So it is possible to recreate the results from ENVI-met with a simple thermal network model with short running times, but the results show several degrees difference with the ENVI-met model turning out hotter. Also the thermal network model still depends on the solar radiation input from ENVI-met to calculate how much solar radiation falls on the façade and floor with a tree on the balcony. It would be more suitable to model green balconies in a tool that shows geometry visually. This will be discussed in the next chapter.

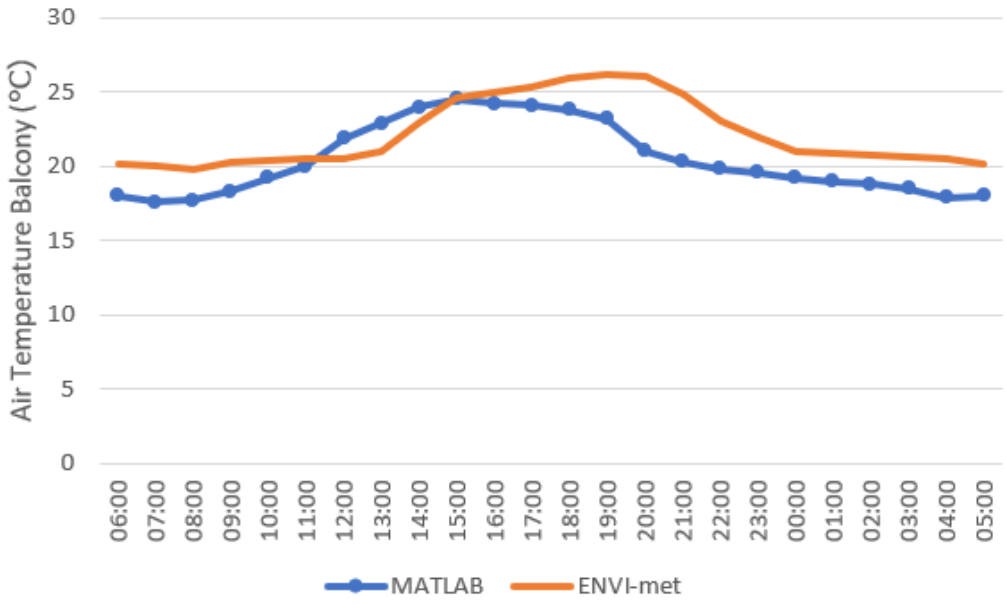

Figure 73: Difference in air temperature balcony between MATLAB en ENVI-met

8 Green Balcony Variant Study

In the previous chapters the microclimate modelling software ENVI-met was validated by first comparing measurements at Bosco Verticale to the microclimate model. Then a simple thermal network was made and compared to ENVI-met for verification. After the validation and verification of ENVI-met, it is now possible to use this method of microclimate modelling as a tool to evaluate the effects of green balconies. The impact of different green balcony parameters is evaluated by performing a green balcony variant study in the following chapter. First the methodology will be discussed, then the model input and variants and finally the results.

8.1 Methodology

The rationalization behind choosing ENVI-met for microclimate modelling in this case has already been treated extensively in Chapter 6. But ENVI-met generates an extensive amount of output and the improvement of the microclimate can also be evaluated in several ways.

As is discussed in the problem context in Chapter 2, one of the main impacts of climate change is that due to the urban heat island effect temperatures will rise substantially in urban areas and this has negative effects on human health. To evaluate the impact of microclimate improvements in the city it is therefore important to predict the effect of microclimate factors on the human body. But there are several ways in which to describe thermal comfort.

8.1.1 Thermal comfort indices

Over the past decades several methods were developed to asses how humans perceive the thermal environment and how their thermal response to different climatic conditions works. Most recent indices capture the performance of in a single value as this is easy to interpret. These indices usually serve three purposes: (i) to identify the possible risk to human health, (ii) to asses the thermal perceptions by humans of the environment both outdoor and indoor and (iii) to assess the climate (Carlucci, 2013). MacPherson (1962) made a classification between different types of thermal comfort indices resulting in three different categories. The first category based on the the calculation of the heat balance of the human body, the second based on physiological strain and the third based on measuring of physical parameters (MacPherson, 1962).

Indices based on the heat balance of the human body combine physiological parameters (wetness and temperature of the skin) with behavioral parameters (metabolic rate and thermal resistance of clothing) and the factors of the thermal environment (air temperature, mean radiant temperature, relative humidity, air velocity, etc). The most widely used early comfort model was proposed by Fanger and based on two indices: the Predicted Mean Vote (PMV) and Predicted Percentage Dissatisfied (PPD) (Fanger, 1972).

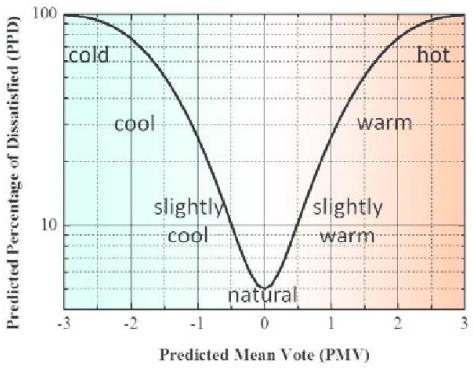

Figure 74: Relationship between PMV and PPD (Fanger, 1972)

The Munich Energy balance Model for Individuals (MEMI) is an example of an energy balance of the human body:

$$M + W + R + C + E_D + E_{Re} + E_{Sw} + S = 0 \qquad (8.1)$$

Where M is the metabolic rate, W is the physical work output, R is the net radiation, C is the convective heat flow, E_D is the latent heat flow through the skin, E_{Re} is the heat flow due to sweat evaporation and S is the storage heat flow for

heating and cooling. The terms in this equation are positive if they result in energy gain (*M)* and negative if they result in energy loss (*W*, E_D and E_{Sw}). The unit of all heat flows is Watt.

The meteorological factors air temperature, air humidity, wind velocity and mean radiant temperature directly influence several factors of the energy balance equation. But it is not accurate to describe thermal comfort with these meteorological factors alone, since that would disregard the thermoregulatory response of the human body. For example, on a day with low wind speed, the mean radiant temperature can have the same importance to the human body as air temperature. But with high wind speed, air temperature could be of more importance (Matzarakis & Amelung, 2008).

This is why the second category of thermal indices was developed. This correlates a wide range of environmental and behavioral parameters with the thermal strain that is put on individuals. The connection between the environmental stress and philological strain is usually expressed mathematically through multiple regression equations. Some examples of physiological strain indices are the Effective temperature, Equatorial comfort index and the Thermal strain index. But most of these were developed to evaluate thermal stress inside buildings.

The Physiological Equivalent Temperature (PET) is one of the most often used thermal comfort indices in the past decades to assess thermal comfort in urban environments (Swaid, et al., 1993). A more recent thermal index is the Universal Thermal Climate Index (UTCI) which also includes acclimatization. However, research in a temperate climate has shown comparable results for UTCI and PET (Matzarakis, Rutz, & Muthers, 2014). In this research therefore the PET will be used.

The PET is defined as the equivalent air temperature required to reproduce in a standardized indoor setting for a standard person the core and skin temperatures that are observed in the real environment. Since PET is expressed in degrees Celsius, it is easy for people to relate to the factor. PMV ranges of satisfaction were translated to corresponding PET ranges, making interpretation of PET even more intuitive. The PET ranges for thermal perception and grade of physiological stress are given in Table 13.

Table 13: Ranges of PET for a standardized person (Matzarakis & Amelung, 2008)

PET	Thermal perception	Physiological stress
4 °C	Very cold	Extreme cold stress
8 °C	Cold	Strong cold stress
13 °C	Cool	Moderate cold stress
18 °C	Slightly cool	Slight cold stress
23 °C	Comfortable	No thermal stress
29 °C	Slightly warm	Slight heat stress
35 °C	Warm	Moderate heat stress
41 °C	Hot	Strong heat stress
	Very hot	Extreme heat stress

The atmospheric output from ENVI-met simulations is used as input for BioMet V1.5. In this module the PET can be calculated for every grid cell based on the Gagge-2-node-model, which combines external heat exchange with a simple two-compartment passive body model and thermoregulatory responses.

8.1.2 Workflow

The choice for ENVI-met software and PET as a thermal comfort index result in the workflow process given in Figure 75. To define the model input, data from Bosco Verticale is used. Tree data from Giacomello is used (Giacomello & Valagussa, 2015) and building information from Stefano Boeri Architetti (Stefano Boeri Architetti, 2018). The model input is then defined in SPACES and saved as an *.inx* file. The ConfigWizard is used to defined the simulation with hourly climate data according to the ASHRAE standard from the EnergyPlus website. The model input and simulation input combined are used to run the simulation in ENVI-met. The simulation in ENVI-met generates a lot of output, but to calculate the Physiological Equivalent Temperature only the air temperature, Mean Radiant Temperature, wind speed and relative humidity are used. The PET

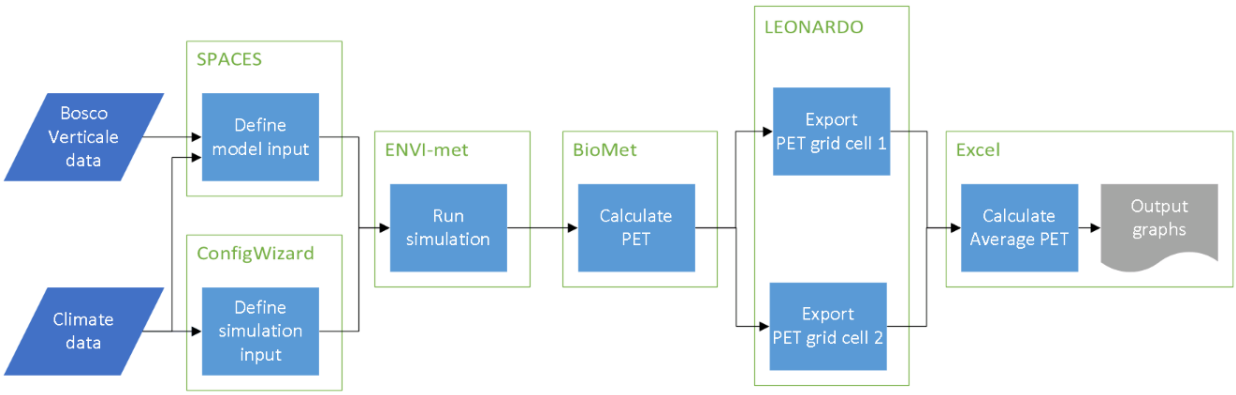

Figure 75: Workflow chart of the variant study

cannot be calculated directly in ENVI-met, so the application BioMet is used for this.

In BioMet some input needs to be defined, such as the metabolism rate and the specific characteristics of the standard human. Then BioMet generates the PET based on the atmospheric output data from ENVI-met. To determine the PET on one specific grid cell, the PET map from BioMet is opened in the visualizer LEONARDO. Then the grid cell 1 (29,38) and grid cell 2 (29,33) are inspected. All relevant factors of the PET and the PET are exported to *.dat* format which can be directly opened with Microsoft Excel. In Excel the export from both grid cells is combined to calculate the average values. This finally results in the output graphs which give information on the thermal comfort on the balcony.

8.2 Model setup

To setup a simulation in ENVI-met first the model and space must be defined, then the simulation input. Both setups will be discussed below.

8.2.1 Model input

The area input is a combination of the material properties and profiles edited in the database manager and the building and environment defined in SPACES. The main model area has a size of 72 x 72 x 48 (x, y, z) with 5 nesting grids (pavement/loamy soil) as an optimal consideration between keeping enough free space around the building for free wind flow and keeping the model area small enough so the run time is not too long. To model at balcony accuracy, the grid size is 1 meter in all directions. The grid size in the z-direction is set to a telescoping grid starting after 26 meters (the height of the building). Location is set to Milan, as is described in Paragraph 6.3.2. The soil profile properties are also similar to that described in Paragraph 6.3.2, but in this case the entire main model area is modelled with concrete pavement.

Building

The modeled building size is 12 x 24 x 24 (x, y , z). The building envelope construction is based on that of Bosco Verticale as described in Paragraph 6.3.2. The only difference in the building envelope is that in this chapter also the glass in the building envelope are modelled. This is done because in

Bosco Verticale every apartment features large glass sliding doors providing a connection to the outside of the building. On a typical balcony sliding doors are of 3 m height and 2 m width. This is modeled as a double glazing unit of similar size. The cross section of the double glazing can be seen in Figure 77, it consists of two float glass panels and an insulation layer. An overview of the glazing material properties are given in Table 14. The material properties of the rest of the building can be found in Table 11.

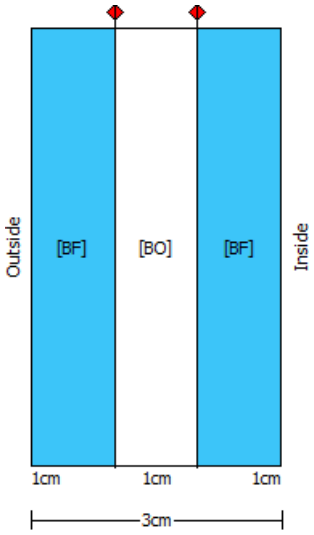

Figure 77: Glazing construction

Table 14: Glazing material properties

Parameter	Value
[BF] Float glass	
Thickness	0,01 m
Absorption	0,05
Transmission	0,9
Specific heat capacity	750 J/(kgK)
Thermal conductivity	1,05 W/(mK)
Density	2500 kg/m^3
[BO] Air	
Thickness	0,01 m
Transmission	1
Specific heat capacity	1006 J/(kgK)
Thermal conductivity	0,025 W/(mK)
Density	1,2 kg/m^3

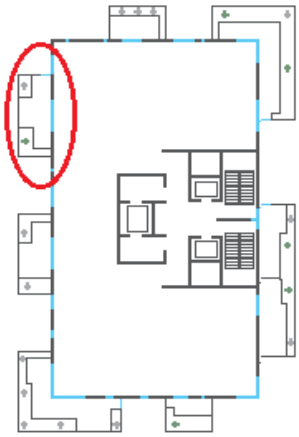

Figure 76: Typical balcony geometry of Bosco Verticale

The input wind speed in ENVI-met is given at 10 m height and the height of the standard human in the thermal comfort model PET is 1,8 meters. To accurately predict the incoming wind speed the floor of the balcony is placed at a height of 8 meters. Since the cooling effect of vegetation is expected to be most significant at the west façade this is the standard orientation of the balcony.

A typical balcony geometry is chosen for modelling (Figure 76). A typical balcony is 8 m wide and 3 m deep with a parapet of 1 m high. Two trees are placed on opposite sides of the balcony and the 2 m wide glazing is located in the center of the balcony. The construction material of the balcony platform and parapet are reinforced concrete and the details can be found in Table 11.

Vegetation

Modeled tree properties are based on the data gathered at Bosco Verticale by Giacomello in 2013 (Giacomello & Valagussa, 2015). Giacomello measured the height of 26 trees on balconies while the building was still under construction. The average tree height was 4,62 m with a minimum of 3,5 m and a maximum of 6,2 m. The medium growth rate of trees is 33-61 cm per year (Dirr, 1990). Assuming a more conservative growth rate due to space constraints, the average tree height is expected to have increased around 1 meter over the course of the past five years. This is in line with the tree design heights of 3, 6 and 9 meters according to Stefano Boeri Architetti. In ENVI-met the smallest resolution to define 3D vegetation is 1 meter and therefore the modelled tree height is chosen at 6 meters.

The tree types studied by Giacomello were mostly of the type European Beech (*Fagus Sylvatica*) and Holly Oak (*Quercus Ilex*). For modeling purposes the European Beech tree type was chosen because this type is readily available in the ENVI-met plant database. Giacomello measured the crown radius of the tree which had a maximum projection of 1,5 m from the tree trunk. The shape

typology of the European Beech is conical (see Figure 78).

Figure 78: European beech photographed on a balcony of Bosco Verticale (Giacomello & Valagussa, 2015)

ENVI-met was not designed to model trees on balconies. In ENVI-met it is only possible to model trees directly on the ground surface or on the rooftop of a building. In order to place trees on the horizontal single wall of a balcony, custom 3D trees were designed with empty (LAD of 0) grids beneath the tree crown. To simulate realistic conditions the tree is lifted 8 meters from the ground to reach the height of the balcony platform and another 1 meter to simulate the height of the plant container on the balcony.

All plants can be categorized according to their carbon concentrating mechanisms. There are three categories of carbon fixation: CAM plants, C_4 plants and C_3 plants. The large majority of plants is of the type C_3 which has the highest carbon dioxide compensation. The European Beech is also a C_3 plant. The characteristic Leaf Area Density (LAD) is an indication of the one sided green leaf area per unit volume of the tree canopy. It describes the vertical and horizontal structure of the tree canopy. The foliage albedo indicates how much short-wave radiation is reflected by the leaves of the tree and for deciduous trees this is typically 18%. A summary of the tree characteristics that were used to define the 3D tree in Albero are given in **Error! Reference source not found.**.

Table 15: Tree properties

Parameter	Value
[F1] Fagus Sylvatica	
Cells (x, y, z)	3 x 3 x (6 + 9)
Shape typology	Conical
Resolution	1 m
Leaf Area Density	2,0 m^2/m^3
CO_2 fixation	C_3 plant
Leaf type	Deciduous leaves
Foliage albedo	0,18
Root depth	1 m

Receptors

Output is automatically generated for all grid cells in the model space and can be viewed in Leonardo. However, to generate more elaborate output of one specific grid cell at different heights in the model space receptors can be placed. This will generate output from the receptors in a spreadsheet format that can be directly imported into Excel. To evaluate the course of climate factors in proximity to the trees, 6 receptors are placed between the trees and the building, see Figure 79.

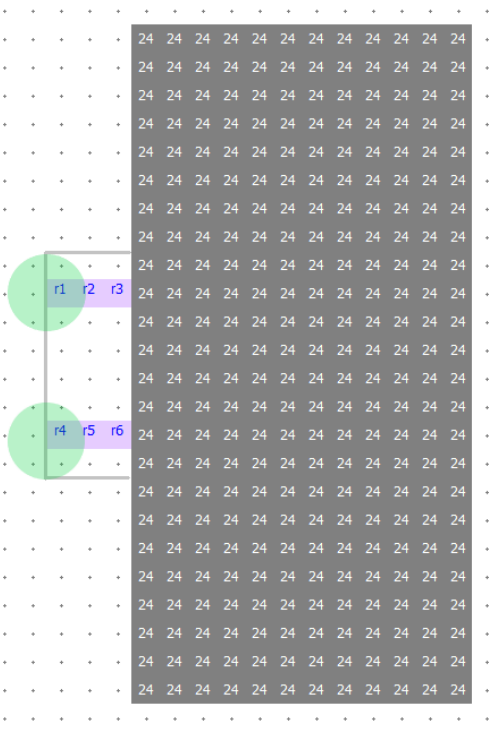

Figure 79: Top view of the building (grey) with green balcony and receptors (purple)

8.2.2 *Simulation input*

In the Configuration Wizard the following simulation input was used.

Time and Date

Since the cooling benefits of trees are expected to be the greatest in summer, the simulation is set to the 21st of July 2018. According to the average daily solar radiation data in July the sun comes up around 5:00 and goes down around 20:00 (see Figure 80). Since the model needs some initialization before the sun comes up it starts at 5:00 and runs until 20:00 (15 hours). The simulation output is written every hour.

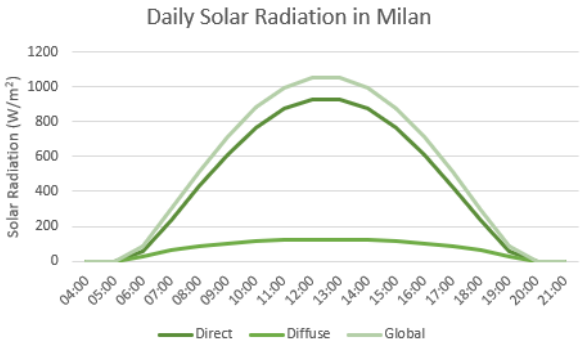

Figure 80: Incoming solar radiation Milan 21st of July 2018

Table 16: Incoming solar radiation Milan 21st of July 2018

Time	Direct radiation (W/m²)	Diffuse radiation (W/m²)	Global radiation (W/m²)
05:00	0	0	0
06:00	59,42	26,34	85,76
07:00	235,7	63,24	298,94
08:00	430,4	87,17	517,57
09:00	613,22	103,56	716,78
10:00	765,72	114,72	880,44
11:00	874,63	121,72	996,35
12:00	931,12	125,1	1056,22
13:00	930,72	125,08	1055,8
14:00	873,44	121,65	995,09
15:00	763,79	114,58	878,37
16:00	610,66	103,35	714,01
17:00	427,36	86,86	514,22
18:00	232,44	62,74	295,18
19:00	56,62	25,44	82,06
20:00	0	0	0

Meteorology

According to the climate files of Milan used in Chapter 7, the average daily wind speed over the month July is 1,3 m/s. This is used as input wind speed in ENVI-met. The roughness length is set to 0,01 m which equals an open flat terrain (see Table 3). The wind direction is set towards the green balcony coming from the west with 270°. The relative humidity is set to 60% which is the average of the hourly humidity data in July according to the climate files. The initial dry bulb temperature at 4:00 is set to 17,8 °C also based on the climate data.

Solar radiation

The total incoming solar radiation is a combination of the direct solar radiation and diffuse solar radiation. In ENVI-met the solar radiation data is calculated automatically based on the sun path for a given location and the input date. The location is set to Milan and the date to the 21st of July 2018. The global, direct and diffuse radiation data is given in Table 16 and is plotted in Figure 80. In the model the cloud cover is set to zero to exclude cloud effects.

Lateral Boundary Conditions

In ENVI-met the Lateral Boundary Conditions (LBC) for turbulence can be set to forced, open or cyclic. In the case of forced or closed LBC the values of the one-dimensional turbulence model are copied to the border. This might be accurate in the case we have a building with absolutely no surrounding obstacles, but in reality the inflow turbulence model is usually somewhat similar to the outflow turbulence model. The forced model is the most stable condition, but shows strong dependency on the one-dimensional inflow model. If instead the choice would be made for open LBC, the turbulence values of the grid point closest to the border are copied to the border for each time step. This would be accurate in the case that the neighborhood of the building is similar to the model area, but there is some room of recovery for the turbulence model. An advantage of this type of LBC is that the boundary has the minimum influence on the results in the middle of the main model. Lastly, in the case of cyclic LBC,

the values downstream of the model are copied to the upstream inflow of the model. Then there is no space for recovery of the turbulence model. This would be an accurate model in for example an urban environment where the inflow is equal to the outflow field.

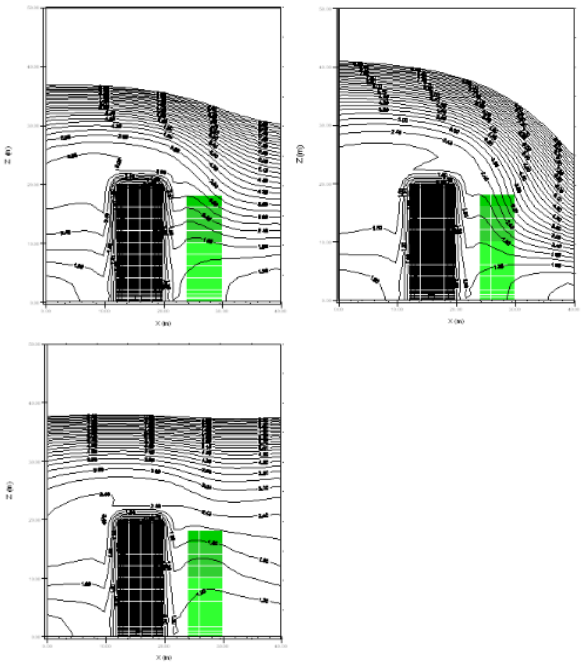

Figure 81: Example of K_m profile with forced, open and cyclic LBC (ENVI-met, 2017)

Figure 81 shows an example which clearly illustrates the effect of the different LBC (forced, open and cyclic) on the vertical K_m profile. The K_m profile is the Von Karman constant times the height in meters and represents the turbulence exchange coefficient. In Figure 81 the turbulence exchange profile is calculated for a simple building with a tree in front of it and the cross section is shown in the x-z direction.

For this variant study the surrounding area is assumed to be empty and the model complexity is high because of the single walls that make up the balcony. To avoid model instability and to simulate empty conditions, the closed Lateral Boundary Conditions are chosen as most suitable.

Model timing

The time step interval of the simulation can be adjusted by the user. A time step that is too small will lead to extremely long run times, whereas a time step that is too large will lead to numerical instability. This makes it challenging to find suitable time steps. Originally the time step in ENVI-met was set to a standard 10 seconds, but in the newer versions of the software the time step varies as the position of the sun changes. This is preferable because smaller time steps are needed when the solar radiation is high in the middle of the day, whereas bigger time steps can be used in the morning or evening. To accommodate this, time step intervals can change as the solar angle changes. When the solar angle is lower than 40° the time step is set to 10 seconds, at a solar angle between 40° and 50° the time step is 5 seconds and at a solar angle higher than 50° the time step is 2 seconds. In the first 30 minutes of the simulation the time step is automatically set to 2 seconds as well, to minimize the chance of numerical instability in the initiation phase. The update timing of the model was not changed from the standard minimum settings.

8.2.3 BioMET input

To calculate the thermal comfort in BioMet the ENVI-met data of the air temperature, mean radiant temperature, horizontal wind speed and specific humidity is used. For the calculation a standard human according to ISO 7730 is used. The standard human in this case is a male of 35 years with a weight of 75 kg and a height of 1,75 m. The metabolic work is set to the standard value of 164,49 W.

Table 17: Typical clothing insulation ensembles (ASHRAE, 2005)

Ensemble description	Insulation (clo)
Walking shorts, short-sleeved shirt	0,36
Trousers, short-sleeved shirt	0,57
Trousers, long-sleeved shirt	0,61
Same as above, plus suit jacket	0,96
Same as above, plus vest and T-shirt	0,96
Trousers, long-sleeved shirt, long-sleeved sweater, T-shirt	1,01
Same as above, plus suit jacket and long underwear bottoms	1,30

The thermal insulation provided by clothing may be expressed in units clo. A single clo equals a resistance of 0,155 W/(m^{2}K) which equals the amount of insulation required to maintain a thermal equilibrium in an environment of 21°C in a normally ventilated room. In Table 17 some typical clothing ensembles with associated clo values are given according to ASHRAE. On a summer day in Milan the average clothing ensemble for males would be (based on a summer visit to Milan) trousers and a short-sleeved shirt, which equals an insulation of 0,57 clo.

The BioMET run times are substantial, therefore the thermal comfort will only be calculated at a certain height. The balcony platform is at a height of 8 meters so calculating the PET given a standard human height of 1,75 m is best approximated with the given resolution at 10 m.

8.3 Variants

The goal of this research is to get a better understanding of the impact of green balconies on the microclimate. For this purpose a variant study is done using ENVI-met. In the previous paragraph the basic model setup was described. But several variants of this basic model will be tested to investigate how individual parameters influence the local microclimate. An overview of all variants with a small illustration is given in subparagraph 8.3.1 and in the following subparagraphs these variants are discussed more elaborately.

8.3.1 Overview of variants

Balcony orientation

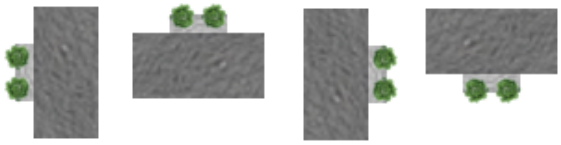

O1 West | O2 North | O3 East | O4 South

Climate

C1 Milan summer | C2 Milan winter | C3 Utrecht summer | C4 Utrecht winter

Wind speed

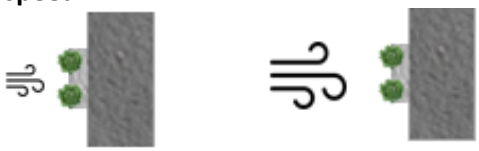

W1 Low wind speed | W2 High wind speed

Wind direction

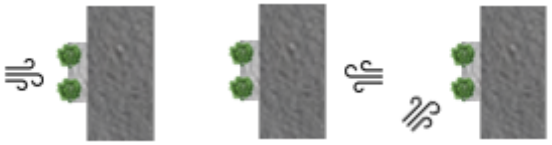

D1 From west | D2 From east | D3 From south west

Tree properties

T1 Normal density, normal albedo | T2 Low density, normal albedo | T3 Normal density, high albedo

8.3.2 Orientation variants

The purpose of the orientation variants is to determine the differences in microclimatic effects as the orientation of the balcony changes. The standard balcony orientation is towards the west. In the space editor the 'model rotation out of grid north' can be defined. This is the number of degrees that the model space is rotated clockwise. Turning the model space 90° out of grid north for example, changes the balcony orientation from its original west orientation to face north.

However, only changing the orientation of the main model area does not change the direction from which the wind enters the model space. So in the example where the model space is turned 90° out of grid north, the wind that would originally be coming from the west direction after rotation of the model space comes from the south. In the variant study it is desirable to change one factor at a time, so to investigate the impact of the balcony orientation the relative direction of origin of the wind should remain the same as the base case. This would be a wind arriving perpendicular to the balcony orientation. To achieve this result both the model rotation out of grid north and wind direction should be perpendicular to one another. Four variants in the main wind directions are considered. The resulting orientation variants are given in Table 18.

Table 18: Orientation variants

Parameter	O1	O2	O3	O4
Balcony orientation	West	North	East	South
Model rotation	0°	90°	180°	270°
Wind direction	270°	0°	90°	180°

8.3.3 Climate variants

The purpose of the climate variants is to investigate under which climate conditions it is most beneficial to place a green balcony. Since the first vertical forest was located in Milan and a new vertical forest is planned in Utrecht, these two locations will be considered.

To compare the climate of Utrecht and Milan, it is useful to evaluate how the climate classifications of the Netherlands and Italy compare. One of the most widely used climate classification systems is the Köppen climate classification. This system makes a distinction between five main climate types: *A* (tropical), *B* (arid), *C* (temperate), *D* (continental) and *E* (polar). The second letter in this classification system indicates the seasonal precipitation and the third letter the level of heat (Chen & Chen, 2013). According to this system Milan has a *Cfa* climate, which is a temperate climate without a dry season (*f*) and with a hot summer (*a*). The climate of Utrecht is classified as *Cfb*, which is also a temperate climate without a dry season, but with a warm summer (*b*).

In Figure 82, the average daily solar radiation in both Milan and Utrecht on the summer day 21st of July and winter day 21st of January are visualized. This data was retrieved from ENVI-met, which automatically calculates the incoming horizontal solar radiation based on the given location and date. Since the difference in location between Utrecht and Milan is relatively limited, so is the difference in incoming solar radiation. The combined direct and diffuse solar radiation on a horizontal plane in summer reaches a maximum of 1056 W/m^2 in Milan and 986 W/m^2 in Utrecht. The solar radiation in winter reaches a maximum value of 377 W/m^2 in Milan and 246 W/m^2 in Utrecht.

Additional climate data was retrieved per location from the EnergyPlus website (EnergyPlus, 2018). The city of Utrecht is located in closer proximity to the sea than Milan. This partially explains the difference in relative humidity between Milan and Utrecht, which are 60% and 87% respectively. Also the height above sea level differs, whereas Utrecht is only 2 m above sea level Milan is located at 103 m above sea level. The exact location coordinates for Bosco Verticale and Wonderwoods were retrieved from Google Maps and used as input in ENVI-met SPACES.

In a different climate it is to be expected that people will dress accordingly. In the summer a clo of 0,57 was chosen, as explained in paragraph 8.2.3. In winter in both locations it is to be expected that people will wear trousers combined

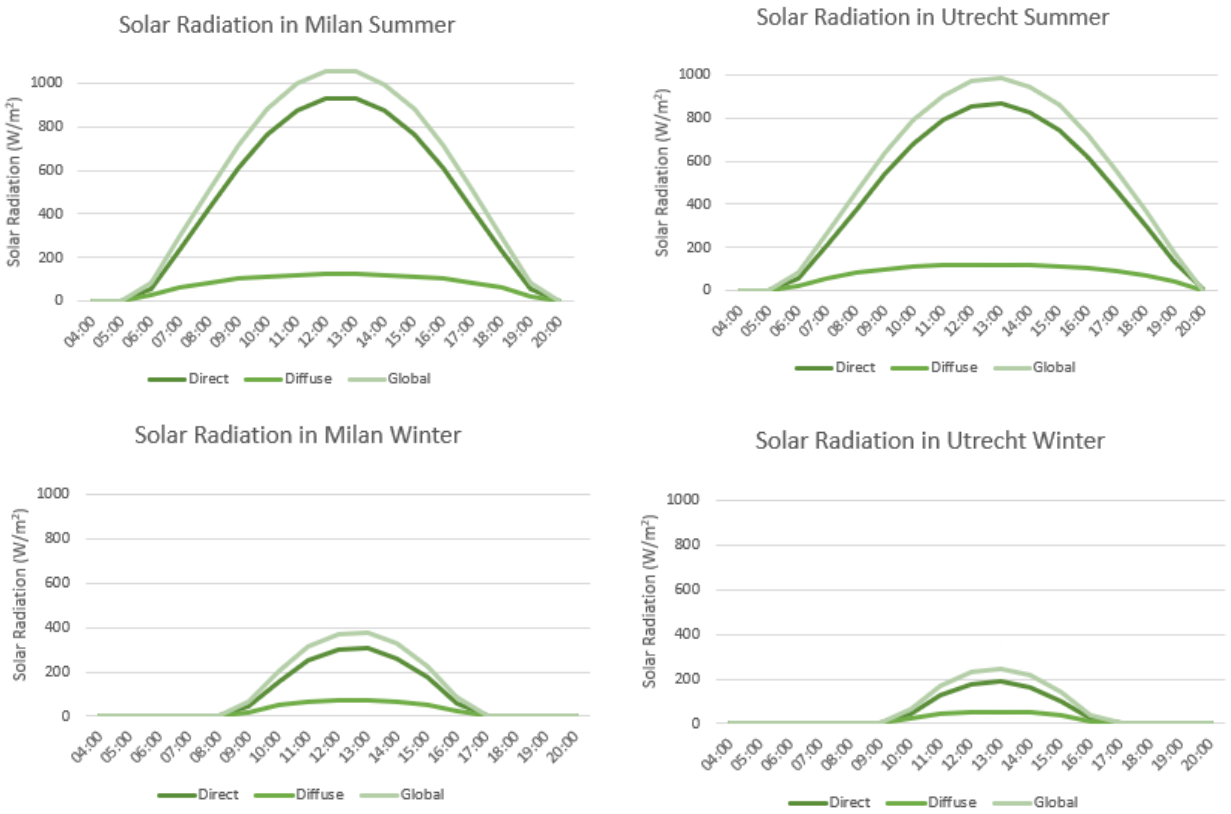

Figure 82: Daily average horizontal solar radiation in Milan/Utrecht on the 21st of July 2018 (summer) and the 21st of January 2018 (winter)

Table 19: Climate variants

Parameter	Variant C1	Variant C2	Variant C3	Variant C4
Location	Milan		Utrecht	
Latitude/Longitude	45,29°N 9,11°E		52,08°N 5,11°E	
Above sea level	103 m		2 m	
Date	21-07-2018	21-01-2018	21-07-2018	21-01-2018
Relative humidity	60%	60%	87%	87%
Initial temperature	17,8 °C	-0,3 °C	14,0 °C	4,0 °C
Clothing insulation	0,57 clo	1,49 clo	0,57 clo	1,49 clo

with a T-shirt, long-sleeved shirt and long-sleeved sweater (1,01 clo). Outdoors this clothing will be complimented with a thick jacket (0,48 clo) (ASHRAE, 2005). This results in a total clothing insulation of 1,49 clo in winter.

An overview of the four chosen climate scenario's is given in Table 19. Variant C1 and C2 are both located in Milan, C1 on a summer day and C2 on a winter day. Variant C3 and C4 are both located in Utrecht, with C3 on a summer day and C4 on a winter day.

8.3.4 *Wind speed variants*

The purpose of the wind speed variants is to determine how the wind influences the spread and intensity of the microclimate effects. The original wind speed in Milan was 1,3 m/s, then the double wind speed was tested and ran without issues. But the turbulence model runs into stability issues at the triple wind speed of 3,9 m/s, therefore only two wind speeds are evaluated. Variant W1 has the original wind speed of 1,3 m/s and variant W2 has the double wind speed of 2,6 m/s. The wind speed variants are given in Table 21.

Table 21: Wind speed variants

Parameter	W1	W2
Wind speed	1,3 m/s	2,6 m/s

8.3.5 Wind direction variants

The purpose of the wind direction variants is to determine how the wind direction of origin influences the spread and intensity of the microclimate effects of green balconies. The wind is coming from the west in the original scenario D1 since this was the wind direction at which the cooling effect at the building façade was expected to be the largest as it moves from the vegetation to the façade. The opposite effect is studied at variant D2 where the wind comes from behind the building and the effect is expected to be more minimal. The third variant considers how the wind effects will spread when the wind direction is not orthogonal to the building but comes from a cross direction, such as the south west. For all variant the wind direction of origin is given in degrees, where 0° means the wind is coming from the north and 90° means the wind is coming from the east. An overview of the wind direction variants are given in Table 22.

Table 22: Wind direction variants

Parameter	D1	D2	D3
Wind direction	270°	90°	225°

8.3.6 Tree type variants

The standard variant tree has a foliage albedo of 0,18 and Leaf Area Density of 2 which is derived from measurements by Giacomello. The standard values for foliage albedo can be found in the Albero database for thirty deciduous tree types which are common the Northern European regions. Several variables are defined for the trees, but the ones that directly impact the evaportranspiraiton and shading properties are the leaf area density and the leaf albedo. The albedo is expressed as a number between 0 and 1 where an albedo of 0,18 means 18% of the short-wave radiation received at the surface of the tree canopy is reflected back to the sky. However, there are also tree types for which the albedo can reach up to 0,7 since the leaf color of these trees is different and the surface has a more reflective surface properties. The tree types with a higher foliage albedo than 0,18 are listed in Table 20 below.

Table 20: Tree types with higher albedo than 0,18

Foliage albedo	Tree types
0,50	*Citrus Aurantium* *Populus Nigra* *Privet* *Tilia*
0,60	*Albizia Julibrissin* *Cercis Siliquastrum* *Fraxinus* *Jacaranda Mimosifolia* *Palm Washingtonia* *Senegalia Greggii* *Sophora Japonica*
0,70	*Koelreuteria Paniculata* *Populus Alba*

To investigate the impact of choosing a tree type with a higher foliage albedo compared to the original scenario, a variant with an albedo of 0,70 is also investigated which is common for the *Koelreuteria Paniculata* and *Populus Alba* tree types. The standard Leaf Area Density was based on the measurements from Bosco Verticale, but in literature both higher and lower values for the Leaf Area Density were found. Since the case of a lower Leaf Area Density is more likely for this case since the trees are relatively small in size, this variant is also investigated. An overview of the three tree type variants that were studied is given in Table 23.

Table 23: Tree type variants

Parameter	T1	T2	T3
Leaf Area Density	2,0 m^2/m^3	1,0 m^2/m^3	2,0 m^2/m^3
Albedo	0,18	0,18	0,70

8.4 Sensitivity analysis

A sensitivity analysis is done to check how the model works dynamically. This is done by changing the input of the model and evaluating how this influences the model outcome.

8.4.1 Sensitivity of receptor height

The height of the receptors was chosen to approach the height of a standard human (1,75 m) on the balcony platform with the given resolution (1 m). Since the platform is located at 8 m height this results in a receptor at a height of 10 m. To research how this choice affects the simulation outcomes, an analysis is done of results for a different receptor height. The lower receptor heights closer to the balcony platform are not evaluated, since the PET at these heights is expected to be higher as a result of a high Mean Radiant Temperature. The MRT will be higher closer to the balcony platform since the grid cell will be enclosed on three sides by the building, balcony platform and parapet. This rationalizes why the sensitivity analysis is only done for greater heights than the original height of 10 m. Also a height of 11 m and 12 m is evaluated. The analyzed receptor heights are depicted in Figure 83.

At the chosen heights the PET is calculated with BioMet at 16:00 since the cooling effect is substantial at this time. Then in LEONARDO the values of the two receptor grid cells are exported and the average values are calculated. Table 24 shows the results of the sensitivity analysis of the receptor height. Remarkably, the cooling effect of the PET at a height of 10 and 12 m is similar. The PET cooling at the intermediate height 11 m is 19,8% higher. The sun moves from a higher position to a more horizontal position around 16:00 which would result in a greater shading effect and therefore lower MRT around the center of the tree crown. This shading effect might explain the cooling differences. The difference in temperature caused by the receptor height seems significant. But still the choice for a receptor height of 10 meter is most sensible, since it is common practice to calculate thermal comfort close to the height of a standard human.

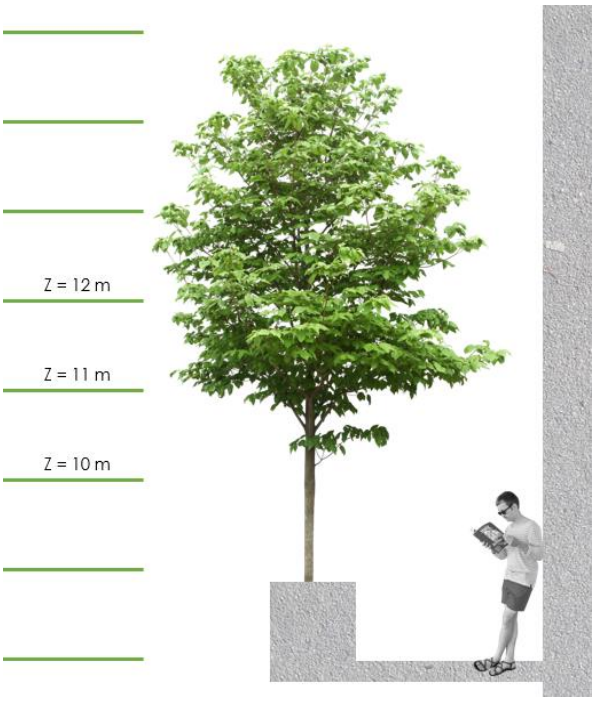

Figure 83: Analyzed receptor heights (illustration by author)

Table 24: Sensitivity analysis receptor height at west orientation 16:00

Receptors Height	Average PET without Trees	Average PET with Trees	Average PET Cooling
Z = 12 m	50,5 °C	37,9 °C	12,6 °C
Z = 11 m	52,4 °C	37,3 °C	15,1 °C
Z = 10 m	51,1 °C	38,5 °C	12,6 °C

8.4.2 Day cycle simulation time

Figure 84: Simulation time 24 hours

For the first simulation of the model the simulation time was set to 24 hours to evaluate the behavior of the PET over a longer period of

time. The results of this long run time is given in Figure 84. As was to be expected, the cooling benefit only occurs during the day time when there is incoming solar radiation, since only in this case there is any evapotranspiration and shading by the trees. The sun goes down after 20:00 so the simulation time can end at this time. This shorter simulation time will reduce the run time of the model, without influencing the relevant model output. The cooling effect by the vegetation is noticeable from 13:00 to 20:00 when the direct shading effect from the tree on the building is the largest. If only the vegetative cooling effect is the subject of interest, it is also possible to diminish the run time to this period, with an hour of initialization time.

8.5 Results

The variants described in the previous paragraph were simulated according to the workflow given in Figure 75. The results of the simulations are given in this paragraph.

8.5.1 Standard variant

The standard model was described elaborately in paragraph 8.2. Here the results from the simulations will be discussed.

PET parameters

In Figure 85 the results of the situation with and without trees are given for the standard model variant. Both graphs show the PET and three factors that influence the size of the PET: air temperature, humidity and Mean Radiant Temperature.

The specific humidity graph does not show a significant difference in both scenarios, the humidity was expected to be higher in the case with trees due to evapotranspiration by the leaf stomata. At closer inspection of the model results it appears that the vapor flux from the leaves at the receptor height is only in the range of 0,01-0,05 g/kg*m/s which is almost negligible. The evapotranspiration rate is low since there are only two small trees present. Even though the wind speed is also a factor that influences the PET, it is not shown in the graphs because this is fairly constant. The average wind speed is 0,14 m/s with a maximum of 0,16 m/s and minimum of 0,12 m/s. These low wind speeds are a result of the already low incoming wind speed caused by a high roughness length in the urban environment and the diminishing of the wind speed by the building façade and balcony parapet. Another cause of the low evapotranspiration is the root size of the trees. The root size determines the amount of water the tree can absorb from the soil and therefore transpire. Since the tree is located in a dimensionally constrained container, the root size is limited.

The air temperature curve also only shows a small response to the presence of the trees. A change in air temperature could be caused by a change in wind speed or direction and moisture content in the air. But since the wind speed is relatively low and evapotranspiration as well, the change in air temperature is not considerable.

As the other factors only show slight changes as a result of the presence of trees, the decline in the PET seems to be mainly caused by the change in Mean Radiant Temperature. The MRT in Figure 85

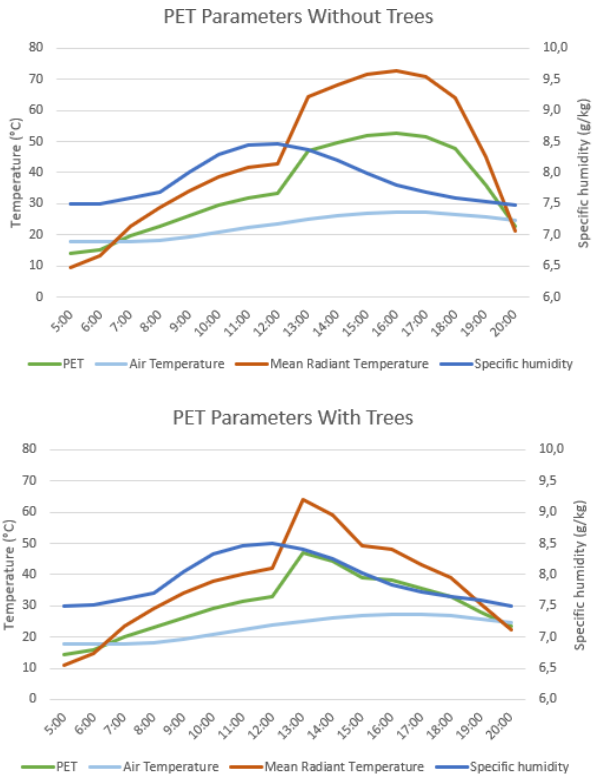

Figure 85: PET parameters without/with trees in Milan

shows two critical points: at 12:00 and at 20:00. At 12:00 the sun turns around the corner of the building and the western façade receives direct solar radiation for the first time. At 20:00 the sun goes down behind the parapet of the balcony and no more direct solar radiation is received.

PET over time with and without trees

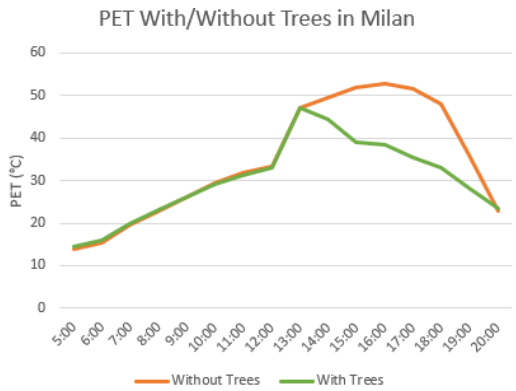

Figure 86: PET with/without trees in Milan

In Figure 86 the PET with and without trees are compared. It can be noted that these curves generally follow the shape of the MRT. The first tree provides solar shading at 14:00 and as the sun turns towards the west, the other tree also provides shade. As the sun goes down and amount of solar radiation increases, the cooling effect of the trees also diminishes. After the sun has gone down, the PET curve of the scenario with trees returns to normal. The area under the orange graph represents the cooling effect caused by the vegetation.

8.5.2 Orientation variants

The results of the PET calculation for different orientations is given in Figure 87. As is to be expected the east and west orientation show many similarities and the north and south orientation also.

The west orientation only receives indirect solar radiation in the morning and as a result the PET already increases steadily. Around 13:00 the solar path turns across the corner of the building to reach the west façade and the tree shading provides a sharp decline in the PET where otherwise the maximum would be reached around 16:00 in the afternoon.

The east orientation results in a lower maximum temperature than the west orientation, but the extent to which the trees cool the microclimate is similar. At the eastern orientation, the direct solar radiation is already received at the start of the simulation. Without trees the PET increases until it reaches a plateau around 46 °C. When the sun disappears behind the building between 12:00 and 13:00 this results in a sudden drop in PET.

In contrast with the east and west orientation that only show one critical point, the north and south orientation show two critical points in the course of the PET. As the sun travels from the east to the south, around 8:00 the path turns the building corner and the northern balcony no longer receives direct solar radiation because of shading by the building. Between 16:00 and 17:00 the direct solar radiation appears again from the west side of the building and causes another peak in the PET. Again the temperature at the end of the day is significantly higher than earlier due to thermal storage of the building materials. Since the solar radiation is interrupted by the building shade in the middle of the day, the cooling effect of the trees is limited. During the shading time the PET recovers and the temperature with trees rises again to meet the temperature of the scenario without trees. Even though the starting temperatures are very different, the range of cooling by the trees at the beginning and the end of the day show great similarity.

The south orientation PET behaves different. In this variant the green balcony is in the shade of the building at the beginning and end of the day. Due to the increased air temperature the PET slowly increases as the day progresses. The trees provide a cooling effect much larger than with a northern orientation, but at the end of the day the PET returns to the same level as it would be at without tree shading. The cooling benefits of the trees are limited in time.

To easily compare the benefits of the different orientations, a new term is introduced, namely

Figure 87: Thermal comfort with/without trees for west, east, north and south orientation

the PET degree hours. This parameter indicates how much the thermal comfort improves by either cooling or heating of the microclimate. For example the PET cooling degree hours can be calculated in the following manner. In Figure 87 the area between the graph without trees and the graph with trees is determined. The PET cooling degree hours are positive if the values with trees are smaller than the values without trees, since this means the trees provide a cooling effect. However, under the thermal heat stress threshold of 23 °C it is undesirable to provide cooling, since this is already in the comfortable range. So only above this line the areas between the two curves are calculated. The same kind of calculation is done for the PET heating degree hours. Under the threshold of 18 °C it is beneficial if the trees would provide an increase in temperature, so this effect is perceived as positive.

The PET degree hours make it possible to compare the heating and cooling benefits of different variants. The results are given in Figure 88. The PET heating benefits are negligible in comparison to the cooling benefits. In all cases the trees provide cooling benefits. At the north orientation the benefits are the smallest, followed by the south orientation. At both the east and west orientation the cooling benefits are substantial. The east orientation has a slightly more positive effect reaching a cooling benefit of 1076 PET degree hours.

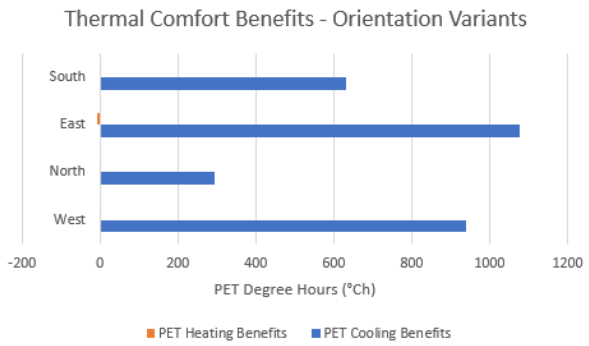

Figure 88: Thermal comfort benefits of orientation variants

These results can be compared to a study done by Simpson & McPherson (1996). In their research the combined cooling effect of trees (shading, increased humidity and less infiltration) has shown to have a significant impact on the energy needed for cooling. A study in California on over 75,000 yard trees shows the significant impact that shade trees can have on the building energy consumption. The potential effects of the tree shading on the air conditioning and heating was considered for different tree orientations, insulation levels and climate zones. It turned out that tree shading on the west side produced the largest annual and peak energy savings, followed by southwest trees and east bound trees (only in annual peak savings). It was found that the placement of three trees close to the residential homes reduced annual energy use for cooling 10-50% and peak electrical use by 23%. With the exception of climates with a low air-conditioning demand, the cooling load reductions were always higher than the increased heating load from south trees in the winter. In warmer climates the air-conditioning savings were largest, whereas the percentage savings were larger in cooler climates (Simpson & McPherson, 1996). The effects in this study were more significant due to three reasons. First of all it did not only evaluate microclimatic effects, but the actual energy use which includes the impact of less infiltration due to tree placement. Also the paper evaluated the energy use over a whole year, whereas this study only considered one day. And finally, the research by Simpson & McPherson was conducted in the climate conditions of California (Köppen classification *Csb*) which in general has higher temperatures in summer than Milan (classification *Cfa*).

8.5.3 Climate variants

An overview of all climate variant PET simulation is given in Figure 89. When comparing the Utrecht summer temperature gradient to that of Milan it is notable that there are fewer hours in which the solar radiation reaches the balcony. As a result the cooling effect of the trees only lasts for three hours as compared to six hours in Milan. The maximum cooling effect is reached at 15:00 in Utrecht, whereas the maximum temperature decrease in Milan is at 18:00 more towards the end of the day.

The boundary values of the PET between which there is no thermal stress, this is between 18 and 23 °C. In the Milan climate the main issue with the climate is that the temperature is too high and there is slight thermal heat stress even before direct solar radiation hits the building façade. In Utrecht there is mainly cold stress before the

	Milan Summer		Milan Winter		Utrecht Summer		Utrecht Winter	
Time	Without trees	With trees	Without trees	With trees	Without trees	With trees	Without trees	With trees
5:00	13,9	14,5	7,9	8,3	12,7	13,1	9,6	9,6
6:00	15,3	15,9	7,4	7,8	13,9	14,4	9,1	9,2
7:00	19,7	20,0	7,0	7,4	17,8	18,3	8,8	8,9
8:00	22,8	23,1	6,6	7,1	20,8	21,1	8,5	8,7
9:00	26,2	26,2	7,9	8,4	23,9	24,0	8,3	8,5
10:00	29,5	29,1	9,9	10,3	26,9	26,8	9,6	9,8
11:00	31,9	31,3	11,0	11,4	29,2	28,8	11,1	11,1
12:00	33,5	33,0	11,5	12,0	30,7	30,2	11,7	11,9
13:00	47,2	47,1	29,1	24,0	46,2	46,7	27,3	27,2
14:00	49,6	44,4	28,9	17,7	49,1	42,1	26,9	26,9
15:00	51,9	38,9	26,3	15,7	51,1	37,2	23,8	15,9
16:00	52,8	38,4	19,1	12,5	52,0	35,8	15,2	11,7
17:00	51,6	35,5	7,4	7,9	51,2	33,3	8,6	8,8
18:00	47,9	32,9	6,9	7,4	48,0	31,0	8,3	8,5
19:00	35,9	28,1	6,5	7,1	40,0	27,7	8,1	8,3
20:00	22,8	23,3	6,3	6,8	21,9	22,3	7,9	8,1

Figure 89: PET for climate variants

direct solar radiation reaches high intensity. In the afternoon the thermal stress only becomes slightly warm, so the thermal stress does not improve significantly by adding trees.

The cold stress is indicated in blue and the heat stress in red. White values indicate that the temperature range is experienced as comfortable for a standard human. The table illustrates the effect of the trees is mainly noticeable in the afternoon, when the sun hits the west oriented balcony.

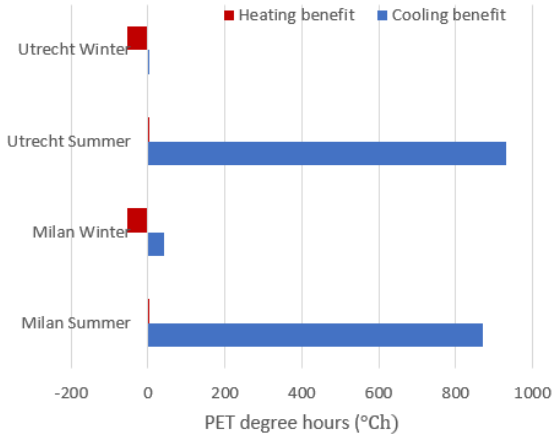

Figure 91: PET heating and cooling for climate variants

In Figure 91 the improvement of thermal comfort both in cool and heat stress is normalized. What this shows is that trees can provide a cooling benefit of up to 16°C in the afternoon in a warm climate, whereas the thermal comfort in a cold climate does not improve significantly. In a cold climate the thermal comfort even slightly decreases in the afternoon as the trees provide shade and drive down the temperature in an already cold environment.

8.5.4 Wind speed variants

The different wind speed variants mainly influence how the cooling effect of the trees is spread along the building facade. Due to the long run time of the simulations, only two variants could be simulated. In Figure 90 the results from the two variants are shown. The figure shows the three-dimensional image of the model from the west orientation with the balcony and building displayed in white. On the balconies actually two trees are present as described before, but they

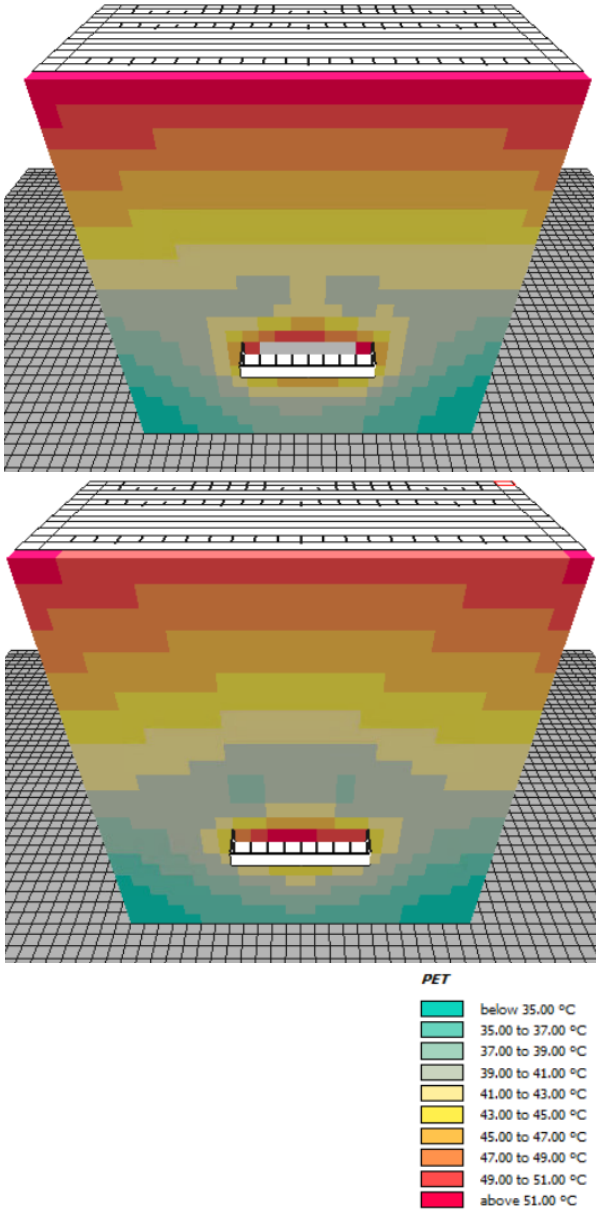

Figure 90: PET along west building facade height at 16:00, variant with low wind speed (top) and high wind speed (bottom)

were left out of this image to show the PET along the height of the west building façade at 16:00. The top image shows the variant where the wind speed is coming from the west (perpendicular to the building façade) and the wind speed is 1,3 m/s. The bottom image shows the variant where all conditions are kept the same, except the wind speed is doubled to 2,6 m/s. By increasing the wind speed the cooling effect of the trees standing directly in front of the façade is projected with more power towards the building. This causes a lower average PET at larger wind

speeds along the façade. The façade around the balcony platform however, shows a higher PET due to the reflection from the balcony itself which causes a higher Mean Radiant Temperature. And the balcony platform also influences the direction at which the lower PET spreads along the building façade. At the lower wind speed the lower PET is mainly directed downwards, but as the PET increases the cooling effect directed downwards stays similar whereas the cooling effect direct upwards from the balcony increases.

8.5.5 Wind direction variants

Different wind directions of origin result in different local wind speeds depending on the geometry of the objects in the area. In Figure 92 the simulation model area is viewed from the top, showing the building roof as a black rectangle and the trees on the balcony as green shapes near the west façade of the building. The cross section is made at the height of 12,5 m and the simulation time is 16:00. The incoming wind speed for all variants is 1,3 m/s, but due to the roughness length of the urban area that is input in the simulation setup (0,001 m) and because there is an invisible nesting grid area around the main model area, the incoming wind speed is already slightly reduced when it reaches the main model area that is depicted here.

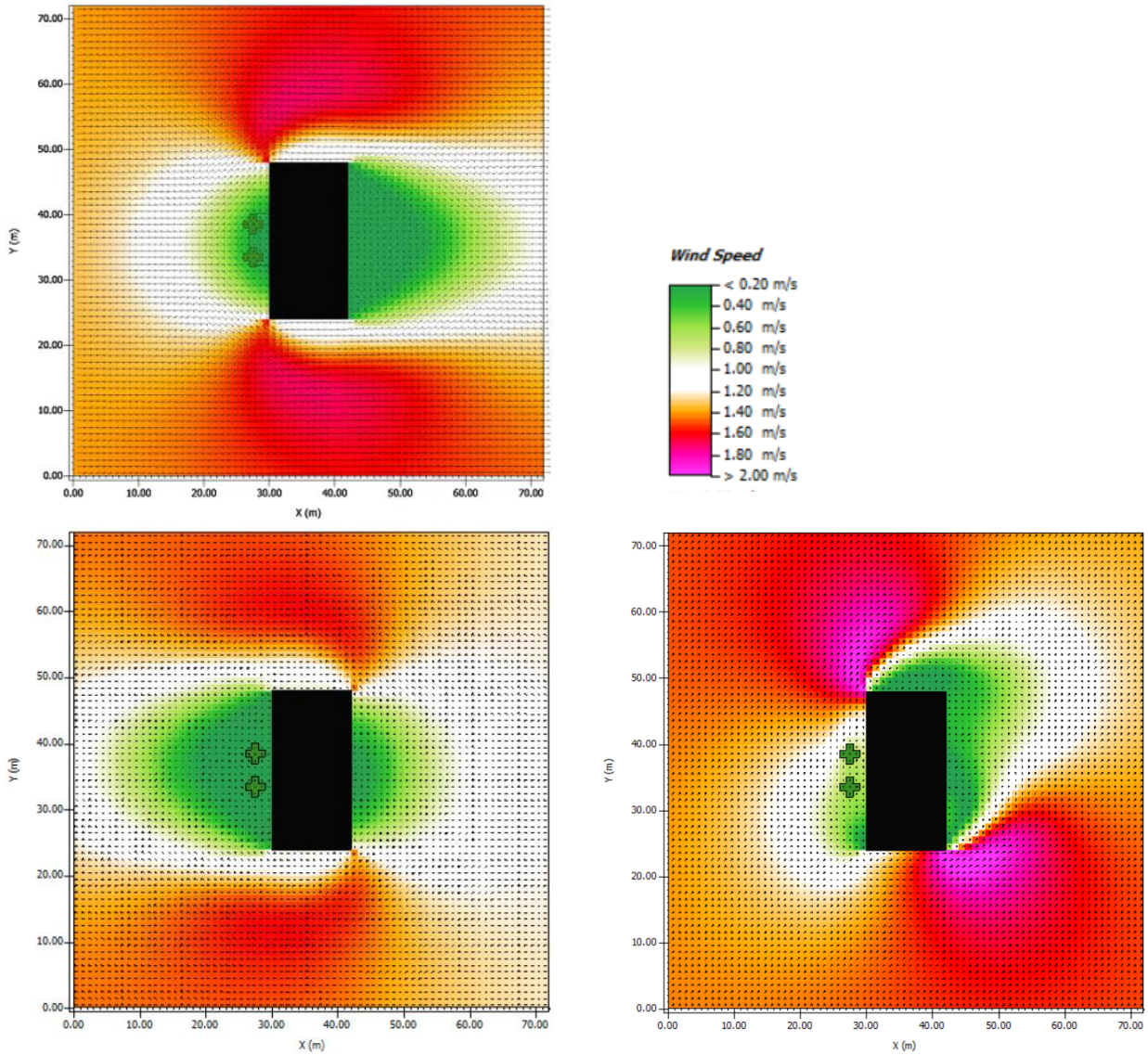

Figure 92: Top view of wind speed with wind from west (top left), from east (bottom left) and from southwest (bottom right)

The top left simulation output in Figure 92 show the variant where the wind comes from the west, perpendicular to the green balcony. The figure is similar to previous research on wind around research (Kleerekoper, et al., 2016) and shows that on the windward side of the building the wind speed reduces to almost 0 m/s as it approaches the building façade. Around the windward corner of the building significantly stronger gusts of wind can be found. The most wind speed reduction can be found on the leeward side of the building where the wind speed slowly increases as the wind flow returns to a more steady and less turbulent flow pattern.

The bottom left simulation output in in Figure 92 shows the case where the wind comes from the back side of the building, so from the east in this case. The pattern is similar to the wind coming from the west and the trees only have a small wind reducing effect on the wind speed in this case which is already very low since this is a model of the urban area of Milan. Finally, the bottom right output in Figure 92 show the case where the wind comes from the southwest. This results in higher wind speeds on the balcony, but also stronger gusts of wind on the north-west and south-east corners of the building. The spread of the lower wind speed reaches less far with a non-perpendicular incoming wind speed. But a larger area of low wind speed is situated directly around the building.

This understanding of the wind flow around the building is necessary to interpret the results that can be found in Figure 93. This shows again a three-dimensional image of the PET along the west façade of the building for the different wind orientation variants. The first variant has wind coming perpendicular to the building. The trees improve the PET and this effect is taken by the wind to move downward towards the street level. The second variant, with the wind coming from the direction behind the building, has a stream of wind moving downwards and out along the west façade of the building. As the wind moves past the trees, the improved PET is also moved downwards but also more towards the lower corners of the building. The scenario with wind coming from the

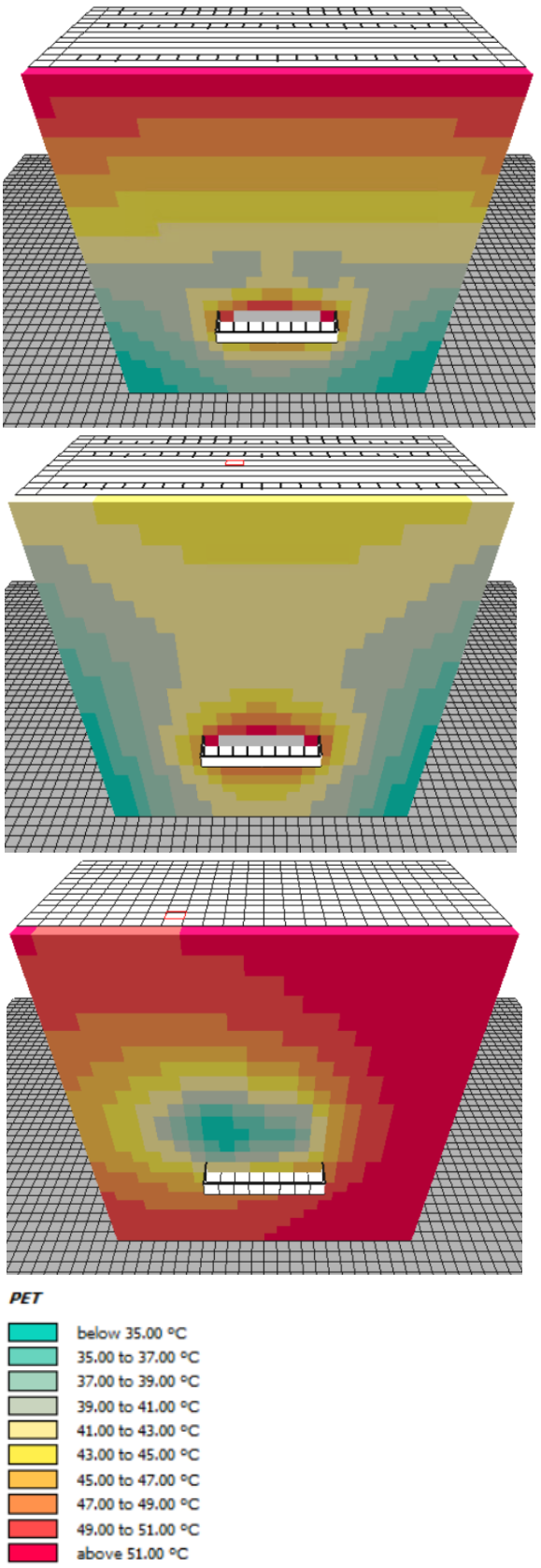

Figure 93: PET along the west facade height for wind from west (top), east (middle) and southwest (bottom)

opposite side of the balcony results in a better thermal comfort near the entire building façade. Finally, the third variant shows the wind from a south-west direction. The first thing that one will notice when comparing this simulation to the other two, is that the PET on this variant is significantly warmer, even not close to the trees. This can be explained due to the fact that this simulation was run for only three hours instead of eight. This makes the modelled behavior still accurate, but it is not possible to directly compare this output to the other two. However, it is clearly visible how the improved PET in this case moves from the trees toward the north eastern part of the model area. The wind blows the cooling effect upwards compared to the balcony instead of mainly downwards as occurred in the other two cases.

8.5.6 Tree properties

Variants for tree properties have a change in either the albedo of the tree or the Leaf Area Density (LAD) of the tree in comparison to the standard variant. These leaf properties have an impact on the amount of solar radiation that is received at the façade of the building. The results for the three different tree property variants is given in Figure 94. The top image is the standard scenario with an albedo of 0,18 and a LAD of 2,0. There is clearly a lower amount of shortwave radiation that reaches the façade in the shadow of the two trees. In the complete shadow at the center of the tree the shortwave radiation received comes below 200 W/m^2 even.

The second variant has a significantly higher leaf albedo of 0,70. The reason the leaf albedo was researched is because on the one hand a higher albedo will lead to more shortwave radiation reflection back to the sky, but also more reflected back to the façade itself. As it turns out the higher albedo leads to more shortwave radiation at the façade, since ENVI-met software takes into account reflections between surface and in this case there is a lot of shortwave radiation reflected from the high albedo tree to the low albedo black building surface.

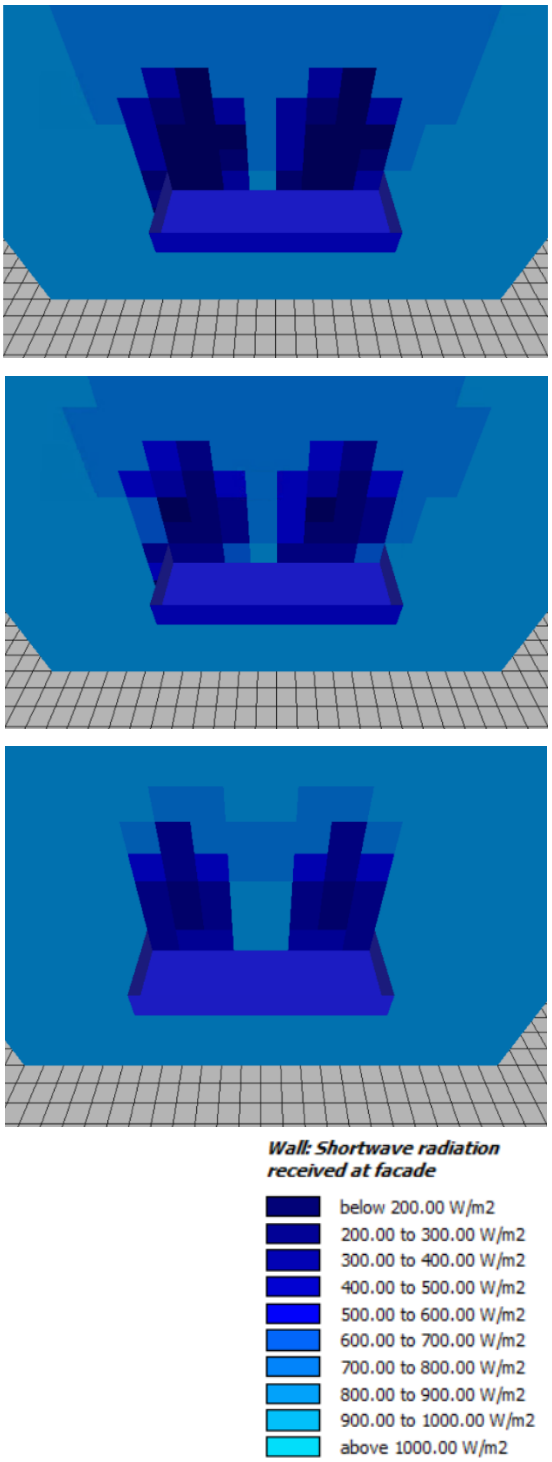

Figure 94: Facade surface temperature with albedo 0,18 and LAD 2,0 (top), albedo 0,7 (middle) and LAD 1,0 (bottom) on west facade at 16:00

Finally, a variant with a lower LAD is tested. Since the LAD is in m^2/m^3, a higher LAD represents a wider tree canopy. This automatically leads to a larger area of the façade receiving solar radiation. As a result of the smaller canopy diameter, the amount of reflected radiation received by the building from the tree foliage is also smaller than in the standard variant.

8.6 Conclusions

In this chapter a variant study was performed on different factors of the environment and green balcony design that have an influence on the microclimate. From this chapter it can be concluded that green balconies show potential in the cooling of the climate. Important factors in determining the amount of cooling of a green balcony and the spread thereof, are the balcony orientation, wind speed and direction and local climate. On a smaller scale the choice for low albedo tree types with a high Leaf Area Density will bring most cooling benefits along the façade of a vertical forest. The conclusions of this variant study will be discussed more elaborately in the final chapter.

.

La Tour des Cedres, Stefano Boeri

Part IV

Final Remarks

9 Conclusion

This chapter contains the concluding remarks on this research on the impact of green balconies on the microclimate. First the research will be critically discussed, then the conclusion will give an answer to the initial research questions and finally recommendations for further research will be given.

9.1 Discussion

While this research was focused on microclimate modelling, this field of study is inherent to uncertainties. The interaction between the atmosphere, moisture and heat works in a complex way and especially wind modelling can only reach a certain level of accuracy. Measurements in the field again showed that even though microclimate software such as ENVI-met is based on well-founded scientific principles, it is difficult to predict the microclimate exactly since there are so many factors at play. Also the time period over which the measurements were done was limited, making the results less reliable.

Another large uncertainty in this research is the way that the vegetation is modelled. To accurately model vegetation a plant canopy analyzer tool is needed to determine the Leaf Area Index with the highest level of accuracy, but unfortunately this type of measuring device was not available. This is why the choice was made to rely on previous measurements, but these were measurements of different tree samples. Due to differences in every individual tree type, no sample is the same.

Also the results of this research apply specifically to the case of Bosco Verticale and cannot be generalized for any time and location.

9.2 Conclusion

As was described in Chapter 3, the main research question is:

What is the impact of green balconies on the microclimate by solar shading, evapo-transpiration and wind flow change?

This research question can be answered by giving an answer to the questions posed below.

1. *How does building integrated vegetation influence the microclimate?*

Building integrated vegetation can provide cooling to a building by solar shading and by evapotranspiration. Also vegetated facades and rooftops can lead to energy savings. Also trees close to the building envelope can provide wind shading by protecting the façade and reducing wind speeds, leading to an extra insulative effect and less infiltration into the building. Air quality improvement by plants is done by intercepting particles, emitting VOC and absorbing carbon dioxide. This can lead to outdoor but also indoor improved air quality. The psychological benefits and physiological benefits of vegetation on humans has been proven numerous times by science. Trees in an urban environment also better the biodiversity and can provide animals with food and shelter. Finally, the substrate of vegetation and the leaf canopy to some extent can reduce noise by scattering of sound and noise absorption.

2. *What are the mechanisms of heat and moisture transfer for trees?*

The most relevant mechanisms for the microclimate are evapotranspiration, solar shading and wind flow effects. Trees increase the amount of moisture in the environment by releasing moisture through their stomata (transpiration) and releasing this into the air (evaporation). Trees also provide solar shading, this can be attributed to the leaf canopy. It depends on the angle of the leaves, the density, tree shape and also reflective properties and transmittance how much solar shading is done. Finally trees influence wind flow. Trees have been used for decades as effective wind breakers. Also the irregular shape of trees increases the turbulence in wind flow. Wind flow change

depends mainly on the porosity of the tree canopy.

3. *How can the microclimatic effects of green balconies be modelled?*

A simple MATLAB model proved valuable in getting a better understanding of the heat and moisture mechanisms at work on a green balcony. However, this is not the most suitable tool to input geometry affecting incoming solar radiation and also not for turbulent wind flow behavior. ENVI-met proved most suitable for modelling purposes, but has the limitation of long run times and fixed solar radiation curves. When comparing ENVI-met simulations to measurements in the field, it turned out that temperature and humidity followed approximately the same trend, whilst solar radiation and wind flow change showed more variety.

4. *How does the environment and design of a vertical forest influence the microclimate?*

A variant study was done to investigate the impact of different factors. The PET on a green balcony in comparison to a non green balcony with two trees can drop up to 14°C in the leeward side of the building. The largest cooling benefit occurs in the late afternoon as the sun is lower in the sky and the trees provide more shade. When considering the four different parameters that influence thermal comfort directly (air temperature, relative humidity, wind speed and mean radiant temperature) it turns out that the mean radiant temperature is most significant. The solar shading of a tree is therefore important in determining the cooling capacity. The wind speed in this case was very low because of the urban setting, but in high rise building this factor might play a more prominent role. The relative humidity change due to two trees was limited, which has to do with the limited root diameter and depth these trees have since they are planted in a container.

In the case of Milan, an east balcony orientation was slightly more preferable over a west orientation because it lead to more PET degree cooling hours. It is also discovered that in the situation where heating is required, the trees on the balcony have a slightly negative effect on the PET. After the east and west orientation, south and finally north orientation show the most PET cooling potential. A west orientation is most beneficial to save cooling later in the day, for example for residential building. Whereas an east orientation could provide energy benefits early in the day, which could be more relevant for commercial real estate.

When considering different climate variants, the climate in Utrecht and Milan were compared. However, these did not have as significant differences as is to be expected considering the differences in the climate. This has to do with the modelling choice to use a start temperature and humidity instead of forcing the temperature and humidity every hour according to a weather station nearby. Now ENVI-met calculated the incoming solar radiation with the help of the geographical location and time of the year. Solar radiation was interpolated from available data but comparison between ENVI-met calculated solar radiation and weather station data showed significant differences for one example (9%). Since the incoming solar radiation directly influences the mean radiant temperature, this could explain why results from Milan and Utrecht are so similar.

But it is possible to compare the results from Milan in summer and winter. In summer the trees provide significant improvement of the PET, especially when solar intensity is high. In winter the effects are less remarkable and could even provide a slight less comfortable situation. But the benefits in summer easily outweigh the negatives in winter.

The wind variants showed that a stronger cooling of the building façade will be reached with higher wind speeds. Also the downwash along the building façade from wind coming from behind the green balcony was more effective in spreading the cooling benefits than wind coming from the perpendicular front side of the building.

Finally different tree properties were evaluated. A higher LAD led to a greater protection of the façade against incoming solar radiation, whereas an increase in the albedo of the plant led to more received solar radiation at the façade due to stronger reflection of solar radiation back to the building.

9.3 Recommendations

While this research tackled several topics related to green balconies, there is still a lot of research to be done in this field.

It would be interesting to measure the microclimate impact of green balconies over a longer period of time during the construction of a vertical forest. By comparing microclimate measurements before and after placement of the tree, a better understanding of the impact of green balconies will be reached.

This research focused on the effects on the microclimate and showed that trees do influence their microclimate. This will also impact the energy use of the building and might provide cooling benefits in summer, whereas it might be disadvantageous to have green balconies in winter. Therefore the impact of green balconies on the energy performance of buildings throughout the year would be an interesting topic for further research, also in the context of energy friendly building and climate change.

One of the issues with vertical forests that came up during this research, is that the trees also block desirable daylight from entering the building. The effect of trees near the building envelope on incoming daylight is not part of the Building Decree in Holland, but should also be considered. Here a trade-off has to be made to minimize overheating and glare, while maximizing the natural daylight entering the building.

Finally, the scope of this research was limited to the cooling, evapotranspiration and wind effects. However, vegetation is also known to have a positive impact on air quality. The air quality improvement by vertical forests specifically has not been researched to the author's knowledge, but can be very relevant for megacities where air pollution by anthropogenic sources is already a serious health issue.

References

Abbass, O. A., Sailor, D. J. & Gall, E. T., 2017. Effectiveness of indoor plants for passive removal of indoor ozone. *Building and Environment*, July, pp. 62-70.

Afrin, S., 2009. *Green Skyscraper: Integration of Plants into Skyscrapers,* Stockholm: KTH.

Akbari, H. et al., 1992. *Cooling Our Communities: A Guidebook on Tree Planting and Light-Colored Surfacing,* Berkeley: U.S. Environmental Protection Agency.

Allen, R. G., Pereira, L. S., Raes, D. & Smith, M., 1998. *Crop evapotranspiration - Guidelines for computing crop water requirements - FAO Irrigation and drainage.* Rome: Food and Agriculture Organization of the United Nations.

Allmond, G., 2017. The First Garden City? Environment and utopianism in an Edwardian institution for the insane poor. *Journal of Historical Geography*, April, pp. 101-112.

Alvey, A., 2006. Promoting and preserving biodiversity in the urban forest. *Urban Forestry and Urban Greening,* pp. 195-201.

An, K. J. et al., 2015. Multi-purpose rainwater harvesting for water resource recovery and the cooling effect. *Water Research,* pp. 116-121.

Aronson, M. et al., 2014. A global analysis of the impacts of urbanization on bird and plant diversity reveals key anthropogenic drivers. *Proc. Biol. Sci..*

Arrau, C. P. & Peña, M. A., 2016. *The Urban Heat Island (UHI) Effect.* [Online] Available at: http://www.urbanheatislands.com/home

ASHRAE, 2001. *Handbook Fundamentals SI Edition.* Atlanta: American Society of Heating, Refrigerating and Air-Conditioning Engineers.

ASHRAE, 2005. *ASHRAE Handbook: Thermal Comfort Fundamentals.* Atlanta: ASHRAE.

Banting, D., Doshi, H., Li, J. & Missios, P., 2005. *Report on the Environmental Benefits and Costs of Green Rooft Technology for the City of Toronto,* Toronto: Ryerson University.

Barber, D. A. & Putalik, E., 2018. *Forest, Tower, City: Rethinking the Green Machine Aesthetic.* [Online] Available at: http://www.harvarddesignmagazine.org/issues/45/forest-tower-city-rethinking-the-green-machine-aesthetic

Benessaia, I., 2011. *Bioclimatic design principles,* Athens: Technical Chamer of Greece.

Berry, R., Livesley, S. J. & Aye, L., 2013. Tree canopy shade impacts on solar irradiance received by building walls and their surface temperature. *Building and Environment,* Volume 69, pp. 91-100.

Berry, S., Whaley, D., Davidson, K. & Saman, W., 2014. Near zero energy homes – What do users think?. *Energy Policy*, October, pp. 127-137.

Bluyssen, P., Bayon, R. & Hamilton, K., 2007. *The Indoor Environment Handbook: How to Make Buildings Healthy and Comfortable,* 2014: CRC Press.

Boonyayothin, V. et al., 2016. Ventilation Control Approach for Acceptable Indoor Air Quality and Enhancing Energy Saving In Thailand. *International Journal of Ventilation,* pp. 315-326.

Bronsema, B., 2013. *Earth, Wind and Fire,* Delft: TU Delft.

Calcerano, F. & Martinelli, L., 2016. Numerical optimisation through dynamic simulation of the position of trees around a stand-alone building to reduce cooling energy consumption. *Energy and Buildings,* Volume 112, pp. 234-243.

Cao, Y. & Cao, N., 2013. Chinese Urbanization Issues. *Applied Mechanics and Materials,* pp. 986-990.

Carlucci, S., 2013. *Thermal Comfort Assessment of Buildings.* Milan: Springer.

Caspari, H., Green, S. & Edwards, W., 1993. Transpiration of well-watered and water-stressed Asian pear trees as determined by lysimetry, heat-pulse, and estimated by a Penman-Monteith model. *Agricultural and Forest Meteorology,,* Volume 67, pp. 13-27.

Chatzipoulka, C., Compagnon, R., Kaempf, J. & Nikolopoulou, M., 2018. Sky view factor as predictor of solar availability on building façades. *Solar Energy,* Volume 170, pp. 1026-1038.

Chen, D. & Chen, H. W., 2013. Using the Köppen classification to quantify climate variation and change: An example for 1901–2010. *Environmental Development,* pp. 69-79.
Corbusier, L. & Jeanneret, P., 1926. *Five Points Toward a New Architecture.* s.l.:MIT Press.
Country Garden, 2018. [Online] Available at: http://www.forestcityjohor.info/
Dalley, S., 2013. *The Mystery of the Hanging Garden of Babylon: An Elusive World Wonder Traced.* Oxford: Oxford University Press.
de Wit, M. H., 2017. *Heat, Air and Moisture in Building Envelopes.* Eindhoven: TU/e.
Dekking, F., Kraaikamp, C., Lopuhaa, H. & Meester, L., 2005. *A Modern Introduction to Probability and Statistics.* Delft: Springer.
DGMR, 2017. *Naar een gezond gebouw met de WELL Building Standard,* Den Haag: DGMR Raadgevende Ingenieurs.
Difford, R., 2009. Infinite horizons: Le Corbusier, the Pavillon de l'Esprit Nouveau dioramas and the science of visual distance. *The Journal of Architecture 14,* pp. 295-323.
Dirr, M., 1990. *Manual of Woody Landscape plants.* s.l.:Stipes Publisher.
Douglass-Jaimes, D., 2015. *AD Classics: Menara Mesiniaga / T. R. Hamzah & Yeang Sdn. Bhd.*. [Online] Available at: https://www.archdaily.com/774098/ad-classics-menara-mesiniaga-t-r-hamzah-and-yeang-sdn-bhd
Duffie, J. A. & Beckman, W. A., 2013. *Solar Engineering of Thermal Processes.* 4th ed. s.l.:John Wiley & Sons.
Duijvestein, K., 1989. *An Ecological Approach to Building,* Delft: Delft University Press.
Dwivedi, A. & Mohan, B. K., 2018. Impact of green roof on micro climate to reduce Urban Heat Island. *Remote Sensing Applications: Society and Environment, Volume 10,* pp. 56-69.
DWR, 2000. *A Guide to Estimating Irrigation Water Needs of Landscape Plantings in California: The Landscape Coefficient Method and WUCOLS III.* Sacramento: California Department of Water Resources.
EEA, 2014. *Noise in Europe 2014,* Copenhagen: European Environment Agency.
Emporis, 2010. *30 St Mary Axe.* [Online] Available at: https://www.emporis.com/buildings/100089/30-st-mary-axe-london-united-kingdom
EnergyPlus, 2018. *Weather Data.* [Online] Available at: https://energyplus.net/weather
Ennos, R., 2015. *Quantifying the cooling benefits of urban trees,* Manchester: University of Manchester.
ENVI-met, 2017. *ENVI-met Model Architecture.* [Online] Available at: http://www.envi-met.info/doku.php?id=intro:modelconcept
EPA, 2008. *Reducing Urban Heat Islands: Compendium of Strategies: Urban Heat Island Basics,* Washington DC: U.S. Environmental Protection Agency.
Eumorfopoulou, E. & Kontoleon, K., 2009. Experimental approach to the contribution of plant-covered walls to the thermal behaviour of building envelopes. *Building and Environment, Vol. 44*, May, pp. 1024-1038.
European Parliament and Council, 2010. DIRECTIVE 2010/31/EU OF THE EUROPEAN PARLIAMENT AND OF THE COUNCIL. *Official Journal of the European Union.*
Fanger, P., 1972. *Thermal Comfort.* New York: McGraw-Hill.
Fernández-Cañero, R., Urrestarazu, L. P. & Perini, K., 2018. Vertical Greening Systems: Classifications, Plant Species, Substrates. In: *Nature Based Strategies for Urban and Building Sustainability .* s.l.:Butterworth-Heinemann, pp. 45-54.
Fokaides, P. A., Polycarpou, K. & Kalogirou, S., 2017. The impact of the implementation of the European Energy Performance of Buildings Directive on the European building stock: The case of the Cyprus Land Development Corporation. *Energy Policy Volume 111,* pp. 1-8.
Foster & Partners, 2018. *Commerzbank Headquarters.* [Online] Available at: https://www.fosterandpartners.com/projects/commerzbank-headquarters/

Fraser, L., 2005. Paving Paradise: The Peril of Impervious Surfaces. *Environmental Healt Perspectives 113,* pp. 456-462.
Fulcher, M., 2011. *Yeang: 'We need more bioclimatic buildings'.* [Online] Available at: https://www.architectsjournal.co.uk/home/yeang-we-need-more-bioclimatic-buildings/8614279.article
Giacomello, E., 2015. A New Urban Forest Rises in Milan. *CTBUH Journal Issue I,* pp. 11-18.
Giacomello, E. & Valagussa, M., 2015. *Vertical Greenery: Evaluating the High Rise Vegetation of the Bosco Verticale, Milan,* Chicago: Council on Tall Buildings and Urban Habitat.
Gkatsopoulosa, P., 2017. *A Methodology for Calculating Cooling from Vegetation Evapotranspiration for Use in Urban Space Microclimate Simulations.* Greece, International Conference on Sustainable Synergies from Buildings to the Urban Scale.
Gou, Z., Prasad, D. & Lau, S. S.-Y., 2013. Are green buildings more satisfactory and comfortable?. *Habitat International*, July, pp. 156-161.
Graamans, L., Dobbelsteen, A. v. d., Meinen, E. & Stanghellini, C., 2016. Plant factories; crop transpiration and energy balance. *Agricultural Systems,* Volume 153, pp. 138-147.
Grimmond, C. & Oke, T., 1998. Aerodynamic Properties of Urban Areas Derived from Analysis of Surface Form. *Journal of Applied Meteorology*, 3 December, pp. 1262-1292.
Gurjar, B., Butler, T., Lawrence, M. & Lelieveld, J., 2008. Evaluation of emissions and air quality in megacities. *Atmospheric Environment*, March, pp. 1593-1606.
Hall, P. B., 2016. *Garden City Mega City: Rethinking Cities for the Age of Global Warming.* Singapore: Pesaro Publishing.
Heinonen, S. & Minkkinen, M., 2016. Interpreting built cityscape: Deconstructing the metaphorical messages of futuristic buildings. *Futures*, November, pp. 163-177.
Hondel, T. & Alibaba, H. Z., 2016. Green Facade as a Prototype Way of Extending Natural Sphere in a Hyper Dense Urban Context. *International Journal of Scientific & Technology Research, Vol. 5.*
Hooff, T. v. & Blocken, B., 2010. Coupled urban wind flow and indoor natural ventilation modelling on a high-resolution grid: A case study for the Amsterdam ArenA stadium. *Environmental Modelling & Software*, January, pp. 51-65.
Howell, J., 1982. *A catalog of radiation configuration factors.* s.l.:McGraw-Hill.
Hsieh, C.-M., Li, J.-J., Zhang, L. & Schwegler, B., 2018. Effects of tree shading and transpiration on building cooling energy use. *Energy and Buildings,* Volume 159, pp. 382-397.
IPCC, 2014. *Climate Change 2014: Mitigation of Climate Change. Contribution of Working Group III to the Fifth Assessment Report of the Intergovernmental Panel on Climate Change,* Cambridge: Cambridge University Press.
Ising, H. & Kruppa, B., 2004. Health effects caused by noise: Evidence in the literature from the past 25 years. *Noise and Health*, January, pp. 5-13.
Jim, C., 2017. An archaeological and historical exploration of the origins of green roofs. *Urban Forestry & Urban Greening,* pp. 31-42.
Jóhannesson, G., 2006. *Lectures on Building Physics.* Stockholm: KTH.
Jones, A., 1999. Indoor Air Quality and Health. *Atmospheric Environment*, December, pp. 4535-4564.
Jones, R., 2013. *AD Classics: The Ford Foundation / Kevin Roche John Dinkeloo and Associates.* [Online] Available at: https://www.archdaily.com/436653/ad-classics-the-ford-foundation-kevin-roche-john-dinkeloo-and-associates
Kats, G. & Glassbrook, K., 2018. *Delivering Urban Resilience,* Washington: USGBC.
Kelso, J. D., 2010. *Buildings Energy Data Book,* Silver Spring: U.S. Department of Energy.
Kleerekoper, L., Taleghani, M., Dobbelsteen, A. v. d. & Hordijk, T., 2016. Urban measures for hot weather conditions in a temperate climate condition: A review study. *Renewable and Sustainable Energy Reviews,* p. 515–533.

Klein, C., 2013. *Hanging Gardens Existed, but not in Bablyon.* [Online] Available at: https://www.history.com/news/hanging-gardens-existed-but-not-in-babylon
KNMI, 2018. *Uurgegevens van het weer in Nederland.* [Online] Available at: http://projects.knmi.nl/klimatologie/uurgegevens/selectie.cgi
Köhler, M., 2008. Green facades-a view back and some visions. *Urban Ecosystems,* pp. 423-436.
Köhler, M. & Ksiazek-Mikenas, K., 2018. Green Roofs as Habitats for Biodiversity. In: *Nature Based Strategies for Urban and Building Sustainability.* s.l.:Elsevier, pp. 239-249.
Köhler, M. & Poll, P. H., 2010. Long-term performance of selected old Berlin greenroofs in comparison to younger extensive greenroofs in. *Ecological Engineering,* pp. 722-729.
Kong, L. et al., 2017. Regulation of outdoor thermal comfort by trees in Hong Kong. *Sustainable Cities and Society,* pp. 12-25.
Krusche, P., Krusche, M., Althaus, D. & Gabriel, I., 1982. Okologisches bauen. *Bauverlag.*
Lechner, N., 2014. *Heating, Cooling, Lighting: Sustainable Design Methods for Architects.* 4th ed. Hoboken: John Wiley & Sons.
Lee, J. & Heaney, J., 2003. Estimation of urban imperviousness and its impacts on storm water systems. *Journal of Water Resources Planning and Management,* September.pp. 419-426.
Li, W., Wang, F. & Bell, S., 2007. Simulating the sheltering effects of windbreaks in urban outdoor open space. *Journal of Wind Engineering and Industrial Aerodynamics*, July, pp. 533-549.
MacPherson, K., 1962. The assessment of the thermal environment a review. *Br. J. Ind. Med.,* Volume 19, pp. 151-164.
Mangone, G., 2015. *Performative Microforests: Investigating the potential benefits of integrating spatial vegetation environments into buildings, in regards to the performance of buildings, their occupants + local ecosystems,* Delft: Delft University of Technology.
Manzano-Agugliaro, r., Montoya, F. G., Sabio-Ortega, A. & García-Cruz, A., 2015. Review of bioclimatic architecture strategies for achieving thermal comfort. *Renewable and Sustainable Energy Reviews*, 18 May, pp. 736-755.
Marín, E., 2009. Linear relationships in heat transfer. *Lat. Am. J. Phys. Educ.,* 2(2), pp. 243-245.
Matzarakis, A. & Amelung, B., 2008. *Physiological Equivalent Temperature as Indicator for Impacts of Climate Change on Thermal Comfort of Humans.* s.l.:Springer Science + Business Media.
Matzarakis, A., Rutz, F. & Muthers, S., 2014. Application and comparison of UTCI and PET in temperate climate conditions. *Finisterra,* pp. 21-31.
Medl, A. & Florineth, F., 2017. Vertical greening systems – A review on recent technologies and research advancement. *Building and Environment,* pp. 227-239.
Mentens, J., Raes, D. & Hermy, M., 2006. Green roofs as a tool for solving the rainwater runoff problem in the urbanized 21st century?. *Landscape and Urban Planning,* pp. 217-226.
Merriam-Webster, 2018. *Balcony.* [Online] Available at: https://www.merriam-webster.com/dictionary/balcony
Mirniazmandan, S. & Rahimianzarif, E., 2017. Biomimicry, An Approach Toward Sustainability of High-Rise Buildings. *Iranian Journal of Science and Technology, Transactions A: Science,* pp. 1-10.
Mirsadeghi, M., Cóstola, D., Blocken, B. & Hensen, J., 2013. Review of external convective heat transfer coefficient models in building energy simulation programs: implementation and uncertainty. *Applied Thermal Engineering,* Issue March.
Monsi & Saeki, 1953. Über den Lichtfaktor in den Pflanzengesellschaften und seine Bedeutung für die Stoffproduktion. *Japanese Journal of Botany,* Issue 14, pp. 22-52.
Monteith, J., 1965. *The State and Movement of Water in Living Organisms.* Cambridge, Cambridge University Press.
Monteith, J. & Unsworth, M., 1990. *Principles of Environmental Physics.* New York: Edward Arnold.
Mousaad, A. et al., 2013. Wind loading on trees integrated with a building envelope. *Wind and Structures, Vol. 17*, pp. 69-85.

Mun, J., Kim, R. & Han, M., 2012. *The Effects of Catchment Materials and Treatment Train on Rainwater Quality in a Rainwater Harvesting System.* s.l., Trans tech Publications, pp. 451-454.
MVDRV, 2018. *Expo 2000.* [Online] Available at: https://www.mvrdv.nl/projects/EXPO/
MVRDV, 2018. *Valley.* [Online] Available at: https://www.mvrdv.nl/en/projects/valley
Napoli, M. et al., 2016. Modeling tree shade effect on urban ground surface temperature. *Journal of Environmental Quality,* 45(1), pp. 146-156.
National Parks Board, 2018. *Skyrise Greenery.* [Online] Available at: https://www1.nparks.gov.sg/skyrisegreenery/incentive-scheme
Ng, E., Chen, L., Wang, Y. & Yuan, C., 2012. A Study on the Cooling Effects of Greening in a High-Density City: An Experience from Hong Kong. *Building and Environment,* pp. 256-271.
Nouri, H. et al., 2016. Comparing Three Approaches of Evapotranspiration Estimation in Mixed Urban Vegetation: Field-Based, Remote Sensing-Based and Observational-Based Methods. *Remote Sensing 8.*
Nouvel, J. & Beissel, B., 2014. Case Study One Central Park, Sydney. *CTBUH Journal Issue 4*.
Noyes, P. D. et al., 2009. The toxicology of climate change: Environmental contaminants in a warming world. *Environment International,* 35(6), pp. 971-986.
Oberndorfer, E. et al., 2007. Green Roofs as Urban Ecosystems: Ecological Structures, Functions, and Services. *BioScience,* p. 823–833.
Oh, R. R., Richards, D. R. & Yee, A. T., 2018. Community-driven skyrise greenery in a dense tropical city provides biodiversity and ecosystem service benefits. *Landscape and Urban Planning*, January, pp. 115-123.
Oke, T., 1981. Canyon Geometry and the Nocturnal Urban heat Island: Comparison of Scale Model and Field Observations. *Journal of Climatology*, 28 April, pp. 237-254.
Olgyay, V., 2015. *Design With Climate.* Princeton: Princeton University Press.
Ong, B. L., 2003. Green Plot Ratio: An Ecological Measure for Architecture and Urban Planning. *Landscape and Urban Planning 63*, pp. 197-211.
Ottelé, M., 2011. *The Green Building Envelope.* Delft: TU Delft.
Paassen, A. v., 2004. *Indoor Climate Control Fundamentals.* Delft: TU Delft Section Energy Technology.
Pajek, L. & Košir, M., 2018. Implications of present and upcoming changes in bioclimatic potential for energy performance of residential buildings. *Building and Environment*, January, pp. 157-172.
Pasquill, F., 1961. The estimation of the dispersion of windborne material. *Meteoroloigcal Magazine*, February, pp. 33-49.
Patz, J. A., Campbell-Lendrum, D., Holloway, T. & Foley, J., 2005. Impact of regional climate change on human health. *Nature*, 17 November, pp. 310-317.
Perini, K. & Magliocco, A., 2012. The Integration of Vegetation in Architecture, Vertical and Horizontal Greened Surfaces. *International Journal of Biology,* pp. 79-91.
Pijpers-van Esch, M., 2015. *Designing the Urban Microclimate.* Delft: TU Delft.
Pikas, E., Thalfeldt, M. & Kurnitski, J., 2014. Cost optimal and nearly zero energy building solutions for office buildings. *Energy and Building,* pp. 30-42.
Piselli, C. et al., 2018. Outdoor comfort conditions in urban areas: On citizens' perspective about microclimate mitigation of urban transit areas. *Sustainable Cities and Society*, May, p. 16–36.
Poddar, S., Park, D. & Chang, S., 2017. Energy performance analysis of a dormitory building based on different orientations and seasonal variations of leaf area index. *Energy Efficiency, Volume 10*, August, pp. 887-903.
Powell, K., 2011. *The Great Builders.* 1st ed. s.l.:Thames & Hudson.
PwC and the Urban Land Institute, 2016. *Emerging Trends in Real Estate - New Market Realities - Europe 2017,* London: PwC and the Urban Land Institute.

Raji, B., Tenpierik, M. J. & Dobbelsteen, A. v. d., 2015. The impact of greening systems on building energy performance: A literature review. *Renewable and Susainable Energy Reviews 45,* pp. 610-623.
Reece, J. B. & Wasserman, S. A., 2016. *Campbell Biology.* 10th ed. s.l.:s.n.
Rehman, N. & Uzair, M., 2017. The proper interpretation of analytical sky view factors for isotropic diffuse solar irradiance on tilted planes. *Journal of Renewable and Sustainable Energy,* 9(5).
Riley, B., 2017. The state of the art of living walls: Lessons learned. *Building and Environment Volume 114*, March, pp. 219-232.
Robine, J. M., Cheung, S. L. K., Le Roy, S. & Van Oyen, H., 2008. Death toll exceeded 70,000 in Europe during the summer of 2003. *Comptes Rendus Biologies*, February, pp. 171-178.
Robinson, J. & Nelson, W., 1995. *National Human Activity Pattern Survey Data Base,* Reserach Triangle Park, NC: United States Environmental Protection Agency.
Ross, J., Ross, V. & Koppel, A., 2000. Estimation of leaf area and its vertical dsitribution during growth period. *Argricultural and Forest Meteorology,* Volume 101, pp. 237-246.
Rubio, E., Caselles, V. & Badenas, C., 1997. Emissivity Measurements of Several Soils and Vegetation Types in 8-14 mm Wave band: Analysis of Two Field Methods. *Remote Sensing of Environment*, March, p. 490=521.
Saiz, S., Kennedy, C., Bass, B. & Pressnail, K., 2006. Comparative life cycle assessment of standard and green roofs. *Environmental Science and Technology, Vol. 40,* pp. 4312-4316.
Samant, S. & Hsi-En, N., 2017. A tale of two Singapore sky gardens. *CTBUH Journal, Issue 3*, pp. 26-31.
Santamouris, M., 2001. *Energy and Climate in the Urban Built Environment,* Oxon: Routledge.
Schröpfer, T., 2015. *Dense + Green: Innovative Building Types for Sustainable Urban Architecture.* Basel: Birkhauser Verlag.
Shan, H., 2011. *Beijing's Air Pollution Index Reaches Alarming Levels.* [Online] Available at: https://www.theepochtimes.com/beijings-air-pollution-index-reaches-alarming-levels_1504326.html
Sharmin, T., Steemers, K. & Matzarakis, A., 2017. Microclimatic modelling in assessing the impact of urban geometry on urban thermal environment. *Sustainable Cities and Society,* pp. 293-308.
Shashua-Bar, L. & Hoffman, M. E., 2003. Geometry and Orientation Aspects in Passive Cooling of Canyon Streets with Trees. *Energy and Buildings 35*, pp. 61-68.
Shashua-Bar, L., Pearlmutter, D. & Erell, E., 2011. The Influence of Trees and Grass on Outdoor Thermal Comfort in a Hot-Arid Environment. *International Journal of Climatology 31*, 2 June, pp. 1498-1506.
Simpson, J. & McPherson, E., 1996. Potential of tree shade for reducing residential energy use in California. *Journal of Arboriculture, Vol. 22*, January, pp. 10-18.
Spala, A. et al., 2008. On the green roof system. Selection, state of the art and energy potential investigation of a system installed in an office building in Athens, Greece. *Renewable Energy, Vol. 33,* pp. 173-177.
Stec, W. J., 2006. *Symbiosis of Double skin Facade and Indoor Climate Installation,* Delft: TU Delft.
Steemers, K. & Manchanda, S., 2010. Energy efficient design and occupant well-being: Case studies in the UK and India. *Building and Environment*, February, pp. 270-278.
Stefano Boeri Architetti, 2018. *Projects.* [Online] Available at: https://www.stefanoboeriarchitetti.net/en/projects/
Stieb, D. M., Doiron, M. S., Blagden, P. & Burnett, R. T., 2005. Estimating the Public Health Burden Attributable to Air Pollution: An Illustration Using the Development of an Alternative Air Quality Index. *Journal of Toxicology and Environmental Health,* pp. 1275-1288.
Straube, J. & Burnett, E., 2005. *Building science for building enclosures.* Westford: Building Science Press Inc.
Stredova, H. et al., 2012. Aerodynamic parameters of windbreak based on its optical porosity. *Contributions to Geophysics and Geodesy*, pp. 213-226.

Sun, J., Liu, J., Wu, F. & Nian, H., 2015. *Research on High-Efficient Balcony Greening Based on the concept of Low-Carbon Green Buildings.* s.l., ICAEES, pp. 1018-1021.
Sutton, O., 1953. *Micrometeorology.* s.l.:s.n.
Swaid, H., Bar-El, M. & Hoffman, M. E., 1993. A Bioclimatic Design Methodology for Urban Outdoor Spaces. *Theoretical and Applied Climatology,* pp. 49-61.
Tan, P. Y., Wang, J. & Sia, A., 2013. Perspectives on five decades of the urban greening of Singapore. *Cities 32*, 22 March, pp. 24-32.
Taylor, T., Counsell, J. & Gill, S., 2014. Combining thermography and computer simulation to identify and. *Energy and Buildings*, March, pp. 130-142.
theOtherDada, 2013. *Biolcimatic Analysis.* [Online] Available at: https://theotherdada.wordpress.com/2013/10/12/bioclimatic-analysis/
Tian, Y. & Jim, C., 2012. Development potential of sky gardens in the compact city of Hong Kong. *Urban Forestry & Urban Greening, Vol. 11*, pp. 223-233.
United Nations, 2015. *World Urbanization Prospects,* New York: DESA.
United Nations, 2016. *The World's Cities in 2016,* s.l.: United Nations, Department of Economic and Social Affairs.
UWO, 2018. *Green Roof Research At Western.* [Online] Available at: www.eng.uwo.ca/research/greenroof/
Venhari, A. A., Tenpierik, M. & Hakak, A. M., 2017. Heat mitigation by greening the cities, a review study. *Environment, Earth and Ecology*, pp. 5-32.
Villalobos, F. J., Testi, L., Mateos, L. & Fereres, E., 2016. The Energy Balance. In: *Principles of Agronomy for Sustainable Agriculture.* Cordoba: Springer International Publishing, pp. 79-90.
Vincent Callebaut Architectures, 2009. *DRAGONFLY.* [Online] Available at: http://vincent.callebaut.org/object/090429_dragonfly/dragonfly/projects [Accessed 21 September 2018].
Voogt, J. A., 2004. *Urban Heat Islands: Hotter Cities.* [Online] Available at: http://www.actionbioscience.org/environment/voogt.html
Wang, J. & He, D., 2015. Sustainable urban development in China: challenges and achievements. *Mitigation and Adaptatopm Strategies for Global Change,* pp. 665-682.
WELL Building Institute, 2018. *The WELL Building Standard,* New York: International WELL Building Institute pbc and Delos Living LLC.
WHO, 2002. *The World Health Report 2002,* Geneva: World Health Organization.
WHO, 2018. *Global Health Observatory (GHO) data.* [Online] Available at: http://www.who.int/gho/phe/outdoor_air_pollution/en/
Wieringa, J., 1998. *How far can agrometeorological station observations be considered representative?,* Albuquerque: Meteorological Social Conference on Agriculture and Forest Meteorology.
Wilby, R., 2003. Past and projected trends in London's Urban Heat Island. *Weather 58,* pp. 251-260.
Wit, M. d., 2017. *Heat, Air and Moisture in Building Envelopes.* Eindhoven: TU/e.
WMO, 2012. *Manual on Meteorological Services,* Geneva: World Meteorological Organization.
WOHA, 2018. *PARKROYAL on Pickering, Singapore.* [Online] Available at: http://woha.net/
Wolkoff, P., 2013. Indoor air pollutants in office environments: Assessment of comfort, health, and performance. *International Journal of Hygiene and Environmental Health*, July, pp. 371-394.
World Health Organization, 2014. *Mental health: a state of well-being.* [Online] Available at: http://www.who.int/features/factfiles/mental_health/en/
Wu, L., 2012. Looking for the lost soul of Chinese cities. *South China Weekend*, 14 October.
Yan, Z. et al., 2018. Impervious surface area is a key predictor for urban plant diversity in a city undergone rapid urbanization. *Science of The Total Environment,* pp. 335-342.
Yeang, K., 1996. *The Skycraper Bioclimatically Considered.* s.l.:Wiley Academy.

Yeang, K. & Yeang, L. D., 2008. *Ecoskyscrapers and Ecomimesis: New Tall Building Typologies.* London, Brook House, pp. 1-11.
Zeiger, E., Farguhar, G. & Cowan, I., 1987. *Stomatal Function.* Stanford: Stanford University Press.
Zhang, H., Simmonds, L. P., Morison, J. I. & Payne, D., 1997. Estimation of transpiration by single trees: comparison of sap flow measurements with a combination equation. *Agricultural and Forest Meteorology,* Volume 87, pp. 155-169.

Appendix A: Measurements Bosco Verticale

A.1 All measurements

Date	Time	Temperature (°C)	RH (%)	Radiation (W/m^2)	Wind speed (m/s)
10-8-2018	11:01 AM	24,1	68,6	32,3	2,4
10-8-2018	11:02 AM	24,3	68,1	32,4	2,4
10-8-2018	11:03 AM	24,5	67,9	32,9	2,4
10-8-2018	11:04 AM	24,6	67,6	33,1	2,4
10-8-2018	11:05 AM	24,8	67,7	33,1	2,4
10-8-2018	11:06 AM	24,9	67,3	33,3	2,4
10-8-2018	11:07 AM	25,0	67,2	33,7	2,5
10-8-2018	11:08 AM	25,1	66,6	34,2	2,5
10-8-2018	11:09 AM	25,2	66,1	34,8	2,5
10-8-2018	11:10 AM	25,3	66,0	35,4	2,5
10-8-2018	11:11 AM	25,4	65,8	35,8	2,5
10-8-2018	11:12 AM	25,5	65,6	36,6	2,5
10-8-2018	11:13 AM	25,5	64,8	37,4	2,5
10-8-2018	11:14 AM	25,6	65,2	38,1	2,5
10-8-2018	11:15 AM	25,6	65,4	38,7	2,5
10-8-2018	11:16 AM	25,9	64,9	54,6	2,5
10-8-2018	11:17 AM	26,0	64,9	44,7	2,5
10-8-2018	11:18 AM	26,1	64,1	45,3	2,5
10-8-2018	11:19 AM	26,2	64,4	46,5	2,5
10-8-2018	11:20 AM	26,2	63,9	47,5	2,5
10-8-2018	11:21 AM	26,2	64,2	49,1	2,5
10-8-2018	11:22 AM	26,3	64,0	50,8	2,0
10-8-2018	11:23 AM	26,3	63,5	51,9	2,5
10-8-2018	11:24 AM	26,4	63,7	52,9	2,5
10-8-2018	11:25 AM	26,4	63,3	53,6	2,5
10-8-2018	11:26 AM	26,5	64,0	53,6	2,1
10-8-2018	11:27 AM	26,5	63,8	53,4	2,5
10-8-2018	11:28 AM	26,5	63,4	53,0	2,1
10-8-2018	11:29 AM	26,5	63,1	51,4	0,0
10-8-2018	11:30 AM	26,6	63,4	49,1	1,2
10-8-2018	11:31 AM	26,7	62,8	96,1	1,2
10-8-2018	11:32 AM	26,8	62,1	94,4	1,2
10-8-2018	11:33 AM	26,8	61,5	93,2	1,2
10-8-2018	11:34 AM	26,8	61,5	92,4	1,2
10-8-2018	11:35 AM	26,8	61,5	93,6	1,2
10-8-2018	11:36 AM	26,7	61,7	93,7	1,2
10-8-2018	11:37 AM	26,7	62,1	93,1	1,2

10-8-2018	11:38 AM	26,7	61,8	90,7	1,2
10-8-2018	11:39 AM	26,7	62,0	88,3	1,2
10-8-2018	11:40 AM	26,7	61,9	87,4	1,2
10-8-2018	11:41 AM	26,7	62,3	85,8	1,2
10-8-2018	11:42 AM	26,7	62,2	82,4	1,2
10-8-2018	11:43 AM	26,7	62,1	81,2	1,2
10-8-2018	11:44 AM	26,7	62,0	81,7	1,2
10-8-2018	11:45 AM	26,7	62,0	82,9	1,2
10-8-2018	11:46 AM	26,7	62,0	3,3	1,2
10-8-2018	11:47 AM	26,8	62,6	59,1	2,3
10-8-2018	11:48 AM	26,8	62,2	59,7	1,2
10-8-2018	11:49 AM	26,8	62,1	59,1	1,2
10-8-2018	11:50 AM	26,7	62,2	59,1	1,2
10-8-2018	11:51 AM	26,7	62,2	58,9	1,2
10-8-2018	11:52 AM	26,7	62,3	59,4	1,2
10-8-2018	11:53 AM	26,7	62,2	57,9	1,2
10-8-2018	11:54 AM	26,6	62,0	57,1	1,2
10-8-2018	11:55 AM	26,6	62,7	57,2	1,2
10-8-2018	11:56 AM	26,6	63,0	57,5	1,2
10-8-2018	11:57 AM	26,5	62,8	57,1	1,2
10-8-2018	11:58 AM	26,5	62,8	56,2	1,2
10-8-2018	11:59 AM	26,5	63,1	56,0	1,2
10-8-2018	12:00 PM	26,5	63,0	55,9	1,2
10-8-2018	12:01 PM	26,5	63,0	24,7	2,5
10-8-2018	12:02 PM	26,6	62,9	27,6	1,2
10-8-2018	12:03 PM	26,6	62,7	27,6	1,3
10-8-2018	12:04 PM	26,6	62,7	28,0	1,3
10-8-2018	12:05 PM	26,6	62,6	27,8	1,3
10-8-2018	12:06 PM	26,6	62,7	27,8	1,3
10-8-2018	12:07 PM	26,6	62,7	27,5	1,3
10-8-2018	12:08 PM	26,6	62,7	28,0	1,3
10-8-2018	12:09 PM	26,6	62,4	28,0	1,3
10-8-2018	12:10 PM	26,5	62,8	28,0	1,2
10-8-2018	12:11 PM	26,5	62,4	28,0	1,2
10-8-2018	12:12 PM	26,5	62,7	28,0	1,2
10-8-2018	12:13 PM	26,5	62,8	27,6	1,3
10-8-2018	12:14 PM	26,5	62,8	27,3	1,3
10-8-2018	12:15 PM	26,6	63,1	27,3	1,3
10-8-2018	12:16 PM	26,7	62,2	44,9	1,3
10-8-2018	12:17 PM	26,8	62,1	44,0	1,3
10-8-2018	12:18 PM	26,8	61,8	44,4	1,3
10-8-2018	12:19 PM	26,8	61,6	44,7	1,2
10-8-2018	12:20 PM	26,8	61,4	46,3	1,2

10-8-2018	12:21 PM	26,8	61,4	48,0	1,2
10-8-2018	12:22 PM	26,7	61,8	49,3	1,2
10-8-2018	12:23 PM	26,7	61,7	50,6	1,2
10-8-2018	12:24 PM	26,8	61,7	51,0	1,2
10-8-2018	12:25 PM	26,8	61,7	50,4	1,2
10-8-2018	12:26 PM	26,8	61,5	50,3	1,2
10-8-2018	12:27 PM	26,8	61,6	49,8	1,2
10-8-2018	12:28 PM	26,8	61,7	48,6	1,2
10-8-2018	12:29 PM	26,8	61,9	47,8	1,2
10-8-2018	12:30 PM	26,8	61,9	48,0	1,2
10-8-2018	12:31 PM	26,8	61,8	66,7	1,2
10-8-2018	12:32 PM	26,9	61,6	68,2	1,2
10-8-2018	12:33 PM	27,0	61,3	68,3	1,2
10-8-2018	12:34 PM	27,0	61,4	66,0	1,2
10-8-2018	12:35 PM	27,1	61,3	68,8	1,2
10-8-2018	12:36 PM	27,1	60,9	69,3	1,2
10-8-2018	12:37 PM	27,1	60,2	69,4	1,2
10-8-2018	12:38 PM	27,2	59,9	68,7	1,2
10-8-2018	12:39 PM	27,2	59,7	68,9	1,2
10-8-2018	12:40 PM	27,2	59,8	70,6	1,2
10-8-2018	12:41 PM	27,1	59,7	72,2	1,1
10-8-2018	12:42 PM	27,1	59,5	72,3	1,1
10-8-2018	12:43 PM	27,1	59,5	73,3	1,1
10-8-2018	12:44 PM	27,1	59,2	74,2	1,1
10-8-2018	12:45 PM	27,2	59,4	75,5	1,1
10-8-2018	12:46 PM	27,1	59,5	5,4	1,1
10-8-2018	12:47 PM	27,1	58,6	26,0	1,1
10-8-2018	12:48 PM	27,1	58,9	25,8	1,1
10-8-2018	12:49 PM	27,1	58,8	26,1	1,1
10-8-2018	12:50 PM	27,1	59,3	27,3	1,1
10-8-2018	12:51 PM	27,1	58,9	27,5	1,1
10-8-2018	12:52 PM	27,1	58,7	27,2	1,1
10-8-2018	12:53 PM	27,1	58,3	24,6	1,1
10-8-2018	12:54 PM	27,2	58,9	23,5	1,1
10-8-2018	12:55 PM	27,2	58,9	23,4	1,1
10-8-2018	12:56 PM	27,3	59,1	22,9	1,1
10-8-2018	12:57 PM	27,3	59,1	23,0	1,1
10-8-2018	12:58 PM	27,3	59,5	23,2	1,1
10-8-2018	12:59 PM	27,2	59,1	23,0	1,1
10-8-2018	1:00 PM	27,3	59,3	23,0	1,1
10-8-2018	1:01 PM	27,3	59,2	34,4	1,1
10-8-2018	1:02 PM	27,3	58,9	33,6	1,1
10-8-2018	1:03 PM	27,4	58,9	32,8	1,1

10-8-2018	1:04 PM	27,4	59,2	32,8	1,1
10-8-2018	1:05 PM	27,4	59,3	32,9	1,1
10-8-2018	1:06 PM	27,4	59,2	33,8	1,1
10-8-2018	1:07 PM	27,5	59,3	34,8	1,1
10-8-2018	1:08 PM	27,5	59,7	36,4	1,1
10-8-2018	1:09 PM	27,5	59,6	37,8	1,1
10-8-2018	1:10 PM	27,6	59,5	38,6	1,1
10-8-2018	1:11 PM	27,6	59,4	38,6	1,1
10-8-2018	1:12 PM	27,6	58,5	38,2	1,1
10-8-2018	1:13 PM	27,6	58,2	38,2	1,1
10-8-2018	1:14 PM	27,7	58,2	38,2	1,1
10-8-2018	1:15 PM	27,7	58,4	38,2	1,1
10-8-2018	1:16 PM	27,7	58,4	5,7	1,1
10-8-2018	1:17 PM	27,8	57,5	30,3	1,0
10-8-2018	1:18 PM	27,8	57,3	30,8	1,0
10-8-2018	1:19 PM	27,8	57,6	31,3	1,0
10-8-2018	1:20 PM	27,8	57,8	31,3	1,0
10-8-2018	1:21 PM	27,8	57,9	31,1	1,0
10-8-2018	1:22 PM	27,9	57,5	27,7	1,0
10-8-2018	1:23 PM	27,9	56,7	27,3	1,0
10-8-2018	1:24 PM	27,9	56,9	27,8	0,0
10-8-2018	1:25 PM	27,9	57,0	28,7	0,0
10-8-2018	1:26 PM	27,8	56,9	30,1	0,0
10-8-2018	1:27 PM	27,9	56,7	31,1	0,0
10-8-2018	1:28 PM	27,9	56,7	32,4	0,0
10-8-2018	1:29 PM	27,9	56,9	35,3	0,0
10-8-2018	1:30 PM	28,0	56,7	37,6	0,0
10-8-2018	1:31 PM	28,0	56,8	50,5	0,0
10-8-2018	1:32 PM	28,0	56,8	43,9	0,0
10-8-2018	1:33 PM	28,1	56,7	43,8	0,0
10-8-2018	1:34 PM	28,1	56,9	43,5	0,0
10-8-2018	1:35 PM	28,2	56,7	43,3	0,0
10-8-2018	1:36 PM	28,3	56,5	43,8	0,0
10-8-2018	1:37 PM	28,4	55,7	44,4	0,0
10-8-2018	1:38 PM	28,5	55,1	44,8	0,0
10-8-2018	1:39 PM	28,5	54,6	45,3	0,0
10-8-2018	1:40 PM	28,6	53,9	45,8	0,0
10-8-2018	1:41 PM	28,5	53,8	45,7	0,0
10-8-2018	1:42 PM	28,6	53,5	44,9	0,0
10-8-2018	1:43 PM	28,6	53,3	44,3	0,0
10-8-2018	1:44 PM	28,7	53,2	44,2	0,0
10-8-2018	1:45 PM	28,7	53,1	44,7	0,0

A.2 Temperature boxplots

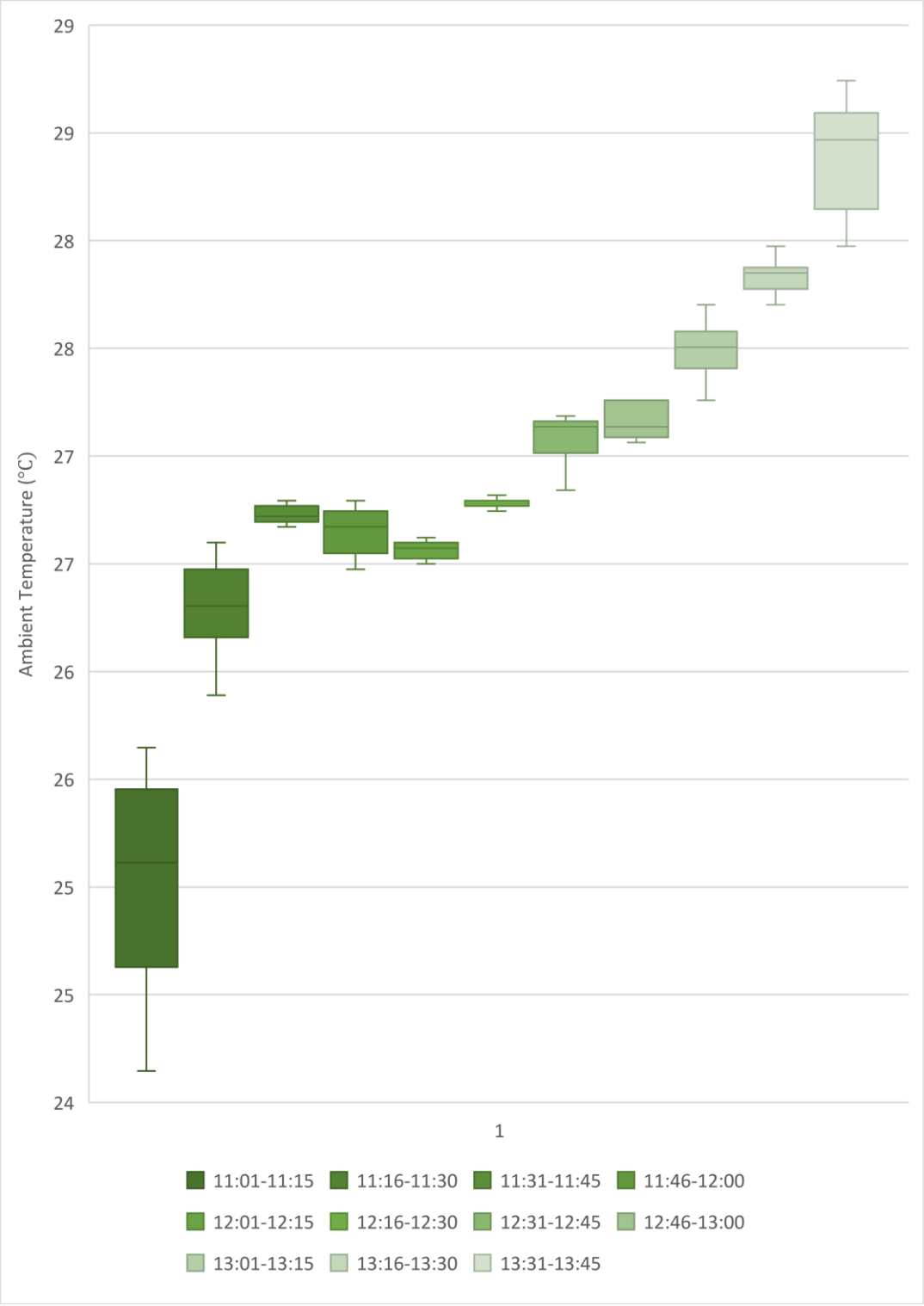

Figure 95: Temperature boxplots

A.3 Relative humidity boxplots

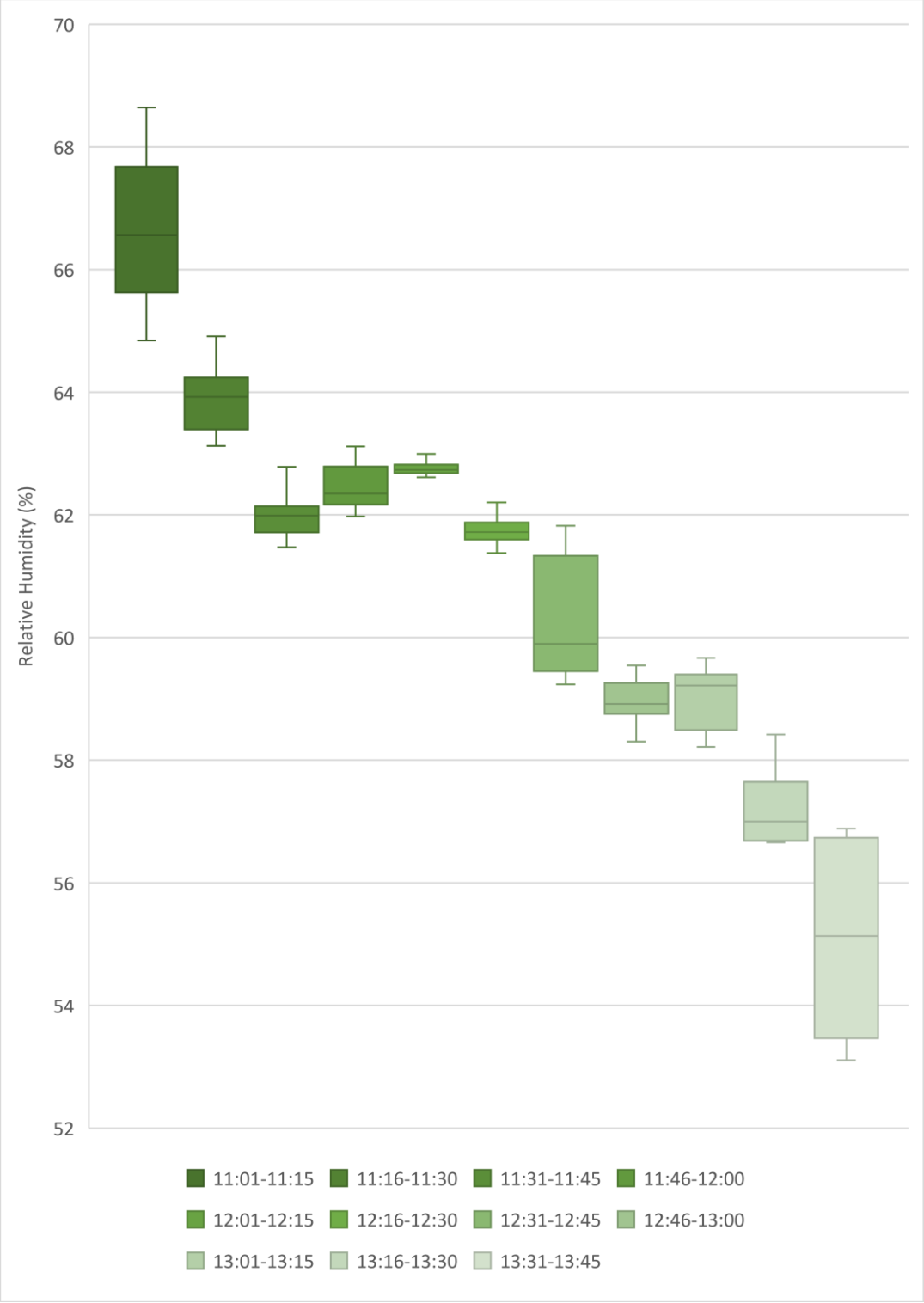

Figure 96: Relative humidity boxplots

A.4 Solar radiation boxplots

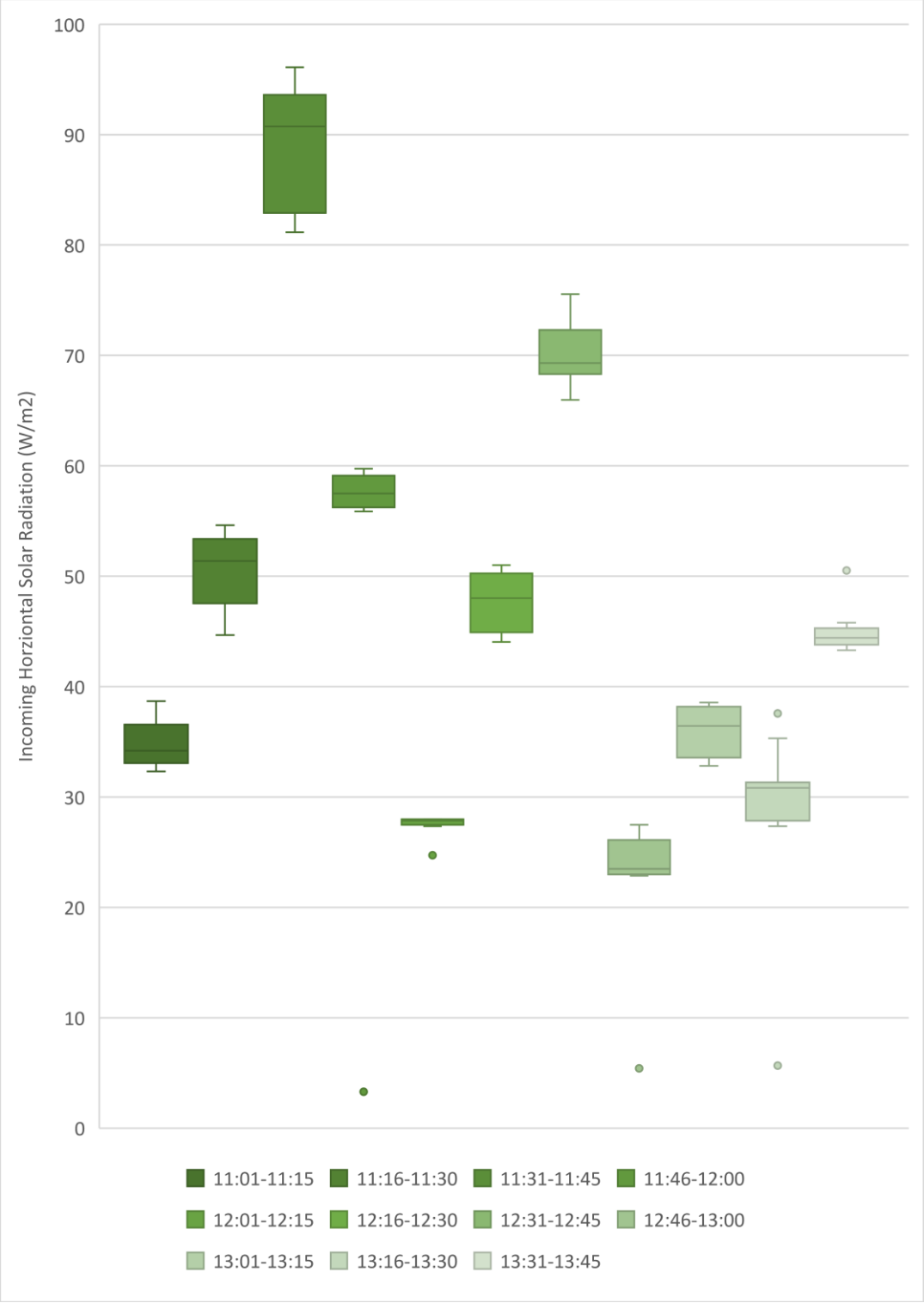

Figure 97: Solar radiation boxplots

A.5 Wind speed boxplots

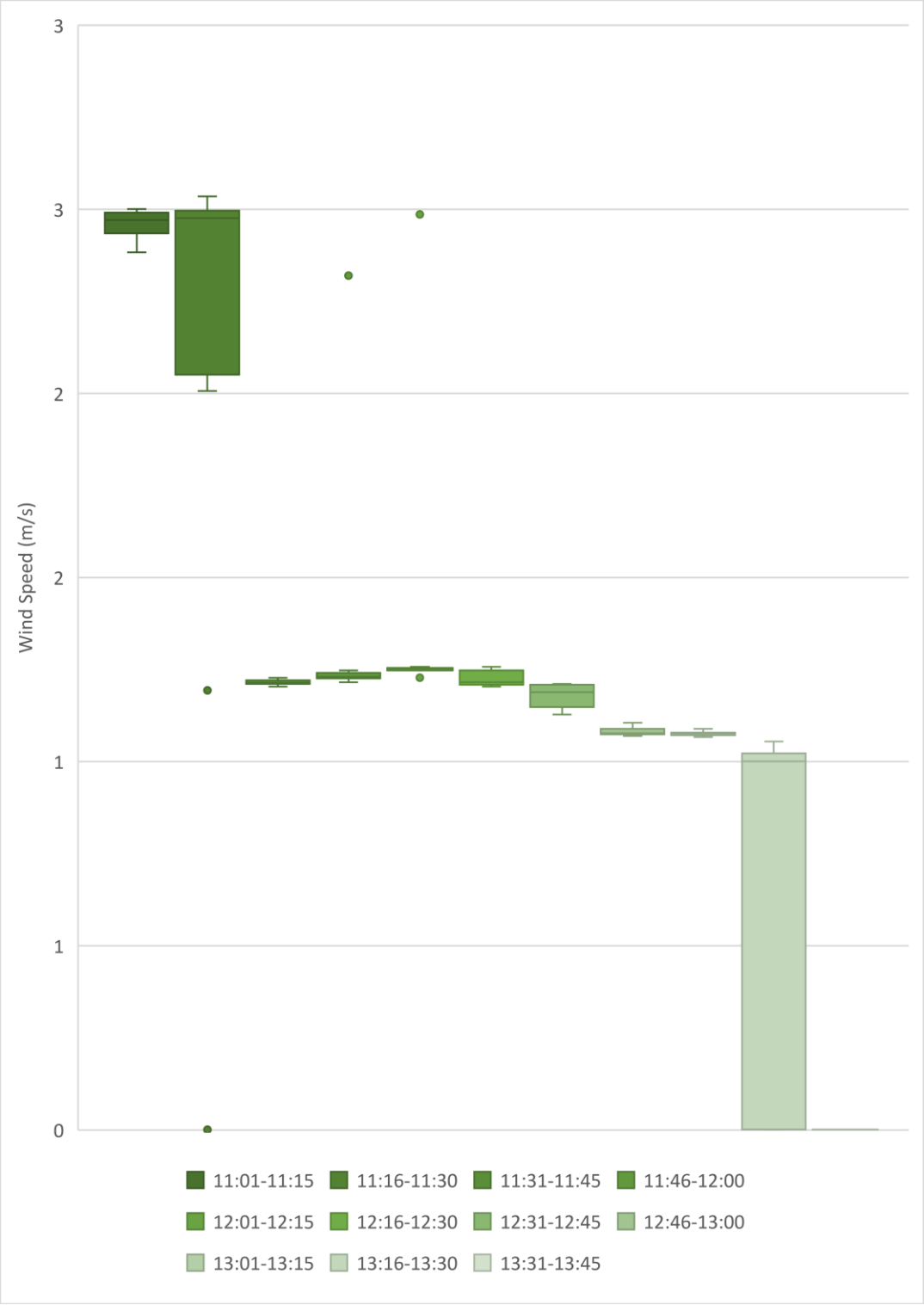

Figure 98: Wind speed boxplots

Appendix B:
Vegetation on green balconies

B.1 Pictures of green balconies

The pictures in the following paragraphs were taken by the author during the moment of measuring. The pictures are ordered from left to right (viewed when entering the balcony) and display the vegetation on the balcony.

B.1.1 Balcony 1

Figure 99: Vegetation on balcony 1

B.1.2 Balcony 2

Figure 100: Vegetation on balcony 2

B.1.3 Balcony 3

Figure 101: Vegetation on balcony 3

B.1.4 Balcony 4

Figure 102: Vegetation on balcony 4

B.1.5 Balcony 5

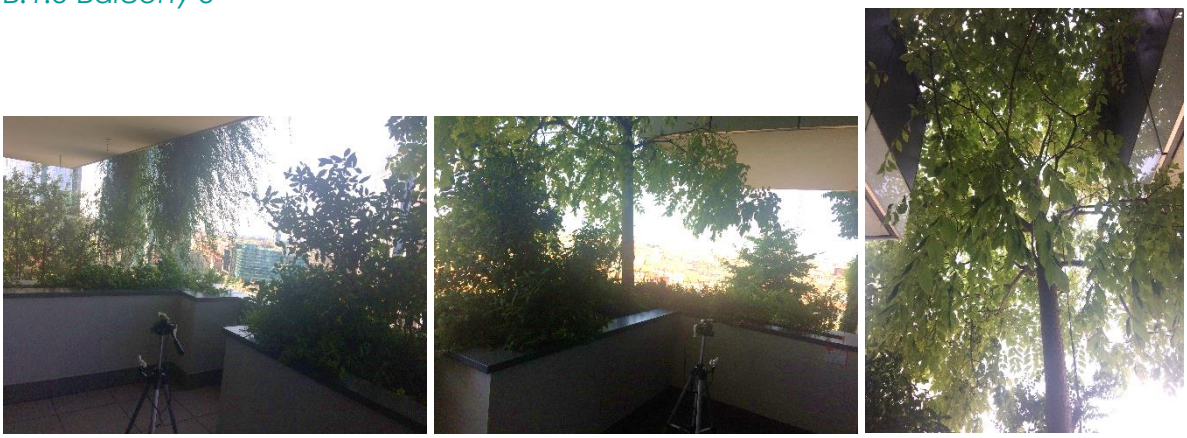

Figure 103: Vegetation on balcony 5

B.1.6 Balcony 6

Figure 104: Vegetation on balcony 6

B.1.7 Balcony 7

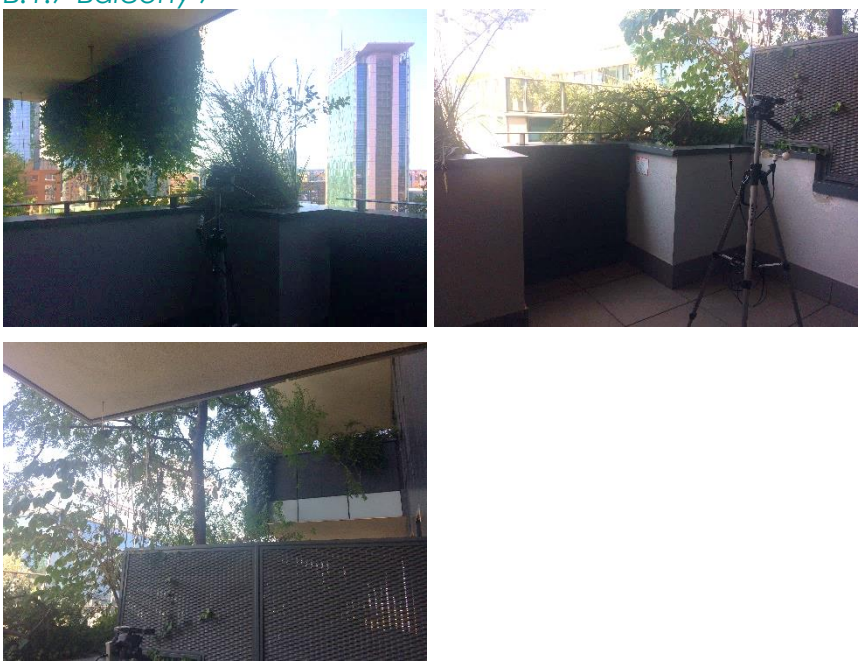

Figure 105: Vegetation on balcony 7

B.1.8 Balcony 8

Figure 106: Vegetation on balcony 8

B.1.9 Balcony 9

Figure 107: Vegetation on balcony 9

B.1.10 Balcony 10

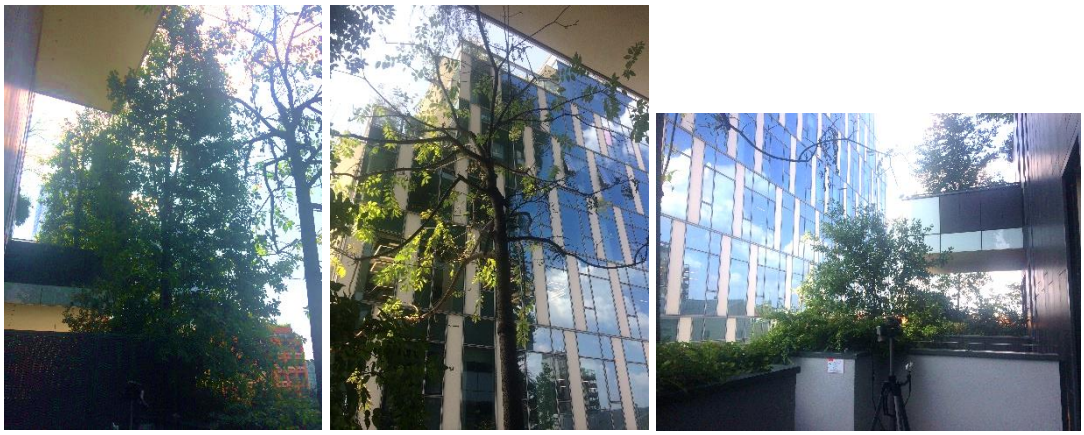

Figure 108: Vegetation on balcony 10

B.1.11 Balcony 11

Figure 109: Vegetation on balcony 11

B.2 Models of green balconies

B.2.1 Explanation of green balcony models

The vegetation on the green balconies has been simulated using Albero 4.3, the 3D plant design tool that accompanies ENVI-met software. To model the plants, a simplification of the actual situation needs to be made. For every balcony assumptions have been made, which are illustrated below. The illustrations below show a top view of all eleven balconies, with the same relative x- and y-coordinates. In the illustration Tower D is depicted in dark concrete with the lighter concrete balcony platform cantilevered from the building. The plant containers with a height of 1 meters are situated on the balcony platform. Inside the plant containers there can be nothing of relevance, bushes or trees. The top view of the bushes also shows their height relative to the plant container with a number. The top view of the trees also displays the height of the trees relative to the plant container. In addition, the canopy height of the tree is given (if this is 1 meter or more) and there is an indication whether the tree canopy Leaf Area Density is high, medium or low. Figure 110 shows a legend for the green balcony illustrations of the following subparagraphs.

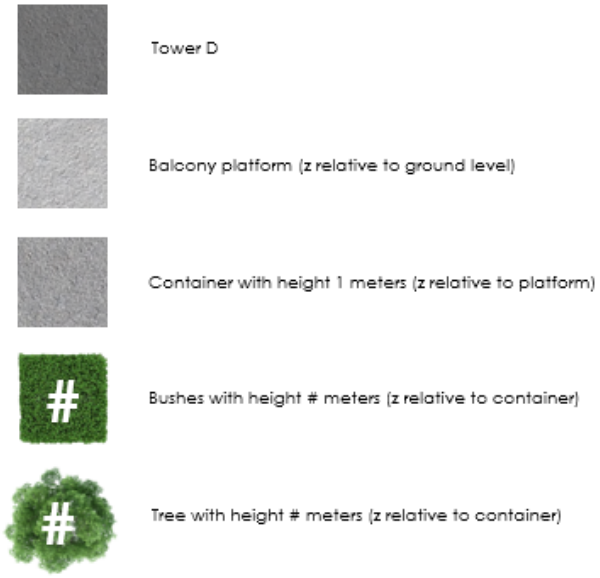

Figure 110: Legend of green balcony illustrations

B.2.2 Top view illustrations of green balcony models

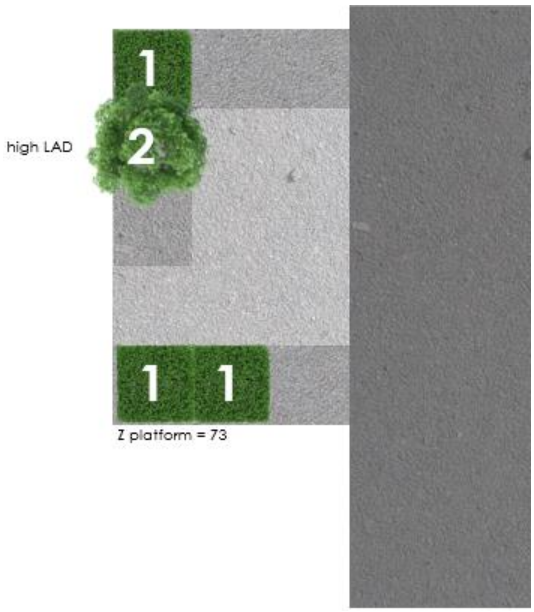

Figure 111: Model of green balcony 1

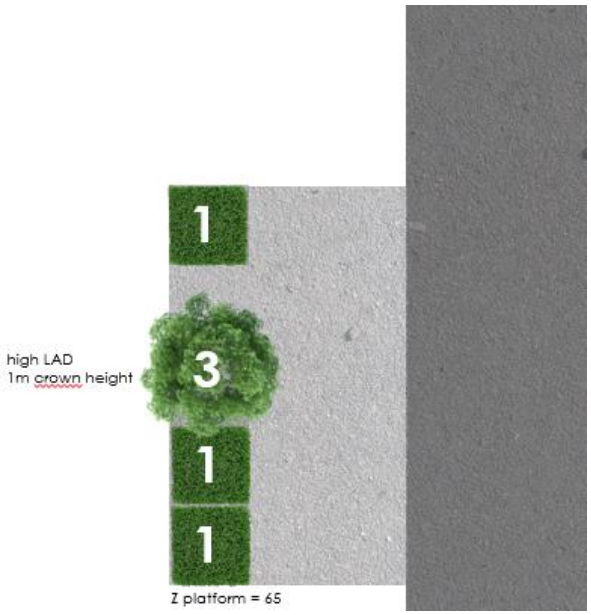

Figure 112: Model of green balcony 2

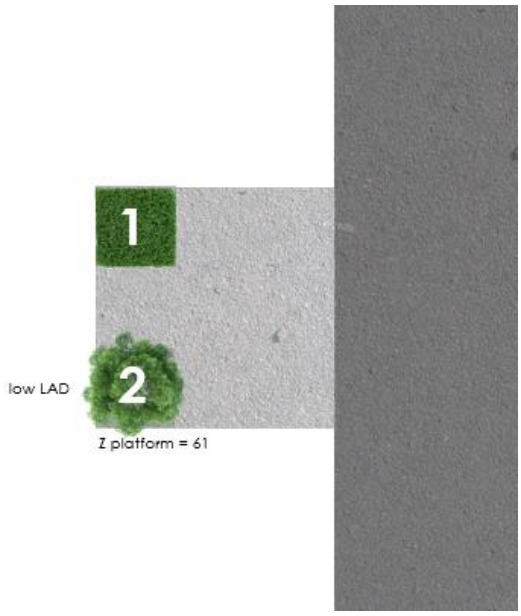

Figure 113: Model of green balcony 3

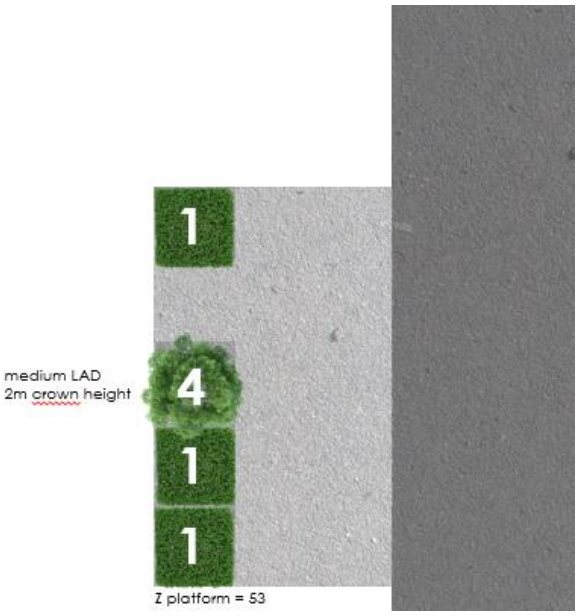

Figure 114: Model of green balcony 4

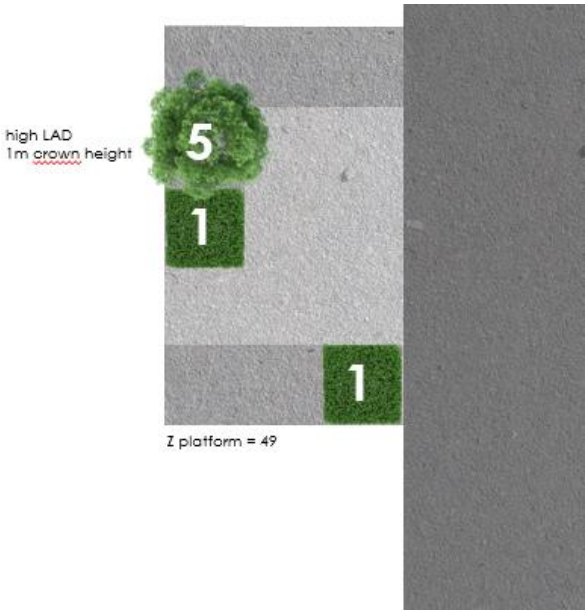

Figure 115: Model of green balcony 5

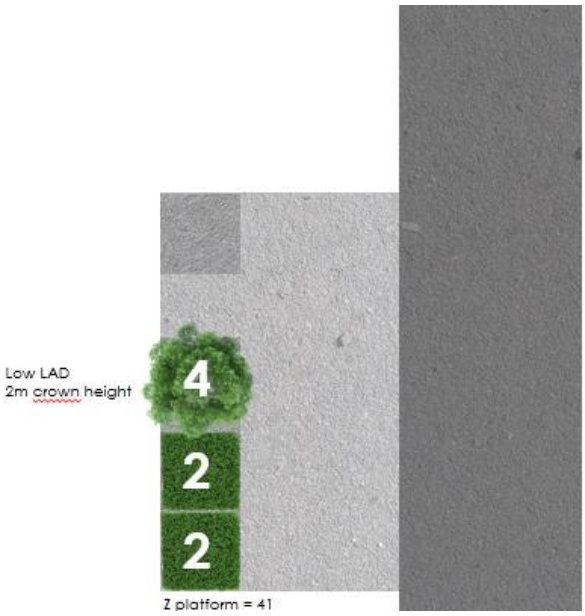

Figure 116: Model of green balcony 6

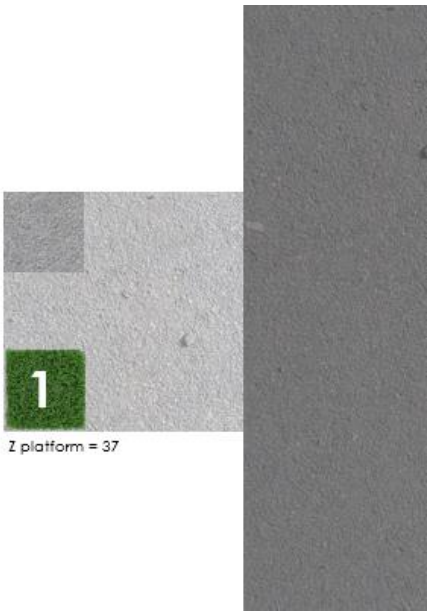

Figure 118: Model of green balcony 7

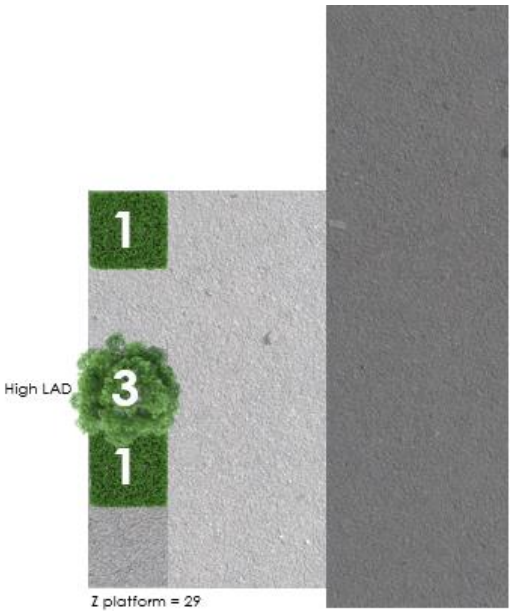

Figure 119: Model of green balcony 8

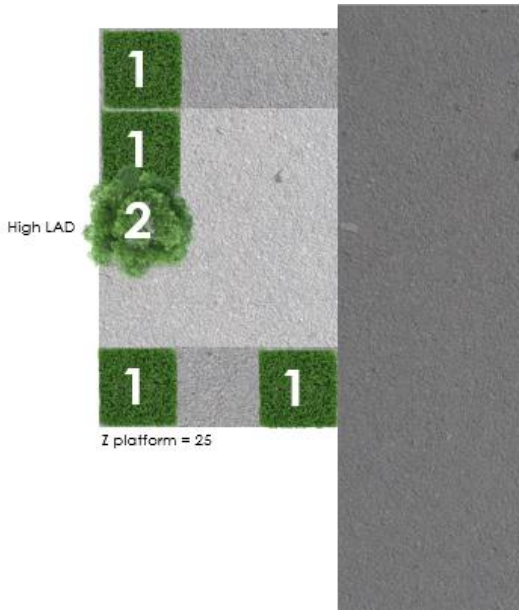

Figure 120: Model of green balcony 9

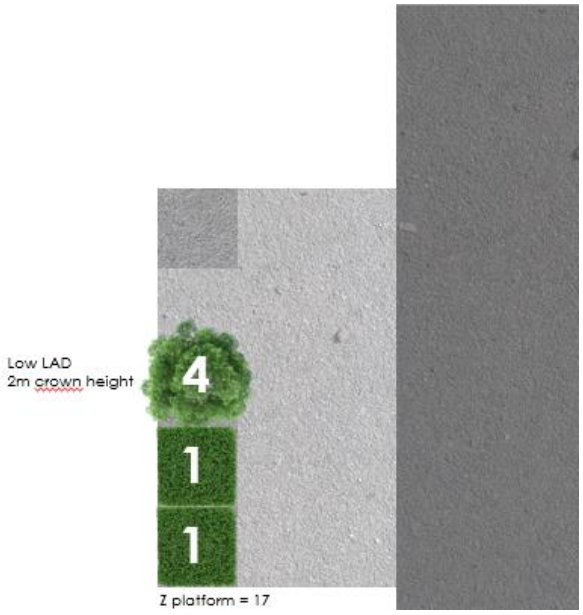

Figure 117: Model of green balcony 10

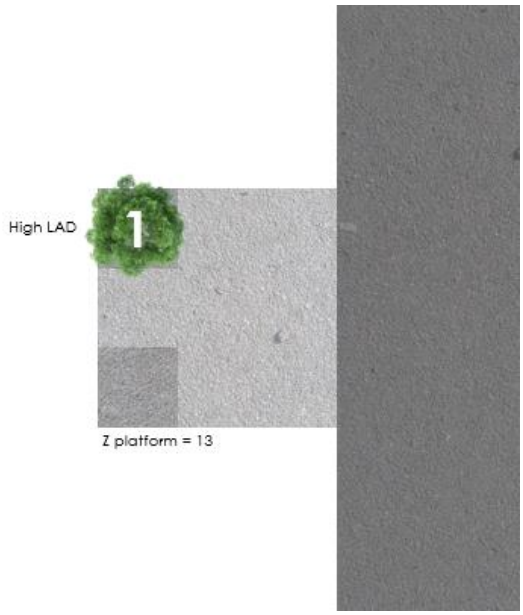

Figure 121: Model of green balcony 11